



Politecnico di Torino

DEPARTMENT OF MECHANICAL AND AEROSPACE ENGINEERING

Master's Degree Course in Mechanical Engineering

Master's Degree Thesis

Prototyping tearing machine

Advisors:

Prof.ssa Daniela Maffiodo
Prof.ssa Raffaella Sesana

Candidate:

Antonio Consiglio
253289

Co-Advisor:

Prof. Juan Zubiri

Academic Year 2018-2019



POLITECNICO DI TORINO

Joint work with:



*“Tu siempre puedes caer pero siempre puedes
levantarte mas fuerte de antes tambien”*

TABLE OF CONTENTS

1	Introduction	10
2	Recycling technologies.....	13
2.1	Primary Approach: Reclaimed Fibers.....	13
2.2	Secondary Approach: Shredding	15
2.3	Third Approach: Chemical recycling.....	17
2.4	Fourth Approach: Thermal method	19
3	Recycling process: <i>obtain reclaimed yarn</i>	20
3.1	Pre-Treatment: disinfection	20
3.2	Cutting and Tearing	21
3.3	Carding.....	22
3.4	Spinning.....	23
4	Tearing machine	24
4.1	PATENT EP0293590 B1 [14]	24
4.2	PATENT US6061876 [15]	27
4.3	PATENT US4484377 [16]	33
4.4	Classification of the machines	34
4.4.1	Rotation part	34
4.4.2	Machine maintenance	34
4.4.3	Ease of manufacture	35
4.4.4	Quality of fibres.....	35
5	Machine analysis and operation.....	36
5.1	Machine description.....	36
5.2	Machine operation	41
5.3	Use of the machine	43
5.3.1	Evaluate the real power required.....	43
5.3.2	Evaluation of the influence of work parameters.....	43
5.3.3	Evaluation the location of metallic pins	47
6	Prototype design for testing.....	49
6.1	Forces involved estimation	49
6.2	Actuation.....	52
6.2.1	Gearmotor.....	52
6.2.2	Toothed belt drive.....	53

6.3	Shaft-hub connections.....	55
6.4	Drive joint	57
6.5	Design: <i>Gear drive</i>	58
6.5.1	Static Design.....	58
6.5.2	Fatigue test: <i>Standard ISO 6336</i>	60
6.6	Static evaluation of metallic pins.....	69
6.7	Estimated of the forces involved: <i>main shaft</i>	71
6.7.1	Design: <i>hollow shaft</i>	71
6.7.2	Design: <i>Internal shaft</i>	74
6.8	Design: <i>Auxiliary shafts</i>	84
6.9	Design: <i>main shaft joint ring</i>	100
6.9.1	Checking the screws used.....	103
6.10	Bearing choose	105
6.10.1	Calculation criteria	105
6.10.2	Bearing for main shaft	110
6.10.3	Bearing for auxiliary shafts	111
7	Conclusion and future development	114

LIST OF FIGURES

Figure 1.1: Common fabrics used in textile industry	11
Figure 1.2: Fiber consumption worldwide	12
Figure 2.1: Tearing Machine - Shunxing - MQK1060.....	13
Figure 2.2: Tearing Machine -Steal Pins- Shunxing - MQK1060.....	14
Figure 2.3: Industrial shredding machine Patent US 2005/0242221 A1	16
Figure 2.4 : Insulation with recycling of post-consumer denim.....	17
Figure 2.5: Chemical Recycling of PET [2]	18
Figure 2.6: Schematic Diagram of Acidolysis Plant [7].....	18
Figure 3.1: Recycling process	20
Figure 3.2: Carding machine	22
Figure 4.1: Shredding machine Patent EP0293590 B1	24
Figure 4.2: Pins on the wooden strip	25
Figure 4.3: Detail of pins.....	26
Figure 4.4: Shredding machine Patent US6061876.....	27
Figure 4.5: Internal parts of shredding machine Patent US6061876.....	28
Figure 4.6: Particular of roll inside the machine	29
Figure 4.7: Particular of the last concave plate	30
Figure 4.8: WP coated wire plate	30
Figure 4.9: Typical Wire coating.....	31
Figure 4.10: Optimum roller and plate configuration covered with wire.....	31
Figure 4.11: GP carding plate.....	32
Figure 4.12: Shredding machine Patent US4484377	33
Figure 5.1: Prototype drawing	36
Figure 5.2: Zoom to the prototype drawing.....	37
Figure 5.3: Zoom to the prototype drawing.....	37
Figure 5.4: Main shaft	38
Figure 5.5: Example of pins on the main shaft.....	38
Figure 5.6: Zoom to the prototype drawing.....	39
Figure 5.7: drawing of the chassis of the tearing machine	39
Figure 5.8: aluminium profiles 40x40	40
Figure 5.9: aluminium profiles 40x16	40
Figure 5.10: aluminium profiles 80x16	40
Figure 5.11: Diagram of the forces involved in the tearing process.....	41
Figure 5.12: Diagram of the forces involved in the tearing process.....	42
Figure 5.13: chassis elements where the auxiliary rollers are mounted	44
Figure 5.14: Device that allows the variation of the distance between the auxiliary rollers.	44
Figure 5.15: Connection between the stem and the component (23)	45
Figure 5.16: Minimum distance between centres condition.....	45
Figure 5.17: Maximum distance between centres condition	46
Figure 5.18: Alternate position of the pins on the main roll	47
Figure 5.19: Main roll full of pins	47
Figure 5.20: Main roll with an alternate row of pins.....	47

Figure 5.21: Conical truncated shape	48
Figure 5.22: Claw shape	48
Figure 6.1: Simple tool used to simulate and measure the force required to tear the cloth	49
Figure 6.2: Dynamometer.....	50
Figure 6.3: Thin cotton fabric.....	50
Figure 6.4: Denim fabric	50
Figure 6.5: Drawing of the motor on CATIA V5.....	52
Figure 6.6: Gearmotor datasheet	52
Figure 6.7. Datasheet of the toothed belt.....	54
Figure 6.8: UNI 6604 standard for the choice of tongues.	56
Figure 6.9: Bolt coupling made by ComInTec.	57
Figure 6.10: Size factor, Y_x , for tooth bending strength.....	60
Figure 6.11: Life factor, Y_{NT} , depending on number of load cycles.....	61
Figure 6.12: Relative notch sensivity factor, $Y_{\delta rel T}$, for reference stress	61
Figure 6.13: Relative surface factor, $Y_{Rrel T}$	62
Figure 6.14: Lubricant factor Z_L	65
Figure 6.15: Velocity factor, Z_v	65
Figure 6.16: Roughness factor, Z_R	66
Figure 6.17: Work hardening factor Z_W for through-hardened gear/case-hardened pinion, reference stress	66
Figure 6.18: Propriety of the steel chosen for the gears.	68
Figure 6.19: graph of the forces acting on the pins	69
Figure 6.20: Shear diagram	69
Figure 6.21: Bending moment diagram.....	69
Figure 6.22: graph of the forces acting on the hollow shaft.....	72
Figure 6.23: Bending moment diagram.....	72
Figure 6.24: graph of the forces acting on the shaft – YX plane.....	74
Figure 6.25: graph of the forces acting on the shaft – YZ plane	75
Figure 6.26: Bending moment diagram – YX plane	75
Figure 6.27: Bending moment diagram – YZ plane.....	75
Figure 6.28: Stress due to bending moment, and its value as the time changes.....	77
Figure 6.29: Sections verified at Fatigue, seen in the YZ plan	77
Figure 6.30: CL and C_s chart depending on load.....	80
Figure 6.31: CF chart depending on the roughness	80
Figure 6.32: A chart depending on $R_{p0.2}$ of the material.....	81
Figure 6.33: K_t chart depending on (r/D) and (D/d)	81
Figure 6.34: drawing of the prototype showing the auxiliary shafts	84
Figure 6.35: Diagram of forces for belt drive.....	85
Figure 6.36: graph of the forces acting on the shaft – YX plane.....	85
Figure 6.37: graph of the forces acting on the shaft – YZ plane	85
Figure 6.38: Shear diagram – YX plane	86
Figure 6.39: Shear diagram – YZ plane	86
Figure 6.40: Bending moment diagram – YX plane	86
Figure 6.41: Bending moment diagram – YZ plane.....	86

Figure 6.42: Section in which carried out the fatigue test.....	87
Figure 6.43: Diagram of forces for gear drive.....	89
Figure 6.44: graph of the forces acting on the shaft – YX plane.....	89
Figure 6.45: graph of the forces acting on the shaft – YZ plane.....	90
Figure 6.46: Bending moment diagram – YX plane.....	90
Figure 6.47: Bending moment diagram – YZ plane.....	90
Figure 6.48: Section in which carried out the fatigue test.....	91
Figure 6.49: graph of the forces acting on the shaft – YX plane.....	94
Figure 6.50: graph of the forces acting on the shaft – YZ plane.....	94
Figure 6.51: graph of the constrain reactions on the shaft – YX plane.....	94
Figure 6.52: graph of the constrain reactions on the shaft – YZ plane.....	95
Figure 6.53: Bending moment diagram – YX plane.....	95
Figure 6.54: Bending moment diagram – YZ plane.....	95
Figure 6.55: Section in which carried out the fatigue test.....	96
Figure 6.56: Datasheet of steel for the main shaft.....	99
Figure 6.57: Datasheet of steel for the auxiliaries shafts.....	99
Figure 6.58: Ring joint.....	100
Figure 6.59: Stress parallel to the axis of the holes to a finite-width thin element [20].....	100
Figure 6.60: A chart depending on $Rp0.2$ of the material.....	101
Figure 6.61: Stress concentration factor Kt for uniaxial tension of a finite-width element. Stress parallel to the axis of the holes.[20].....	102
V Figure 6.62: share force in the screw connection.....	102
Figure 6.63: Viscosity-temperature diagram for ISO viscosity grades.....	107
Figure 6.64: Minimum rated viscosity $v1$ required depending on the average diameter of the bearing.....	108
Figure 6.65: Factor $aSKF$ for radial ball bearings.....	109

LIST OF TABLES

Table 6.1: Testing for thin cotton fabric.....	51
Table 6.2: Testing for denim fabric	51
Table 6.3: Service factor depending on the type of motor and application.....	53
Table 6.4: Shaft-hub connection for the pulleys.....	56
Table 6.5: Shaft-hub connection for the gears.....	57
Table 6.6: ylw depending on Z	58
Table 6.7: Application factor, K_A	63
Table 6.8: $K1$ and $K2$ depending on the accuracy grades	63
Table 6.9: Description and position of the sections verified at Fatigue	78
Table 6.10: Description and position of the sections verified at Fatigue	87
Table 6.11: Description and position of the sections verified at Fatigue	91
Table 6.12: Description and position of the sections verified at Fatigue	96
Table 6.13: Breaking strength according to UNI EN ISO 898-1:2001	103
Table 6.14: Resistant Area for nominal diameter of screw	103
Table 6.15: Values for the ηc for different levels of the contamination, according to SKF standard.....	106

1 Introduction

The problem of waste has always been one of the problems of our society. In particular, the need for textile waste recycling stems from the fact that the world's population is constantly increasing and we will no longer be able to meet the demand for raw materials necessary for the production of clothing (i.e. the demand for organic raw materials) nor will we be able to dispose of and accumulate waste in landfills because there will be a lack of areas that can meet this purpose.

The global production of cotton in 2018 is 123.69 million bales. The global supply of cotton is 246.83 million bales. The global demand for cotton in mill sector in 2018 is to 125.44 million bales. The global cotton production in the world has increased to 41.9 percent during the period 1990 – 2018. The global supply in the world has increased to 72.95 percent during the same period. [1]

Textiles are at the bottom of the league in terms of recycling. While 80% of steel is recycled, 65% of paper and 30% of plastics, recycling of textiles stands at 15-20%. Textiles require indirect inputs such as water (200 litres to a kg of synthetic fibres and 8000 litres to a kg of cotton), energy (100 litres of petrol to one kg of fibre) and land. An American or European consumer requires around 600 m² of land a head to satisfy their annual fibre needs. [2]

The solution to this problem is to be able to recycle fabrics that are left in landfills or incinerators every year. A few communities have textile recycling programs, about 85% of this waste goes to landfills where it occupies about 5% of landfill space and the amount is growing. [3] Up to 95% of the textiles that are land filled each year could be recycled. [4]

After synthetic fibres came onto the market in the 20th century, textile recycling became more complex for two distinct reasons: (i) Fibre strength increased making it more difficult to shred or ‘open’ the fibres, and (ii) fibre blends made it more difficult to purify the sorting process [5]. It is not yet possible to sort the different types of fabrics with which the clothes are made automatically, the collected waste was sorted manually or semi-automatic based on the product type, manufacturing methods, fibre composition and a product condition assessment (by 17 criteria into 25 categories) followed by recycling process. [6]

With the reduction of the areas that can be used as landfills, the cost of disposing of fabrics has increased dramatically, making the practice of recycling increasingly favourable from the economic point of view. In fact, Textile recycling industry can process 93% of the waste without the production of any new hazardous waste or harmful by-products. Further, at the beginning of the 1990s, disposal costs were €5/t for landfilling, but nowadays it is higher than €170/t for incineration. [2]

The fabrics most commonly used in the textile industry can be divided into two categories, as is shown in the *Figure 1.1*. Most of the clothing on the market today is made of mixed fibres, so there is a problem in being able to recycle waste efficiently and economically to obtain from recycling new raw materials that can be used to create new fabrics.

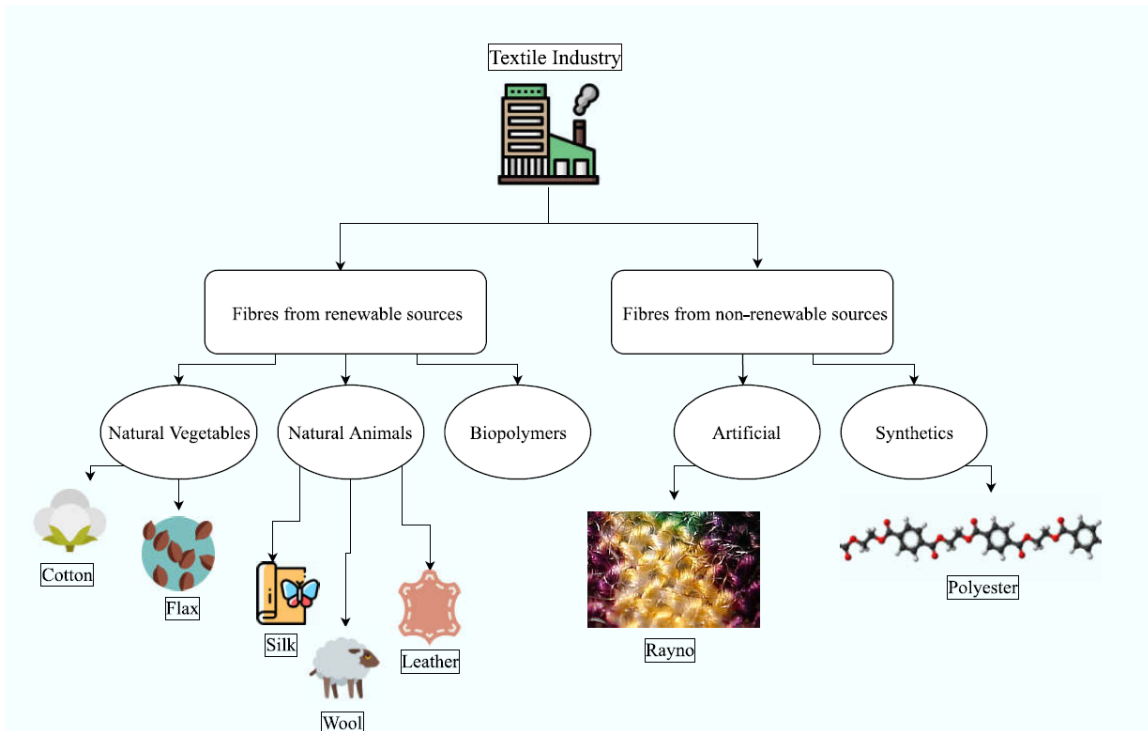


Figure 1.1: Common fabrics used in textile industry

The pie chart below (*Figure 1.2*) shows the distribution of fiber consumption worldwide, by type of fibre in 2018. [7]

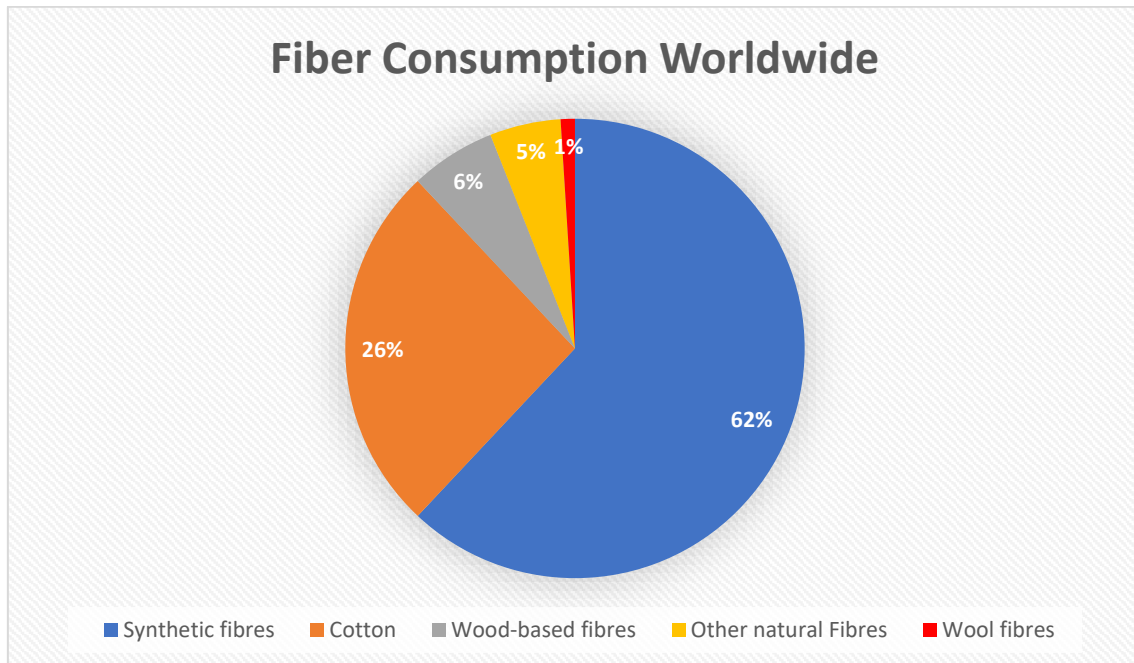


Figure 1.2: Fiber consumption worldwide

The most common mixture in the textile industry is made of Cotton/Polyester, which is used to produce shirts, denim, etc. The scientific world has made great progress in researching procedures for recycling this blend by developing chemical procedures that lead to the effective separation of 98% of the two components, the first in the form of cellulose and the second in the form of solid waste with the possibility of being reworked. Recycling is the recovery for reuse of the economic values of materials and energy from wastes that are usually destined for disposal. The textile recycling industry is one of the oldest and most established recycling industries in the world; It has a myriad of players that includes consumers, policy makers, solid-waste managers, not-for-profit agencies, and for-profit retail businesses [8]. The post-consumer textile waste is a mixture of natural fibers, synthetic fibers, and other substances such as zippers or metallic snap fasteners, which make it hard to degrade. [9] Post-consumer waste can be given to charity and reused as second-hand garments or left in landfills as waste.

2 Recycling technologies

We can classify textile waste into two categories: *pre-consumer waste*, which is all the waste generated by the textile, cotton and yarn industries. It contains biodegradable substances such as fiber waste, yarn waste, fiber lint, and fabric scrap, this waste is reworked by the textile industry and used to create fabrics useful in other fields such as aeronautics, home building, supplies, automotive. *Post-consumer waste* which includes all those textile wastes that arrive in the landfill after they have done their job, such as worn out clothes or out of fashion.

It is a mixture of natural fibers, synthetic fibers, and other substances, such as metallic zippers, acrylic buttons, wood buttons, shell buttons, and metallic snap

Recycling technologies can be classed into four approaches in relation to how textile waste can be processed. The primary approach is to recycle in its original form, which would involve the breakdown of fabrics to fibres and processing of the recycled fibres. The secondary approach is to shredder textile waste, if wastes are only plastics waste it is possible to melt it and process plastics into a new product with lower physical and chemical properties. Tertiary recycling involves converting plastic wastes to basic chemicals or fuels, for example this can be by pyrolysis or hydrolysis reactions. Finally, quaternary recycling is where waste is converted to energy through incineration. [5]

2.1 Primary Approach: Reclaimed Fibers



Figure 2.1: Tearing Machine - Shunxing - MQK1060

The reclaimed fibers are obtained from a second processing cycle. Their characteristic is that at the end of the process, fibres with optimal textile characteristics are obtained.

Currently, the fibres obtained by the process are of short length, which conditions their mechanical properties.

Conventionally, the process consists of a first part in which the waste is pre-treated, cut and collected, and transported through a conveyor belt to a tearing machine (*Figure 2.1*), which allows the textile structure to be broken down into individual fibers, through different stages characterized by steel pins (*Figure 2.2*) which are on the drum surface.

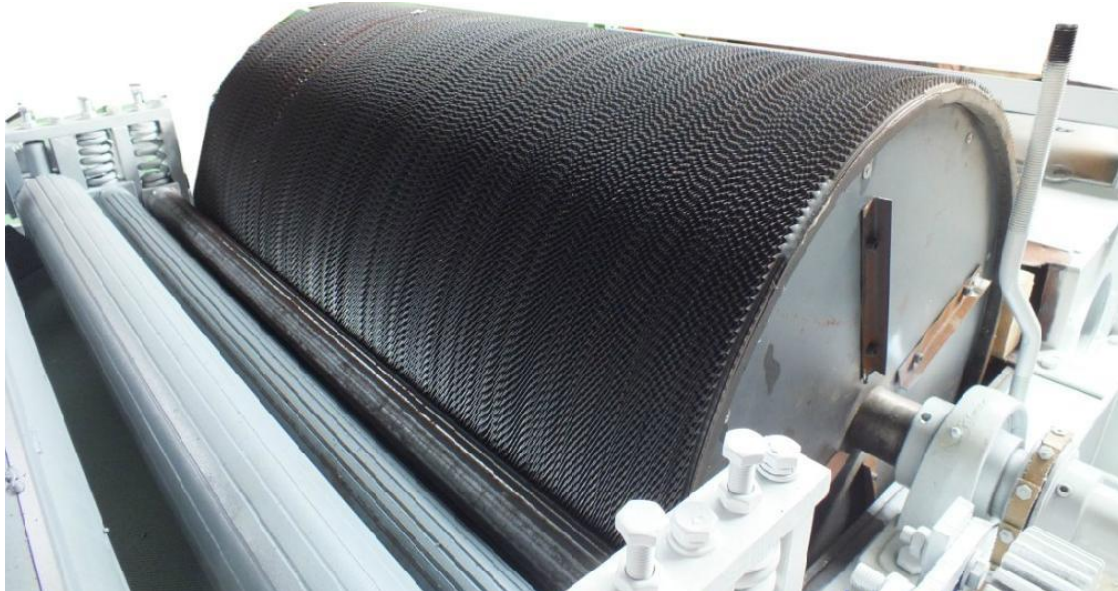


Figure 2.2: Tearing Machine -Steel Pins- Shunxing - MQK1060

In the process, the textile characteristics of the materials are maintained, and this is why functional components of the fibre materials (non-flammability, high fibre strength) can be made use of several times and as for the consumption of energy, breaking down fibres is preferable to other forms of physical and chemical recycling (re-granulation, fibre production). Present-day technologies allow between 25% and 55% of fibres of 10 mm length and longer [5]

Through this process are recycled textile waste from the pre-consumer sector, with an end result that is of excellent quality, and textile waste from the post-consumer sector, from which are obtained regenerated fibers of lower quality and not always homogeneous because there is the possibility to recycle even blends such as cotton/polyester which are used in the non-textile industry.

Regenerated fibres can be used in both the textile and non-textile industries. First of all, new yarns made of regenerated fibres and primary fibres (15%) can be generated in order to obtain better workability, but as the majority of regenerated fibres have a grey or dark colour, they are very often not used to produce new garments or household textiles, but are used to produce technical yarns in which colour is not a relevant parameter.

In this way polyester/cotton threads are machined into open fiber. These fibers can be used for stuffing and for some industrial applications such as filter and caskets.

In general, these fibers may be spun into very coarse count yarns such as mop yarns (a mop cord is made of four to eight plied yarns). Polyester filaments are cut and open end so that the end product can be used as polyester stuffing. Carpet waste can be opened up so that it may be used to produce carpet underlay. Apparel cuttings are processed into the raw materials for sound deadening the pads used in automobiles. Cotton threads are opened to fibers and are used in the absorbent cotton industry.

2.2 Secondary Approach: Shredding

The second approach is highly developed, and it is possible at the end of the shredding process to use the recycled waste as padding or as an insulating material or if it is only plastic (such as Polyester) it is possible to melt the shredded waste to obtain a second Polyester yarn that can be used for the production of new garments. One of the problems with this procedure is the difficulty of separating the shredded material. As already mentioned, modern textile waste is characterised by the fact that its composition is not homogeneous, but is made up of blends, the most famous of which is the cotton/polyester blend.

The main processes in textile recycling are, collection of the waste, sorting, transporting, cutting and shredding with a shredding machine.

A shredder is a machine or equipment used for shredding. Shredding systems are used to reduce the size of a given material. It consists essentially of pairs of steel rolls. The tolerance of the space between cutting edge and sharpness of the cutting edges effect on the shearing efficiency.

Therefore, in *Figure 2.3* an industrial shredder is designed and described to shred the most types of materials, such as rubber, plastic, wood, paper, metals, clothes, and etc. which contain two shafts inversely-rotating and there are parallel to each other (1), where each shaft are keyed disc shaped blades (2) and each blade has one or more teeth (3), separated with bush (4) the thickness of the blade and bush are same, but diameter is smaller than the blades, so that the spacers (4) of the first shaft are blades and a diameter smaller than the blades one, so that the blades (2) of the one shaft are opposed to the spacers (4) of the second shaft, one shafts (1) so spaced that the blades of first shaft cross with other of the shaft to force the material poured into an upper cutting chamber (7) to be sheared between blades, and hollow supports (14) having a circular view (15) it fixed blades (17), which interact with blades (2) to operate cutting process, material already sheared between the opposed blades and fixed supports (14) extending until they almost come into contact with the spacers (4) of the other shaft to perform cleaning thereof [10].

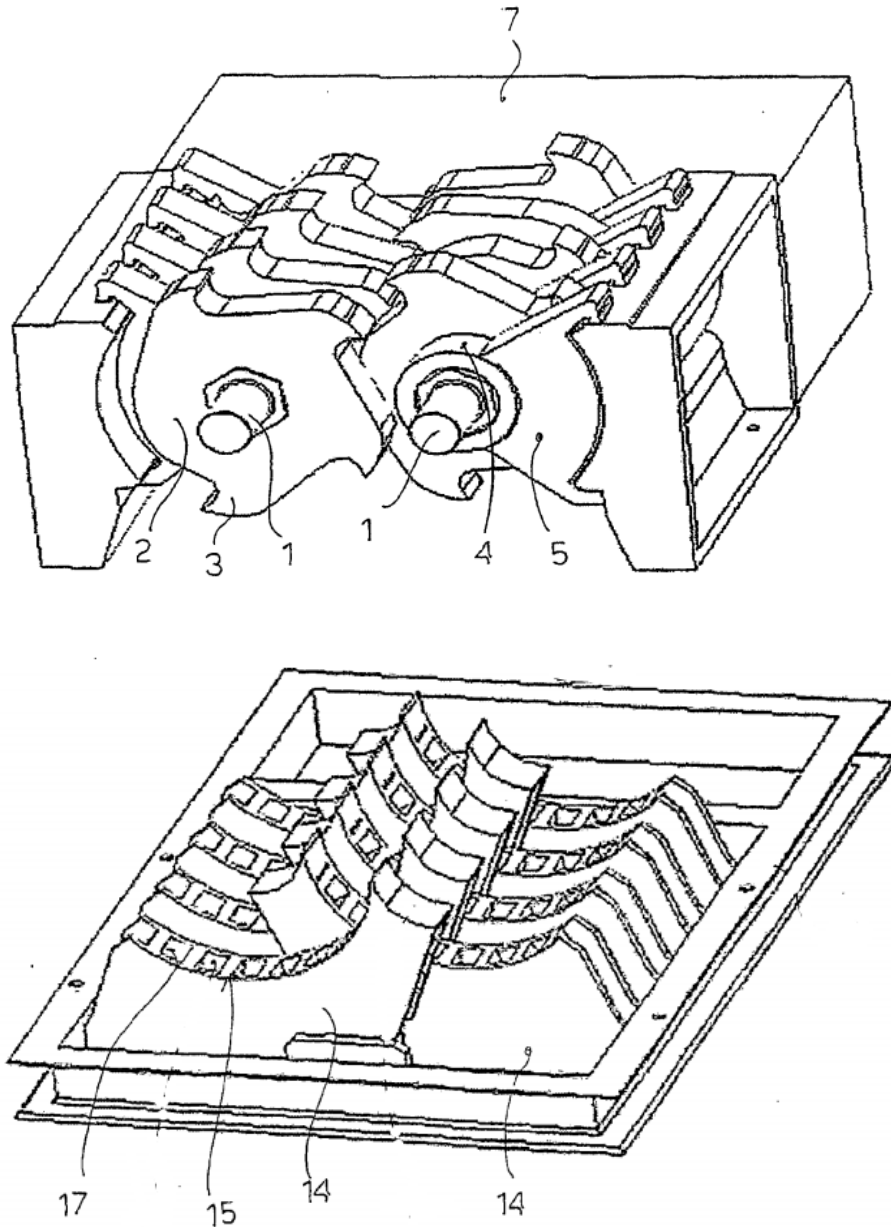


Figure 2.3: Industrial shredding machine Patent US 2005/0242221 A1

The shredding process produces small pieces of fabric that are used mainly for filling car seats, cushions, blankets or as thermal and acoustic insulation for homes or in the automotive field.

It is difficult to determine the physical properties of the output product because it is not a homogeneous product but made of different materials including cotton, polyester, etc. *Figure 2.4* shows an example of a final product obtained through this process.

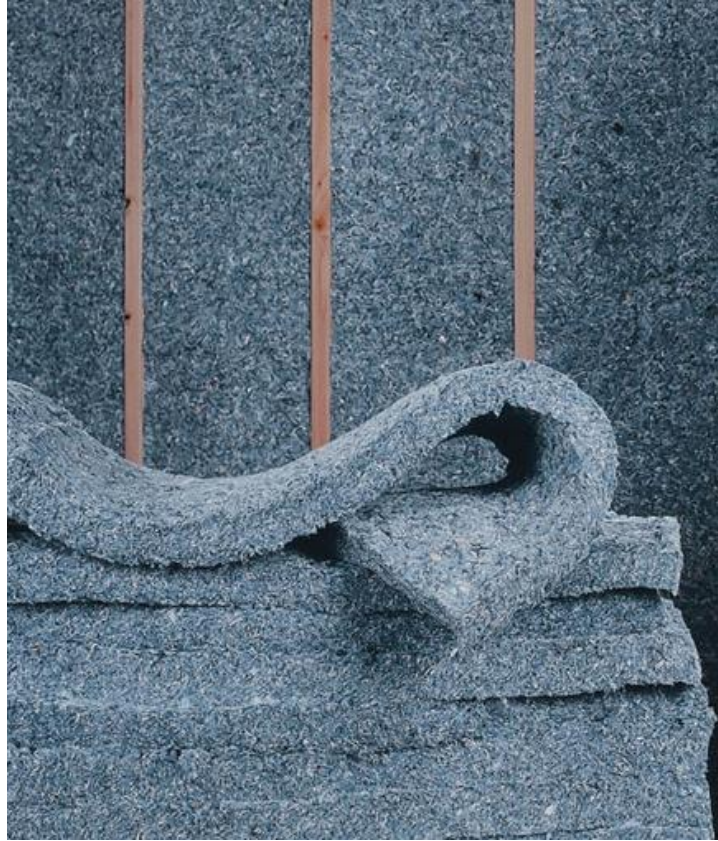


Figure 2.4 : Insulation with recycling of post-consumer denim

2.3 Third Approach: Chemical recycling

The chemical method is a method for depolymerizing a polymer compound in a synthetic fiber by a chemical reagent, converting it into a monomer or an oligomer, and then using the monomer to produce a new chemical fiber.

Chemical recycling overcomes some of the problems that limit mechanical recycling such as the problem of textile's bland.

The products of chemical recycling are easily reintroduced into the production cycle, without any problems of market saturation; another benefit is that the crude products resulting from chemical breakdown can be used without further purification.

The easiest to depolymerise are condensation-type resins (polyester (PET), polyamide (PA), polycarbonate (PC), polyurethanes (PU), etc.). The bonding of molecules in these materials is such that, if appropriate heat and pressure are applied in the presence of a reactive chemical agent, they break into shorter chains in relatively controllable ways. Technologies for the breakdown of such polymers, mainly PET (hydrolysis, glycolysis, methanolysis, aminolysis, etc.) have already been proven, and are viewed as relatively cost-effective [2].

The recycled PET is mostly used in the form of fibres, films, foams, sheets, bottles etc. Thus, chemical-recycling processes for PET are divided as follows (*Figure 2.5*):

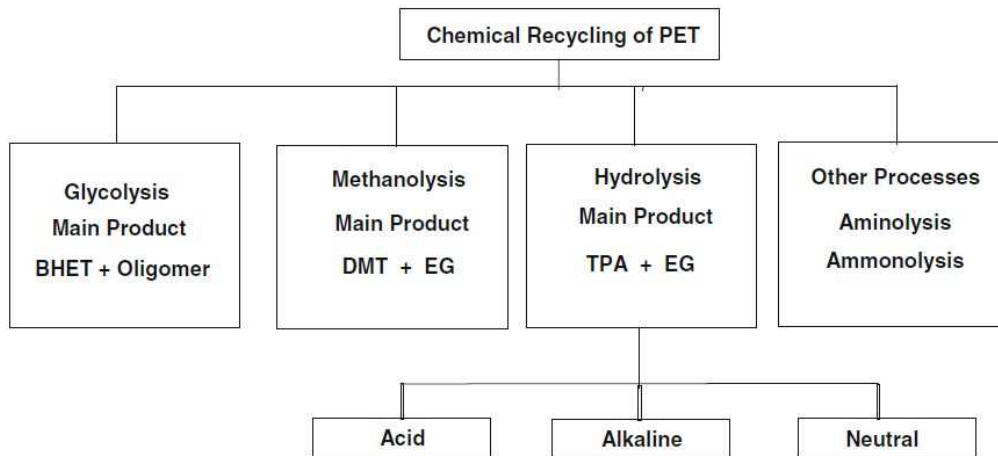


Figure 2.5: Chemical Recycling of PET [2]

For example, this is a popular way of recycling nylon 6 and can be done by acidolysis, hydrolysis or depolymerisation in vacuo. Acidolysis refers to the addition of an acid catalyst to reduce the polymer chain length. However initially nylon 6 is first cut and then melted in a continuous reactor and treated with steam. Hydrolysis of the polymer occurs producing the monomer caprolactam. The caprolactam is then distilled, while the caprolactam-water vapour is concentrated and treated with potassium permanganate which oxidises impurities.

The caprolactam is recovered in a filtration stage, which can then be polymerised to produce a good quality polymer product. *Figure 2.5* shows a plant schematic of the acidolysis process.[11]

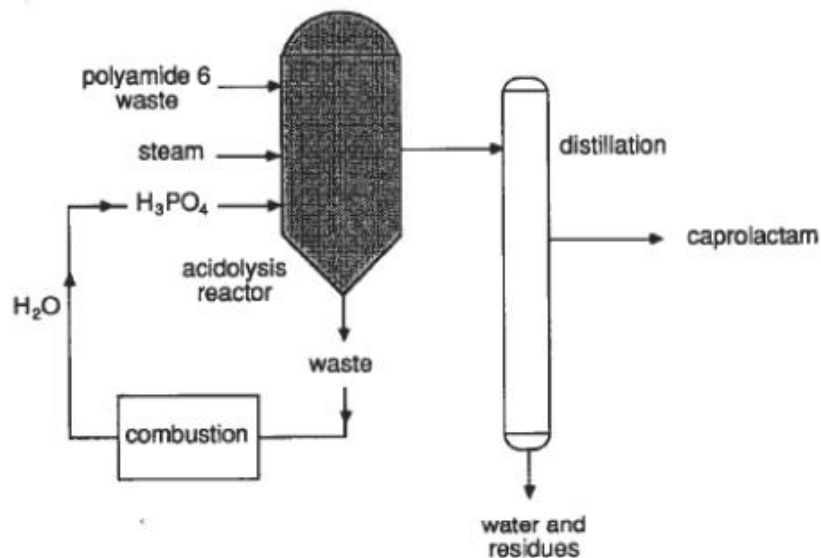


Figure 2.6: Schematic Diagram of Acidolysis Plant [7]

2.4 Fourth Approach: Thermal method

Conventional thermal processing refers to the combustion of solid waste and its conversion into energy. Since solid waste from the textile industry contains a high energy content, it can be used as a raw material to generate heat energy.

A mixture of cotton and polyester contained energy content of 16 MJ/kg. Combustion of the blend fabric at 700 for a few minutes could generate a high heat energy content gas stream at 1100 C as the air flow rate of 819 kg/m²/h (0.186 m/s). Briquette is another product created from the conventional thermal process. Briquette is a solid fuel that is normally made from woody material. Solid waste from the textile industry can also be used as a raw material to produce briquette. Drying and densification processes are required because solid textile waste is bulky and contains high moisture. Once the textile waste is compacted, it can be used for co-combustion with solid fuel, since it contains a similar compound compared to the briquette that is obtained from coal [12].

Biogas production from textile waste via anaerobic digestion is an alternative route to utilize solid waste from textile industry. This process has less requirement on toxic compound removal, therefore the textile waste can be used directly in an anaerobic digestion process. Nevertheless, the pre-treatment is needed in order to obtain high methane concentration [12].

There are many studies involving the use of cotton for the production of ethanol [13], [14]. In particular, the yield of ethanol from the recycling of solid textile waste is not very high, but a study [15] analyses the pre-treatment of waste with ionic liquid that leads to an improvement in the yield of ethanol (>70%).

3 Recycling process: *obtain reclaimed yarn*

The textile waste recycling process consists of several successive steps and can be described as in *Figure 3.1*.

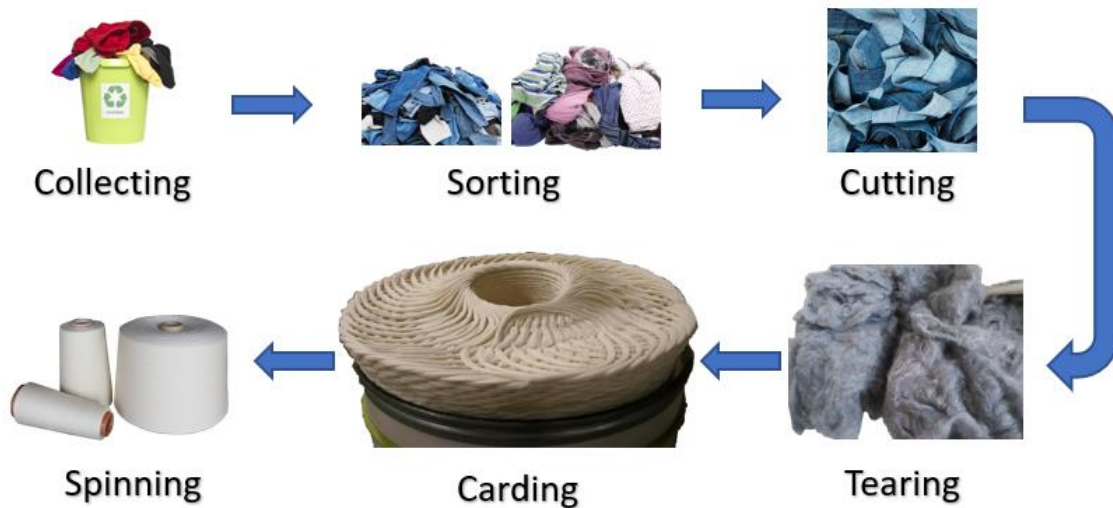


Figure 3.1: Recycling process

3.1 Pre-Treatment: disinfection

After the collection and sorting process, the product that goes through the recovery cycle must be treated and disinfected. In fact, fabrics collected as textile waste may contain bacteria, vomit stains, dirt, fungi, blood stains, sweat, etc.

There are several processes that allow the disinfection of textile waste, this can be done by ultraviolet rays, ozone, high temperature steam or reactive oxygen or the most commonly used chemical disinfectant.

1. **Ultraviolet rays**: this technique allows to destroy the molecular structure of DNA or RNA in bacterial viruses, causing the death of growth cells or the death of regenerative cells. However, although it does not require the use of any chemicals, it is not sustainable because some of the micro-organisms killed can repair damaged DNA or RNA chains in the future.
2. **Ozone**: Ozone destroys the membrane structure of the micro-organism through oxidation of oxygen atoms. It does not cause secondary pollution and has a fast sterilization rate, but excessive inhalation of ozone can cause damage to the human respiratory tract.

3. **High temperature steam:** high temperature and high pressure water vapour is used, it causes the deformation of microbial proteins and nucleic acids. The use of this technique can lead to a qualitative change of the tissue to be sterilized due to the high temperatures, with a consequent deformation.

4. **Reactive oxygen:** The strong oxidative activity of reactive oxygen species can destroy the barrier function of the bacterial cell wall and cell membrane with the oxidative degradation of intercellular proteins, intracellular enzymes until the death of bacteria. At the end of the oxidation process, oxygen and water, non-toxic and odourless substances, are formed.

5. **Chemical disinfectant:** this disinfection process is characterized by the use of two active ingredients, p-chloro-xyleneol, chlorinated phenolic organic compound derived from xylene. It works by disruption of the cell wall and stopping the function of enzymes and hypochlorous acid, which decomposes to form a new ecological oxygen to oxidize the protein. These two products cause some degree of tissue damage due to strong corrosivity and oxidizing properties. In addition, the problem of highly polluted wastewater is not secondary.

3.2 Cutting and Tearing

Once collected, sanitised, separated the textile waste is finally cut into smaller pieces. (for example, in the recycling of denim, studs, buttons and zippers are removed, everything that is not woven in practice). The process of cutting into smaller parts is carried out by an automatic machine, the aim of this step is to make the tearing process easier. Then the cut textile material is torn by a tearing machine (or a shredding machine), thus obtaining the material again in the form of fiber. The quality of the recycling depends mainly on the length of the fibre obtained at the end of the process, because the length of the fibres determines the resistance of the fabric to be produced and because it is not possible to spin fibres that are too short.

3.3 Carding

Once you have obtained our recycled fibre, you need an intermediate process before to spun it. This process is called carding, which results in orderly end parallel fibres that can then be spun. The machine used in this process is called “carding machine”, is possible to see it in *Figure 3.2*

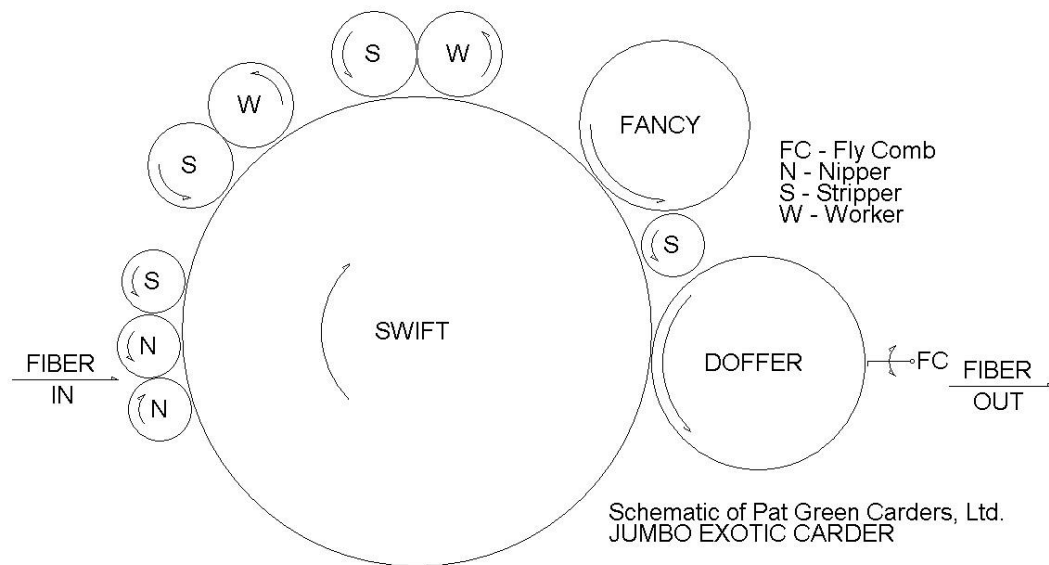


Figure 3.2: Carding machine

A typical cottage carder has a single large drum (the swift) accompanied by a pair of in-feed rollers (nippers), one or more pairs of worker and stripper rollers, a fancy, and a doffer. Raw fiber placed on the in-feed table or conveyor is moved to the *nippers* which restrain and meter the fiber onto the *swift*. As they are transferred to the *swift*, many of the fibres are straightened and laid into the swift's card cloth. These fibres will be carried past the *worker / stripper* rollers to the *fancy*.

As the *swift* carries the fibres forward, from the *nippers*, those fibres that are not yet straightened are picked up by a *worker* and carried over the top to its paired *stripper*. Relative to the surface speed of the *swift*, the *worker* turns quite slowly. This has the effect of reversing the fibre. The *stripper*, which turns at a higher speed than the *worker*, pulls fibres from the *worker* and passes them to the *swift*. The *stripper's* relative surface speed is slower than the *swift's* so the *swift* pulls the fibres from the *stripper* for additional straightening.

Straightened fibres are carried by the *swift* to the *fancy*. The *fancy's* card cloth is designed to engage with the *swift's* card cloth so that the fibres are lifted to the tips of the *swift's* card cloth and carried by the *swift* to the *doffer*. The *fancy* and the *swift* are the only rollers in the carding process that touch.

The slowly turning *doffer* removes the fibres from the *swift* and carries them to the *fly comb* where they are stripped from the *doffer*. A fine web of parallel fibre, a few fibres thick and as wide as the carder's rollers, exits the carder at the *fly comb* by gravity or other mechanical means for storage or further processing.

3.4 Spinning

The product of carding (wick) would be very poorly resistant; to obtain a strong and homogeneous yarn, the carded tape (wick) is directly processed in spinning by continuous ring spinning machine (ring) or by intermittent spinning machine (self-acting or "mule"). The ring spinning machine is currently the most common machine in the world to produce yarn. The main difference between the two systems is that while in the ring spinning machine twisting and drawing are constantly given to the wick during its exit from the feeding rods, in self-acting the twisting is given incrementally during the opening of the machine and therefore the fine points of the yarn in formation, which are those that "absorb" the twists first, are less subjected to the drawing, compared to the large points of the yarn. All this translates into a greater homogeneity in the diameter of the finished yarn. The process can be modified depending on the fiber that want to be spinning.

4 Tearing machine

The first part of my thesis work focused on the search of fundamental notions that describe the functioning of a machine used to tear fabrics, with the aim of obtaining again fiber from outdated or worn garments that are taken to landfill every day.

There is little information in the literature on this subject, which has led us to analyse various patents and make a qualification of the latter considering different parameters, such as:

- Quantity of moving parts
- Machine maintenance
- Ease of manufacture
- Quality of fibre

4.1 PATENT EP0293590 B1 [14]

The machine described in Patent EP0293590 B1 is shown in *Figure 4.1*, where two identical modules are shown in series, with the possibility of extending it by adding other modules.

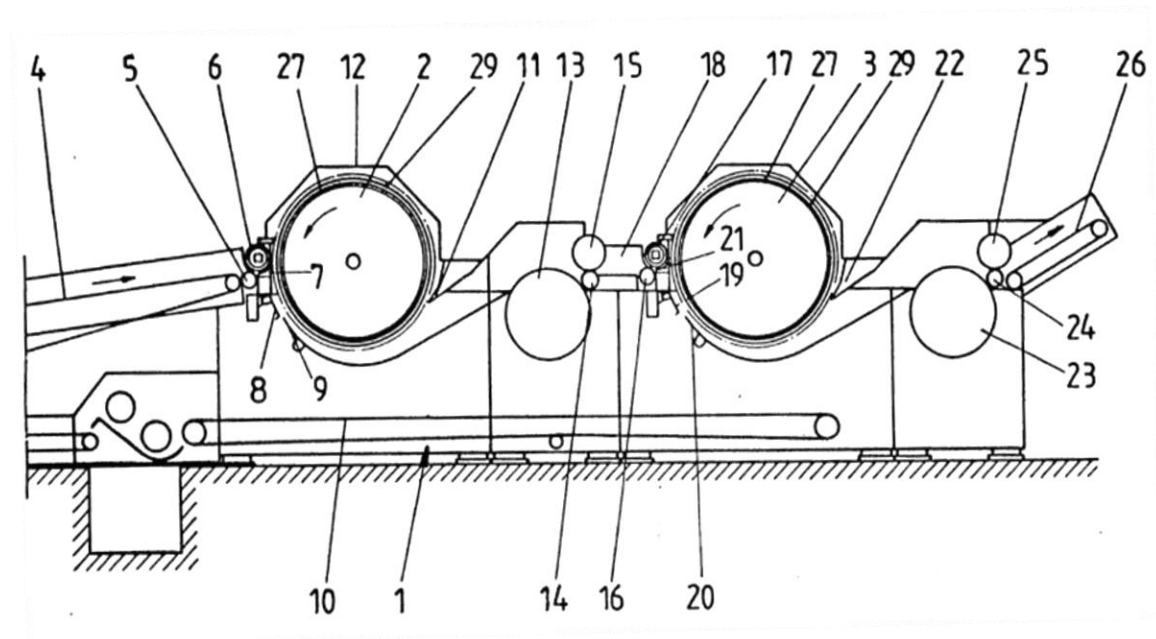


Figure 4.1: Shredding machine Patent EP0293590 B1

The shredder consists of a feeding belt (4) that rotates in the direction of the arrow, at the height of this last one there is a roller (5) that transports the material to be torn in meal to roller 2, in front of this there is a rubber roller (6). The material passes through a cavity (7) and comes into contact with the tearing roller (2), which has sharp pins on the surface inclined 20° with respect to the horizontal in the direction of rotation, indicated by the arrow in the drawing. Once torn, the material passes through the thickness between the

knife (9) and the roller (2). A rotating plate (8), allows to drop the unbroken fabric on a belt (10) that brings it back to the feeding area of the machine. Diametrically opposite the rubber roller (6) there is a scraper (11) whose task is to prevent the torn material from continuing to rotate with the roller (2). Through a perforated roller (13), where a slight underpressure is applied, the torn material is brought into contact with the transport roller (14) where, in combination with a pressure roller (15) placed above it, it represents the passage gap of the torn material. The cycle is repeated, with the torn material continuing through a channel (18) that connects the rollers (14) and (15) with the rollers (16) and (17) that perform the same task as the rollers (5) and (6). The conveyor belt (10) is also present under the roller (3) to allow the material not completely torn to be recovered and returned to the feeding area. At the end of the cycle, the torn material is conveyed by a downstream discharge conveyor (26) which rotates in the direction indicated by the arrow.

Figure 4.2 shows the detail of a roller used to tear the fabric. The tearing pins (28) are held in place by laminated hardwood support strips (29), which are displaced around the drum surface. To accommodate the tearing pins (28), each wooden strip (29) has mounting holes (30) arranged as shown in the Figure 4.2.

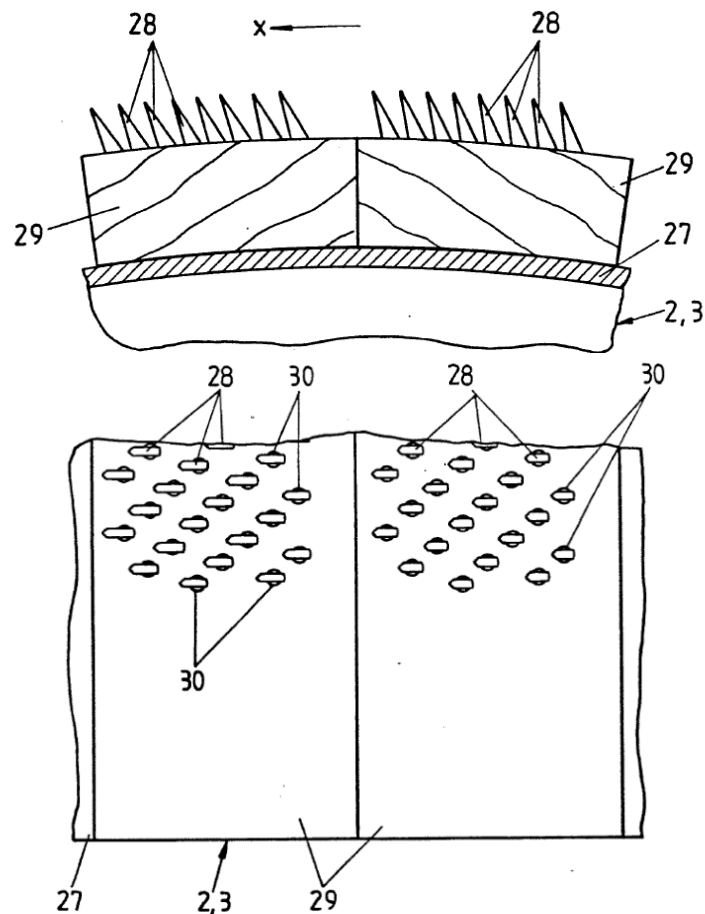


Figure 4.2: Pins on the wooden strip

Each mounting hole (30) runs at an angle to the radial drum R so that the top end of the hole faces the direction of rotation of the drum indicated by X in Figure 4.2.

The performance estimated by the author of the patent is about three times higher than that of comparable shredders. This leads to the possibility of increasing the feed rate of the feed rollers without reducing the quality of dissolution of the fibres. The pins have a rounded tip at the lower end, which is fixed to the drum, and a sharpened part. They are characterized by a flat shape (sword-shaped) that allows a shorter length of the fiber compared to the known tearing rollers used, a schematic drawing is shown in *Figure 4.3*.

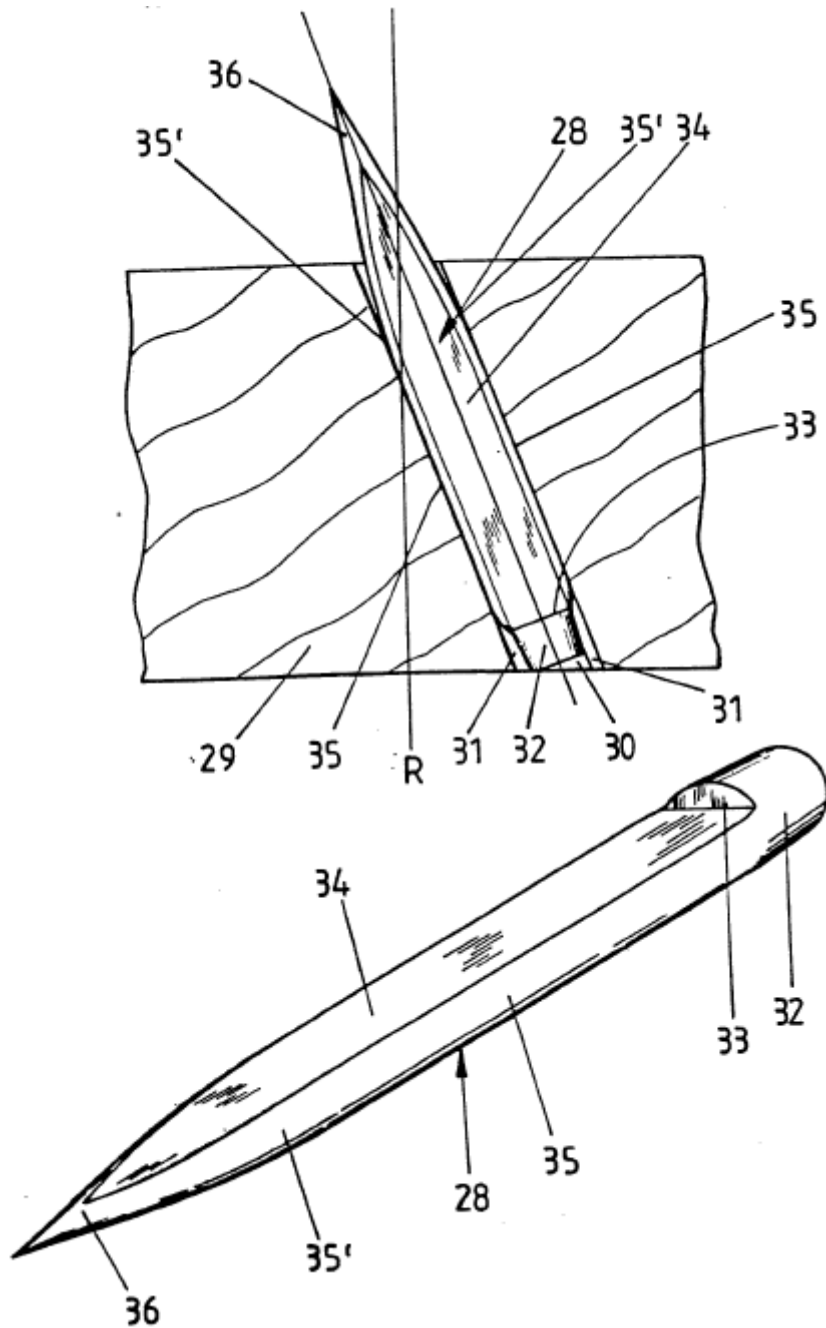


Figure 4.3: Detail of pins

4.2 PATENT US6061876 [15]

The machine described in Patent US6061876 is presented in schematic form in *Figure 4.4*. The present invention includes a machine to recycle fabrics and nonwovens, carpets, upholstery, clothing and other textile products and to produce usable and open fibers that can be used in conventional textile equipment downstream to produce new textile articles. The machine includes a suction conveyor that allows to feed, a series of shredding rollers with the textile material to be recycled. Alternatively, if the material to be recycled is a roll, a roll support system can be used so that the material can be fed into the machine directly from the roll.

The machine has an inlet (12) on one side and an outlet (13) on the other side, from where the fabric emerges in the form of fiber.

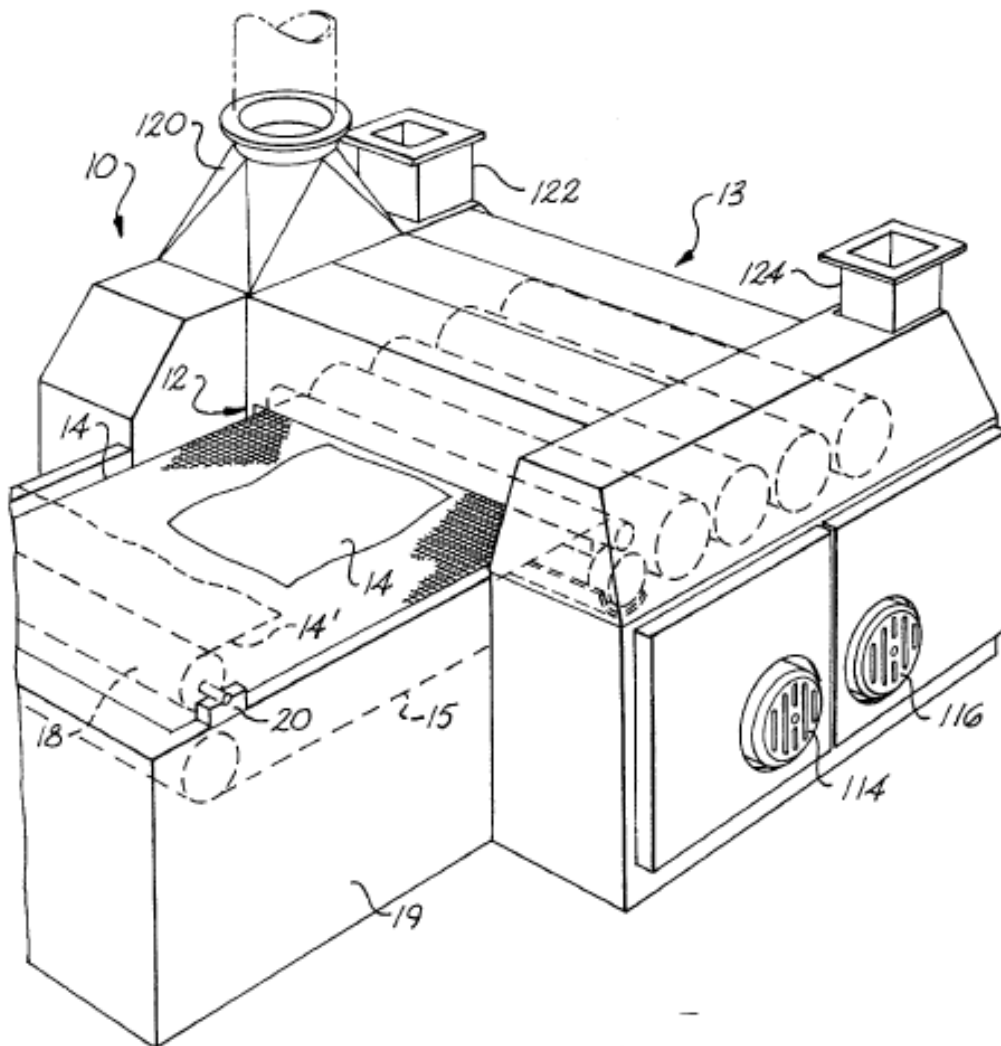


Figure 4.4: Shredding machine Patent US6061876

The machine is fed either by pieces of material (14) deposited automatically or manually on the conveyor belt (15), or if the material (14') to be recycled is in the form of a roll,

this can be fed to the machine directly through the use of an input support (19) and bearing elements (20) connected to the support itself.

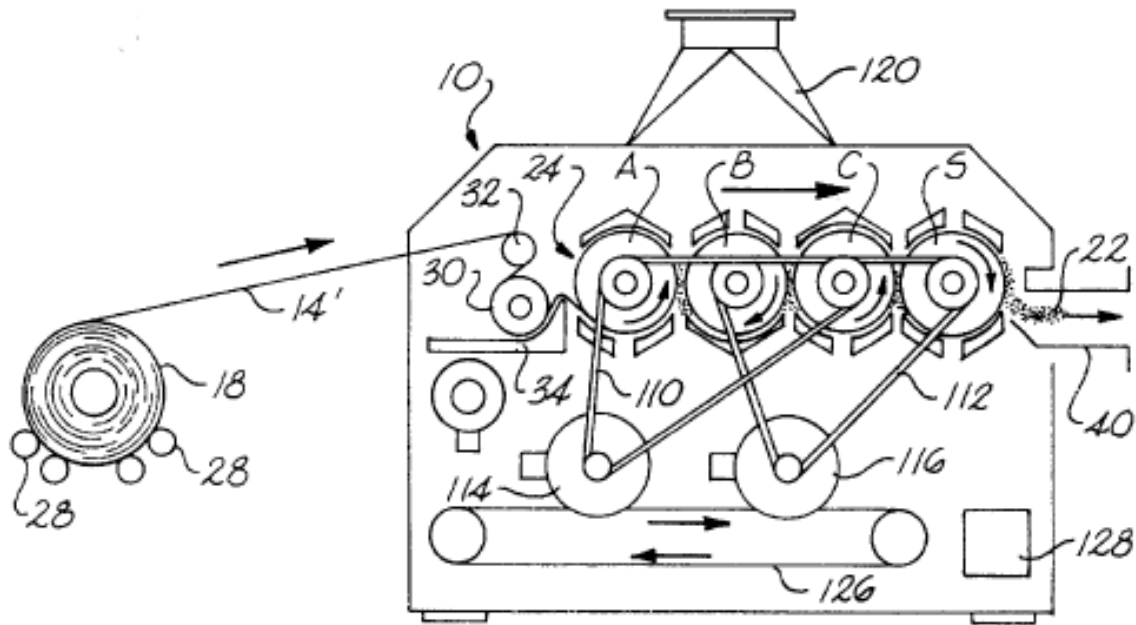


Figure 4.5: Internal parts of shredding machine Patent US6061876

Figure 4.5 shows significant internal parts of the machine, with the material passing through 4 rollers in the form of fabrics (14') and coming out in the form of fibre (22). The machine is preferably composed of four rollers (A, B, C, S) which are clothed with a conventional wire clothing, explained better after.

Obviously, the quality of the final product depends on the number of rollers from which the machine is composed. The rollers are equipped with granular surfaces, such as sandpaper.

In particular, Figure 5.5 shows the machine fed through the material (14') which is in the form of a roll, this is possible through the use of a support (18) and support rollers (28) which are not fed but run passively in response to the load of material recalled by the machine. Alternatively, the latter could be set in motion as an aid to the roller (30). The continuous feeding of the material in the machine is obtained through the rotation of the roller (30) and the roller (A). The material pass on the suction roller (32) and under the roller (30) before taken to fed to the roll (A).

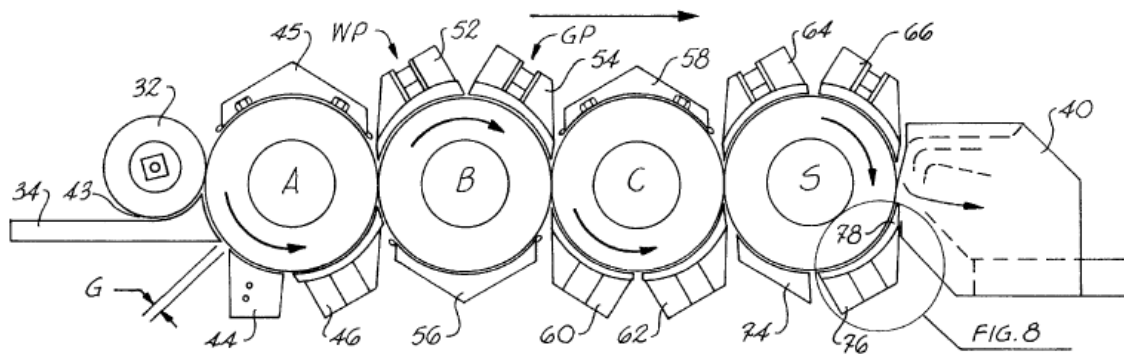


Figure 4.6: Particular of roll inside the machine

Figure 4.6 shows the arrangement of the rollers (A, B, C, S) and their cooperating plates. The material enters the channel (43) between the feeding plate (34) and the roller (32). The roller (A) transports the material (14) beyond the feeding plate (34). An adjustable plate (44) allows the removal of varying amounts of product, trash and/or material debris (14), by adjusting a gap (G) between the plate (44) and the feed plate (34). Smooth plates (45, 46) are formed by concave surfaces which cooperate with the roller surface, thus allowing the material to be in contact with the roller (A).

After passing through the roller (A), the fibre passes through the roller (B), which has a carding plate (52) normally coated with metal wire and also called (WP), the interaction between the surface (52) and the roller (B) allows the opening of the material, then there is also a carding plate of the type (GP), which has a granular surface which, preferably in the form of flexible sandpaper, is used to hold the fibers against the roller (B) and to align them in order to obtain carded fibers. In the lower part there is a smooth plate (56).

Then the fibres pass below the roller (C) which has the same configuration as described for the roller (B), with the plate (60) of type WP and the plate (62) of type GP. The plate (62) can also be replaced by a WP type plate if it is needed.

Finally, the material passes over the roller (S) which has a concave plate (64) of the type WP and a subsequent plate (66) of the type GP. The fibres are then sucked in by the S roller using an air intake duct (40). A smooth carding segment (74) and an adjacent smooth segment (76) are supplied underneath the S roller, where the fibres are removed (22). The smooth segment (76) includes an air duct (78) discussed below and illustrated in detail in Figure 4.7.

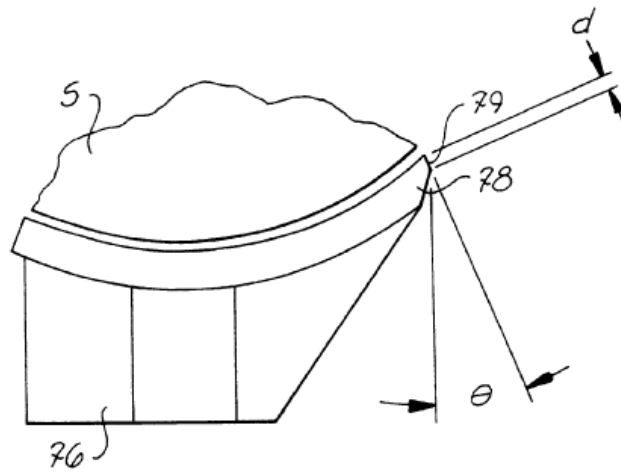


Figure 4.7: Particular of the last concave plate

As shown in *Figure 4.7*, the air channel (78) includes an inclined nose surface (79) that extends downwards at an angle of θ between 20° and 25° from the vertical, preferably 23° .

The surface (79) has a width d , which is preferably about 0.025 inches.

Figure 4.8 shows a typical WP coated wire plate, as one of the plates (52,60 etc.), is formed by a concave surface (80) coated with metal tips (82).

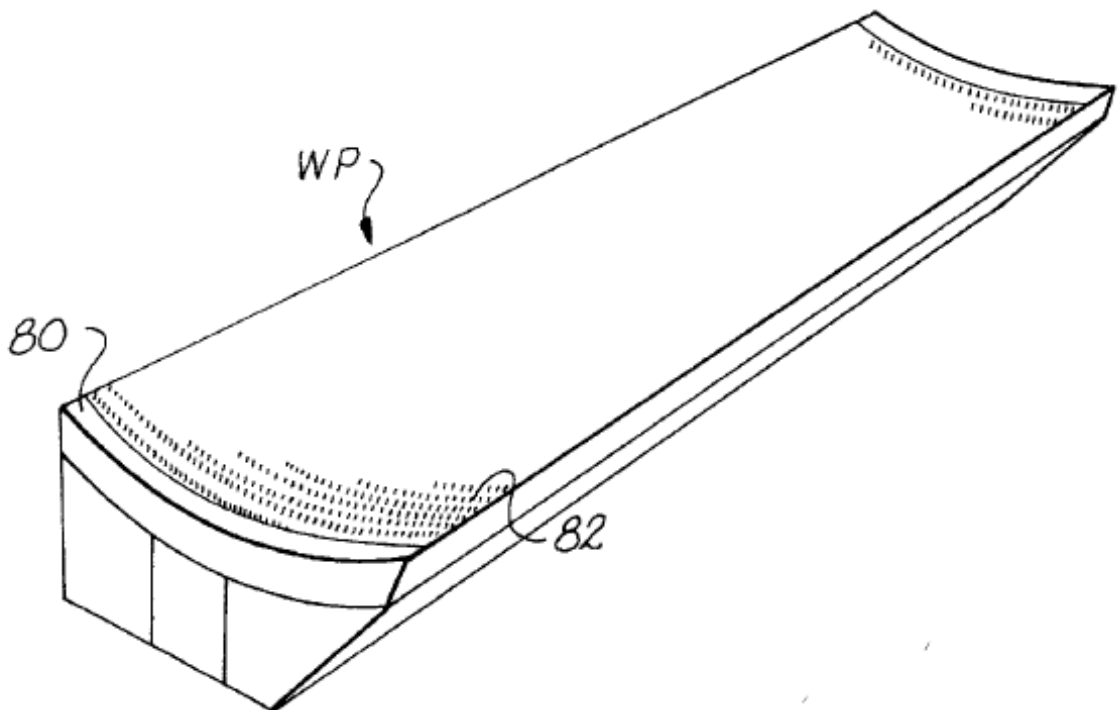


Figure 4.8: WP coated wire plate

An example of the coating is shown in *Figure 4.9*. *Figure 4.10* shows the optimal configuration of the plate, with the wire coating that has an inclination of one angle with respect to the vertical. α equal to 5° .

The roller coating also has an optimal configuration characterized by an angle of inclination to the vertical. β equal to $1-2^\circ$ placed in the opposite direction to the angle α .

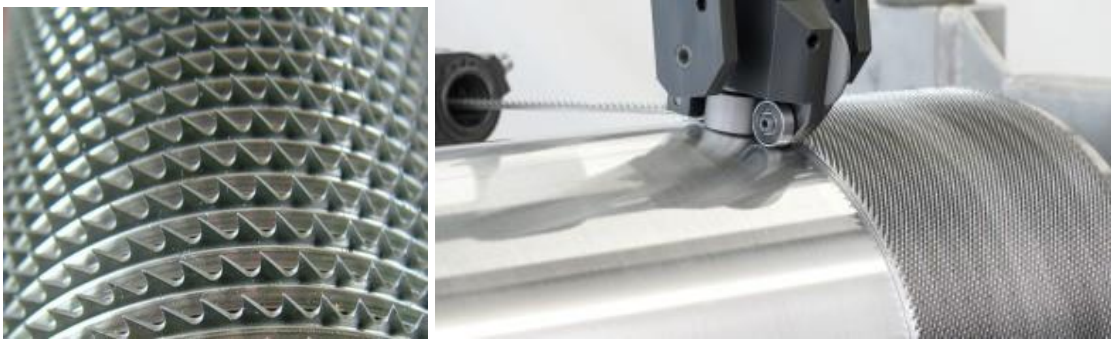


Figure 4.9: Typical Wire coating

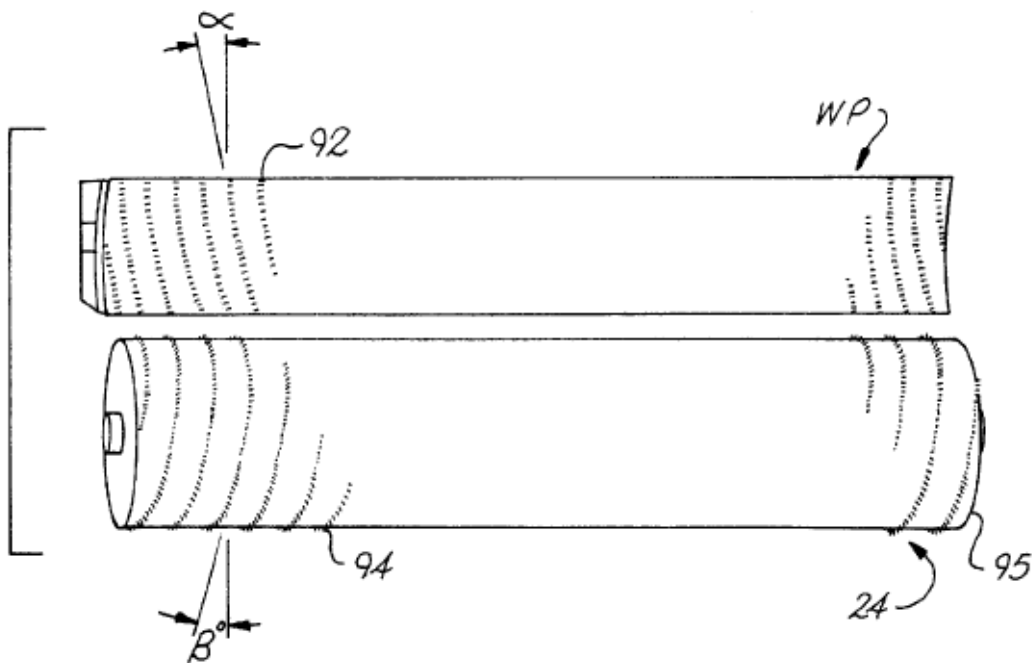


Figure 4.10: Optimum roller and plate configuration covered with wire

Figure 4.11 shows a GP carding plate, the granular coating could be sand, aluminium oxide, tungsten, or some other very hard material typically used on sandpaper and other abrasive materials. The purpose of this plate is to offer a less aggressive carding interface.

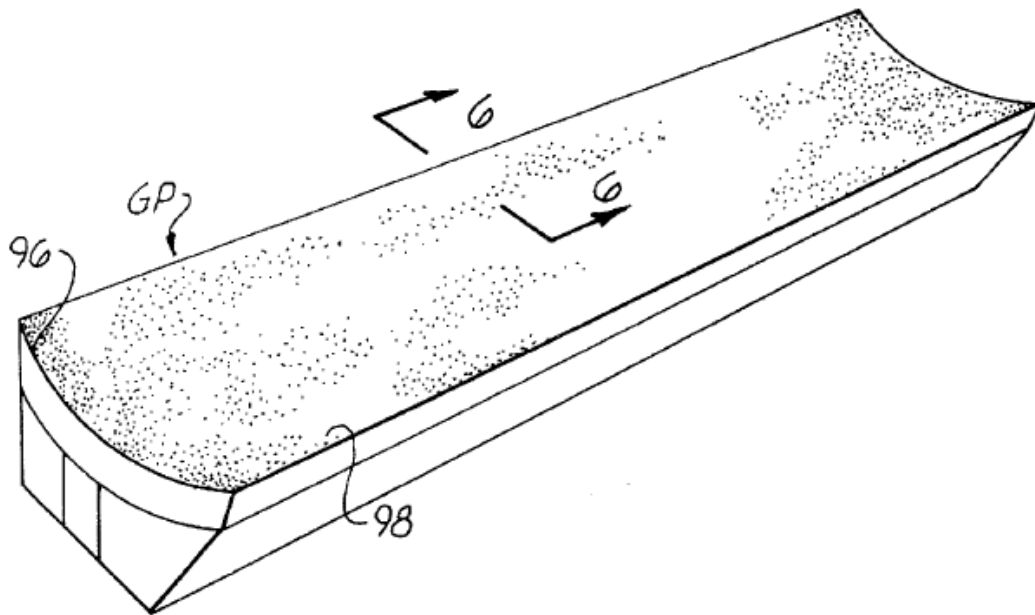


Figure 4.11: GP carding plate

Finally, the patent illustrates some technical data of the machine. It preferably includes four wire wound rollers A, B, C and S. During operation, roller A rotates with a range of 1500 to 2500 rpm, preferably at about 2000 rpm; roller B rotates in a range between 2200 and 3200 rpm, preferably at about 2700 rpm; roller C rotates between about 2900 and 3900 rpm, preferably at about 3400 rpm; and roller S rotates between 3700 and 4700 rpm, preferably at about 4200 rpm.

Conventional steel wire clothing is used on rollers A, B, C and S, with roller A having the thickest wire, and roller B and C having the thinnest wire in relation to each other, so that roller S has the finest wire of all rollers.

The wire clothing used on wire clothed carding plate WP is preferably a finer type of wire, and would generally be like the wire used on roller S. However, a variety of wire configurations could be used on WP sheets and rollers A, B, C, and S, depending on the desired results.

The rollers A and C are driven by the belt (110) that is driven by the motor (114) and the belt (112) drives rollers B and S that is driven by motor (116). The independent drive of rollers A and C and rollers B and S allows you to selectively vary the respective drive speeds of these rollers according to your needs. In general, the distances between the sheaths of the rollers A, B, C, C and S with respect to the carding plates (42) are between 0.022 and 0.040 inches.

4.3 PATENT US4484377 [16]

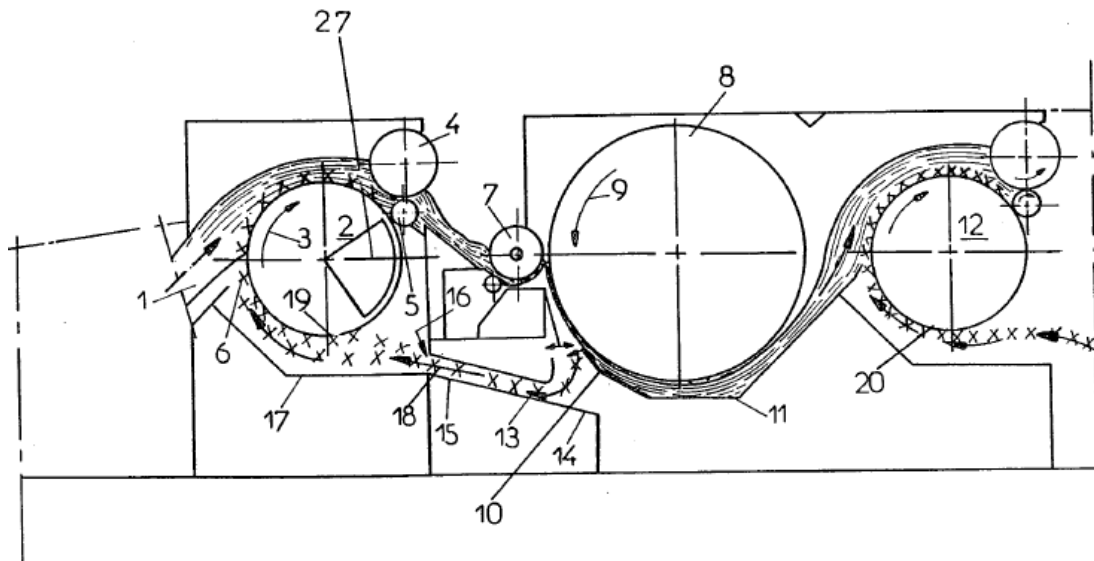


Figure 4.12: Shredding machine Patent US4484377

The machine described in Patent US4484377 is shown in *Figure 4.12*. The material to be recycled (1) is introduced into the machine and is captured by a perforated drum (2) which rotates in the direction of the arrow (3). Inside the drum (2) there is a system that allows to create a strong depression with a fan of known ventilation, not shown. This depression allows the material to be moved through the perforated drum towards two extracting rollers (4) and (5). The material that is brought towards the rollers is formed not only by material (1), but also by the material that is not totally torn (6), which through a selection system, explained later, is separated from the material now open, or torn, and returned to the starting point for further tearing. A cover (27) is placed so as to be orientable toward the interior of the drum (2). It centralizes an angle zone and favors the suction of the waste. The composed wad passes through the rollers (4) and (5) after which it is sent to a feeding system (7). The latter carries the material in contact with the tearing roller (8) represented by a roller characterized by a surface that has metal tips useful to tear the fabric. The cylinder (8) rotates in the direction of the arrow (9). Due to the centrifugal force, the tearing roller transports the defibrated material outgoing to a separation system (10) of a known type, thanks to a predetermined adjustment, makes a selection between the material that is sufficiently teared (11) and that which is not (13). The material (11) is then sucked in by a following perforated drum (12), which has a lower vacuum force than the first one, located downstream of the tearing roller. Depending on the degree of tearing, the machine can be equipped with several steps, which work with the same principle described above.

The material (13) after the selection made by the device (10) falls into the container (14) and is then sucked through the channel (15) by the vacuum force developed in the chamber (17) by the perforated drum (2). Then the material (13) comes into contact with the perforated drum (2) at the bottom of the drum and mixed with the material (1). The container (14) could also be used to eliminate, thanks to the centrifugal force effect, heavy materials (pieces of wood, metal) that are present in the recycled textile waste so as to avoid damage to the tearing roller.

4.4 Classification of the machines

As it was already said, now we can classify the machines described above. The first step is the classification of the number of the rotation parts, the classification for rotating parts is done because more rotating parts also imply a higher probability of machine broke in the future.

4.4.1 Rotation part

The *patent EP0293590 B1* is made by four auxiliary rollers, two to feed the tearing roll (5), (6) of which the second was a rubber roll without motorization and the other two (14), (15) downstream. The tearing roll is covered by a perforate wood clothing and steel pins, in addition there is a perforated roller (13) from which a depression is applied to transport the teared material from the roller to the next roller or the exit of the machine.

The *patent US6061876* is made by, if is considered only the first step, three rollers, the first one (34) is an auxiliary roll to feed the other two rollers that are tearing rollers. These rollers are clothed by wire clothing.

The *patent US4484337* is made by seven rollers, of which (3) and (12) are perforated drums, (4), (5), (7) are auxiliary rollers to feed the last roll (8) that is a tearing roll with steal pins on the surface.

As can be seen from this first classification, *US6061876* patent is made up of less rotating parts, but considering that at least two of these are tearing, they are subjected to greater stress than rollers that perform an auxiliary function, which means a greater probability of failure over time. Regarding the other two patents, both have drums with holes from which a depression is applied, in particular for the *patent US4484377* at least two drums are necessary, one at the inlet and the other at the outlet. This is not the case with *patent EP0293590 B1* where the perforated drum is present only downstream of the tearing drum. Having to make a choice considering this parameter, it falls under *patent EP0293590 B1*.

4.4.2 Machine maintenance

As a second parameter, we tried to suppose which of the patents needed more ordinary maintenance, that means evaluating everything that needs to be done so that the machine always works at maximum performance, which implies obtaining the same results over time.

This parameter is clearly conditioned by the number of moving parts which, during operation, wear out their bearings, for example, which means that more moving parts also lead to more routine maintenance.

It was decided to avoid the wear of the tearing roller tips due to the tearing of the textile fabric, as the material to be lacerated should not cause significant wear.

The type of actuation used in the different machines was also considered, considering belt or chain drives, which are less expensive than a drive with gears and easier to maintain.

The patent US6061876 from patent needs at least two motors to be able to vary the ratio between the speed of the first roller and that of the second roller in a non-proportional way, this therefore means the need for maintenance of at least two electric motors, the motion is transmitted to the various components mainly through belt transmissions as already mentioned before. At the end of the process, it presents an aeration system useful to remove the lacerated material from the last tearing roller and to transport it towards the exit of the machine, which also presents various problems and requires careful maintenance.

For the other two patents the number of motors required is not specified, but from the functioning of the machines it is possible to make them work also with a single motor, using belt or chain drives also in this case.

These two patents, however, present some stages in depression, therefore it is needed to carry out a maintenance of the systems that allow this.

All three machines have a system that allows the reintroduction of the material that, due to a lack of tearing, is discarded, in particular the first two patents provide for the use of a dedicated system, consisting of a conveyor belt placed under the tearing rollers, instead, as regards the last patent, the material is recovered thanks to the depression generated by the perforated drum upstream of the tearing roller, this means the lack of further components that must be taken into account with regard to the ordinary maintenance of the machine.

In addition, patent EP0293590 B1 has a motorized conveyor belt both at the infeed and outfeed for transporting the material, which also implies greater machine maintenance in this case.

4.4.3 Ease of manufacture

The third parameters is the ease of manufacture, there are not many information about this argument in the patent, so it was very difficult to classified the machine by this parameter.

It is possible to say that all the patents have the same difficulty or cost approximately. So, at the end this is not considered as an influent parameter.

4.4.4 Quality of fibres

The quality of the fibres at the end of the process depend from the number of steps, feed rate, rotation speed of the drum. So it is not possible to classified at the most this machine by this parameter.

5 Machine analysis and operation

This section describes the prototype of the designed machine and explains how it works. The prototype in *Figure 5.1* represents a tearing machine, which through the main roller, which has metal pins, allows the tearing of the fiber introduced thanks to the motion of the two smaller auxiliary rollers. The auxiliary rollers, in addition to having the task of introducing the fibre to be recycled into the machine, regulate the flow of incoming material, making it resistant to the advance movement of the fabric that meets the tearing roller. The speed of the main roller is much greater than the speed of the auxiliary rollers, this difference in speed is that which allows the tearing of the textile waste.

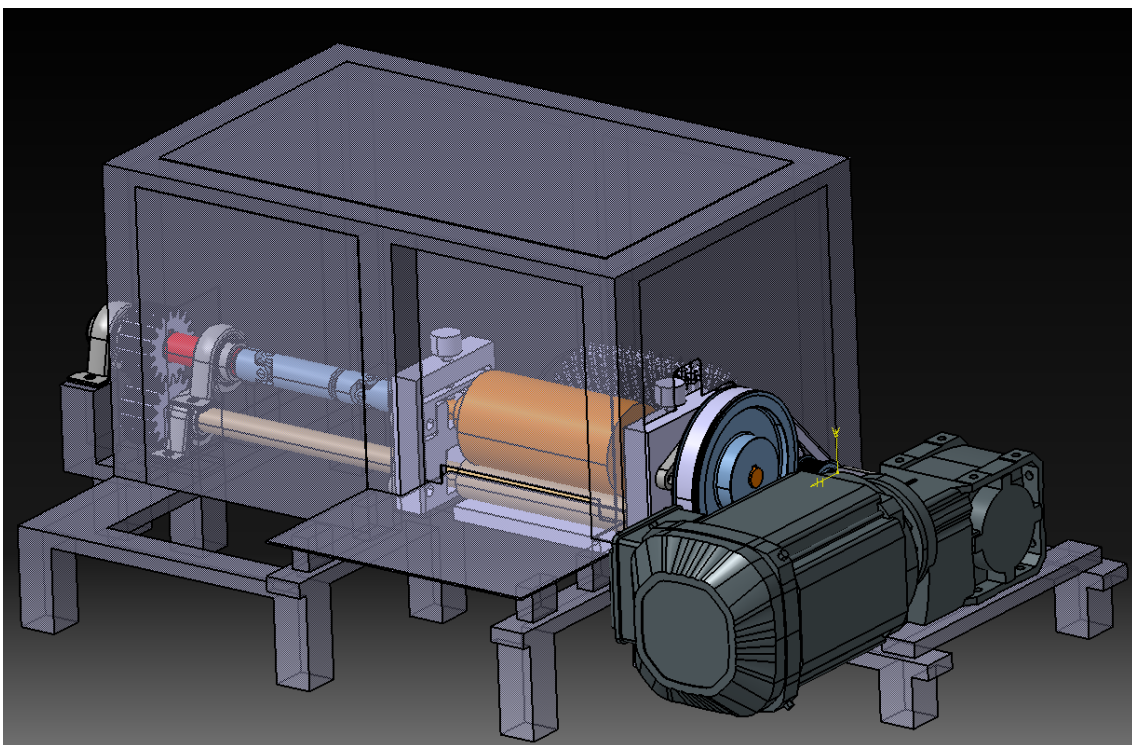


Figure 5.1: Prototype drawing

5.1 Machine description

In the front part of the machine there is a component (1) which in this case, as you can see in *Figure 5.2*, is fixed, but which could be represented by a conveyor belt, which is used to support and transport the material to be recycled.

Referring to *Figure 5.2*, it is possible to identify the two auxiliary shafts, the upper shaft (3), that can be moved, is supported by two flanged supports (6), that host the bearings that allow the shaft to rotate.

In order to allow the shaft to vary its vertical position, and therefore the gap between the rollers, the supports are anchored to the structure (4) by using components (5) that can slide in the slots in the structure (4) that represent linear guides.

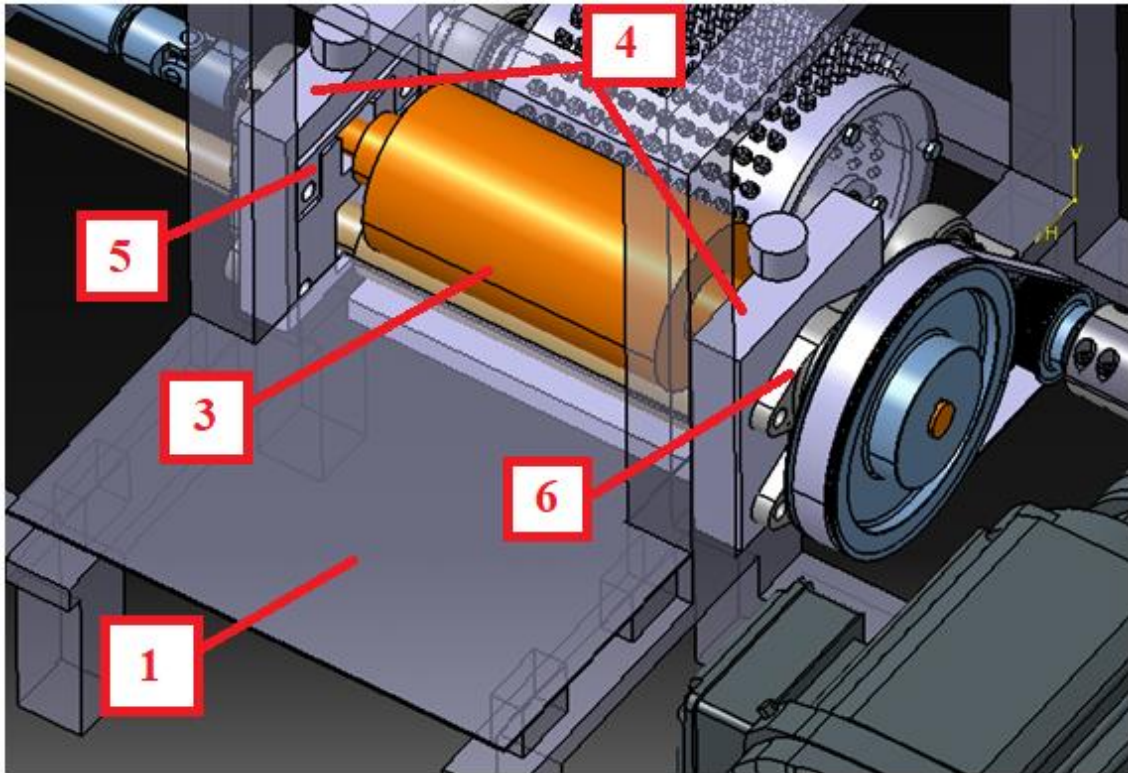


Figure 5.2: Zoom to the prototype drawing

Referring to *Figure 5.3*, the second auxiliary shaft (2) is also supported by three flanged supports (8), which host the bearings inside them. This last shaft, differently from the first one, is fixed to the structure at a certain position that cannot be changed. Connected by a double extendable cardan joint (7) is the third auxiliary shaft (10), which has also mounted a gear (11) that engages with the gear (11) mounted on the second auxiliary shaft (2) thus allowing the transmission of motion with reverse direction of rotation between the auxiliary shaft (3) and the (2). The latter is supported by two supports (9), which contain inside them the bearings that allow the shaft to rotate.

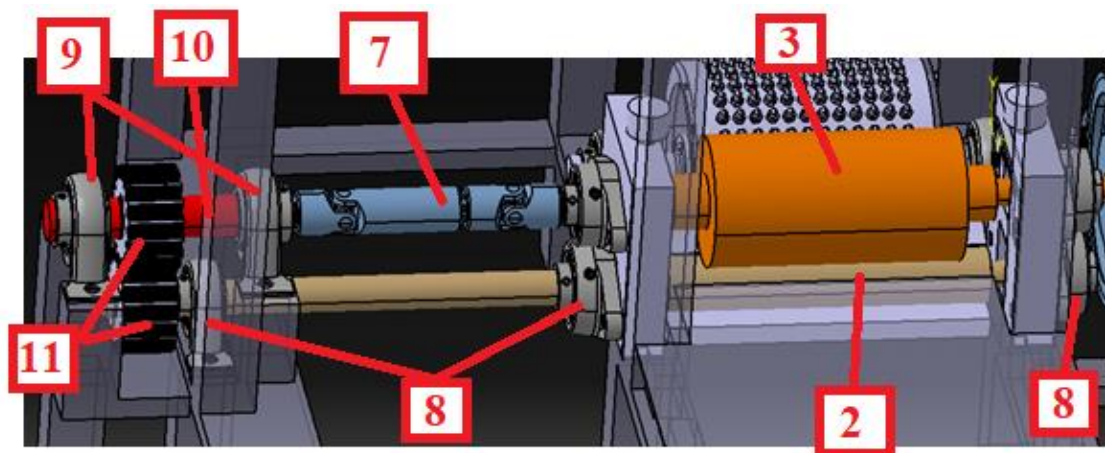


Figure 5.3: Zoom to the prototype drawing

Follow with the description, the machine has a perforated main roller, shown in *Figure 5.4*, which has 12 threaded holes, with a diameter of 5 mm, for each line arranged at a distance of 12 mm from each other. There are 36 rows on the roller, for a total of 432 holes. Another possible solution is to fix on the main roller, by screws, a plate with pins so as to make fewer holes on the main roller and facilitate the assembly.

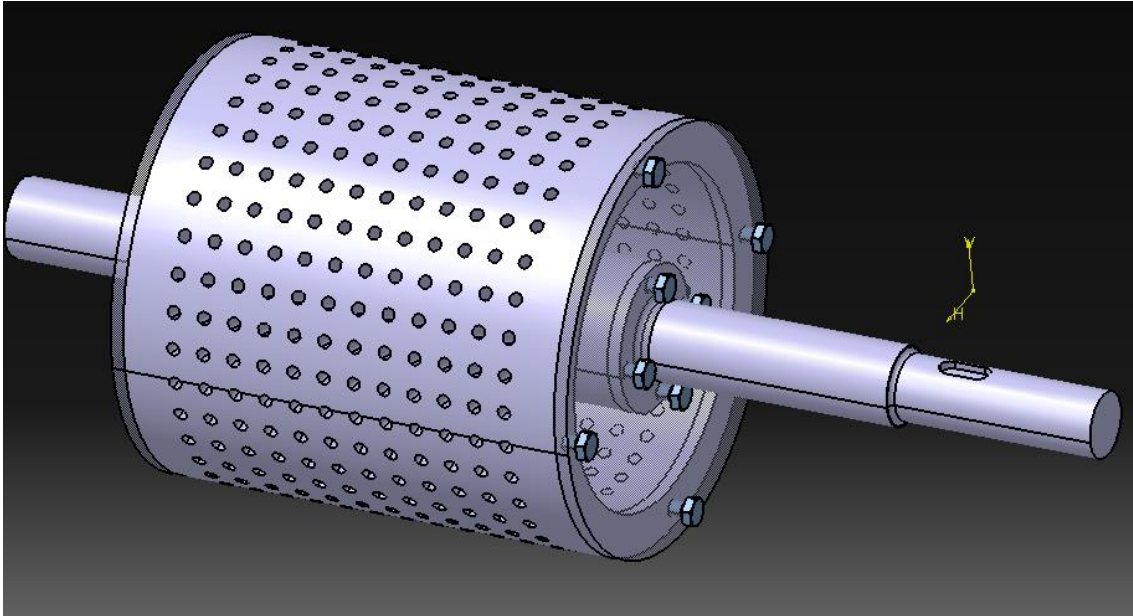


Figure 5.4: Main shaft

Each hole can be equipped with metal pins (*Figure 5.5*), the latter are threaded on one side, to allow them to be fixed on the main roller. The other part is formed by a hexagon combined with a truncated cone. The truncated cone part is the part that comes into contact with the fabric to be recycled, while the hexagonal part, on the other hand, has been designed to make it possible and convenient to fix the metal tips on the roller. Indeed, the possibility of modifying the arrangement of the pines will be, as explained below, one of the parameters taken into consideration to evaluate the result obtained.

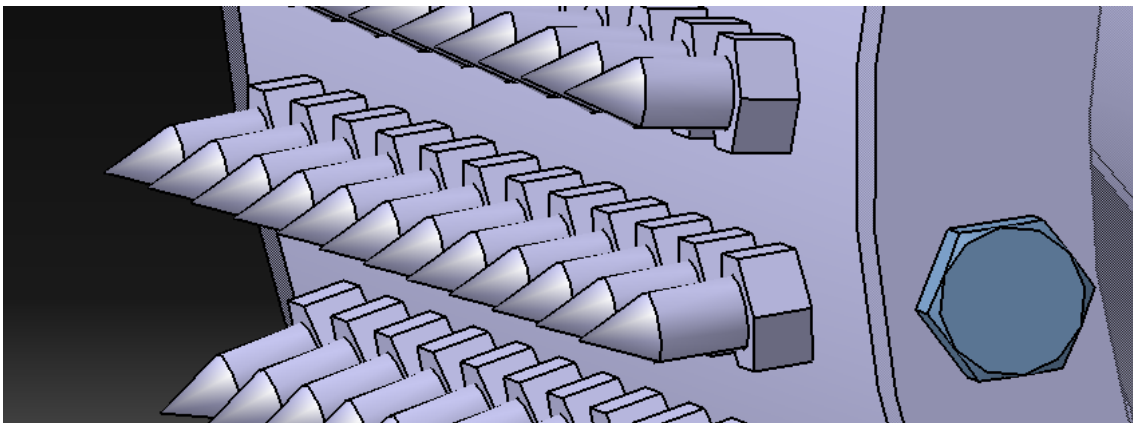


Figure 5.5: Example of pins on the main shaft

Continuing with the description, in the back part of the machine is placed the tearing roller described above, which has a joint ring (12) that allows the main shaft (13) and the hollow roller (14) to be joined. The tearing roller is mounted on two supports (15) that host inside them bearings that allow the roller to rotate. At the end of the main shaft (13) there is the toothed belt drive formed by the driving pulley (16) and the driven pulley (17) mounted on the auxiliary shaft (3). The motor (18) is then connected to the main shaft (13) by a rigid coupling, in particular a bolt coupling (19).

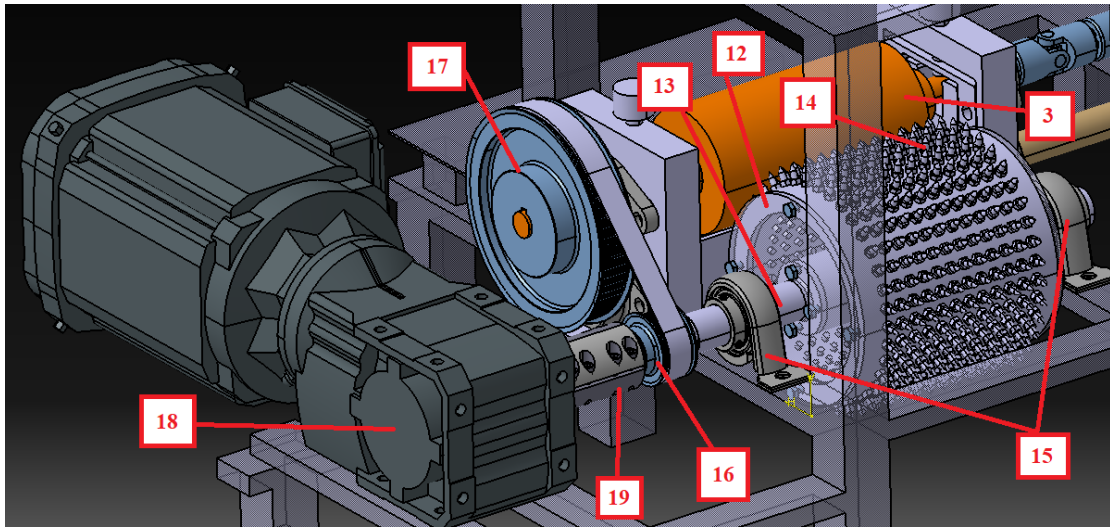


Figure 5.6: Zoom to the prototype drawing

The choice of using a hollow shaft was made to greatly reduce the weight of the structure. The machine chassis (20), in Figure 5.7, is made of commercial aluminium profiles which has three different sections, namely 40x40, 40x16 and 80x16. The characteristics of the profiles are shown in Figure 5.8, 5.9, 5.10 which take as reference the products of the company *Item*. The machine has been equipped with a safety panel (21) fixed on the chassis to prevent the torn cloth from escaping freely from the machine and to secure the work area.

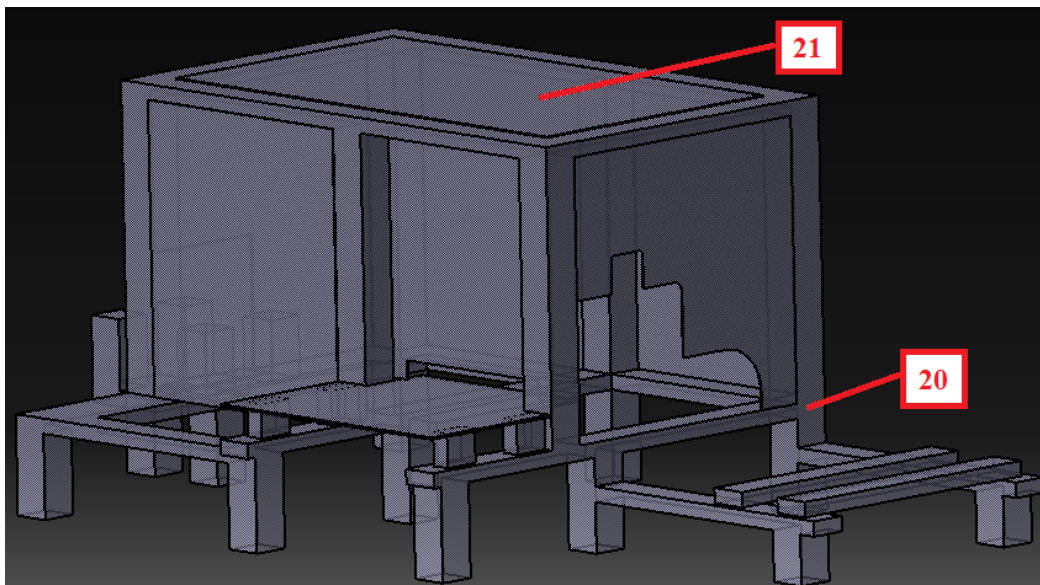


Figure 5.7: drawing of the chassis of the tearing machine

Profilato 8 40x40 3N leggero, naturale
0.0.480.26

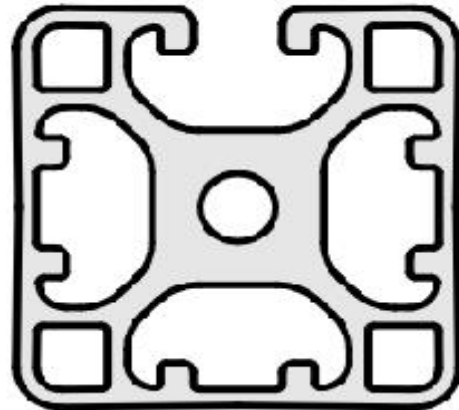


Figure 5.8: aluminium profiles 40x40

Profilato X 8 40x16 leggero, naturale
0.0.652.12

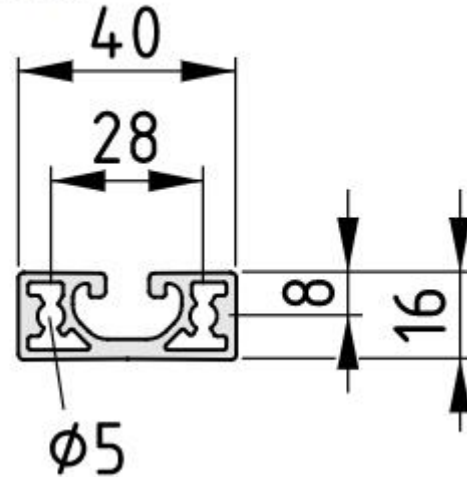


Figure 5.9: aluminium profiles 40x16

Profilato 8 80x16, naturale
0.0.364.72

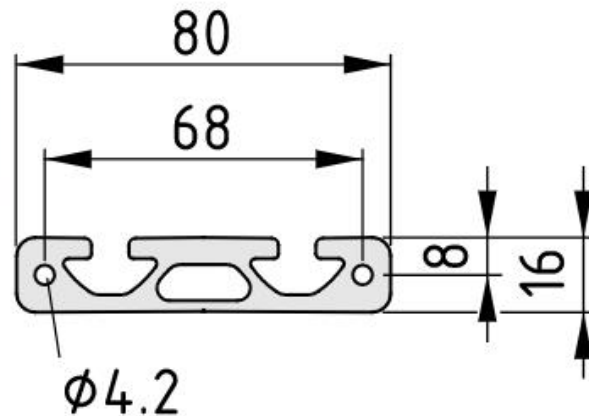


Figure 5.10: aluminium profiles 80x16

5.2 Machine operation

The machine in question works like a normal tearing machine, i.e. the main roller rotates at a certain speed and coming into contact with the fabric tears it generating new fiber that if it has appropriate characteristics, can be spun again with virgin fiber.

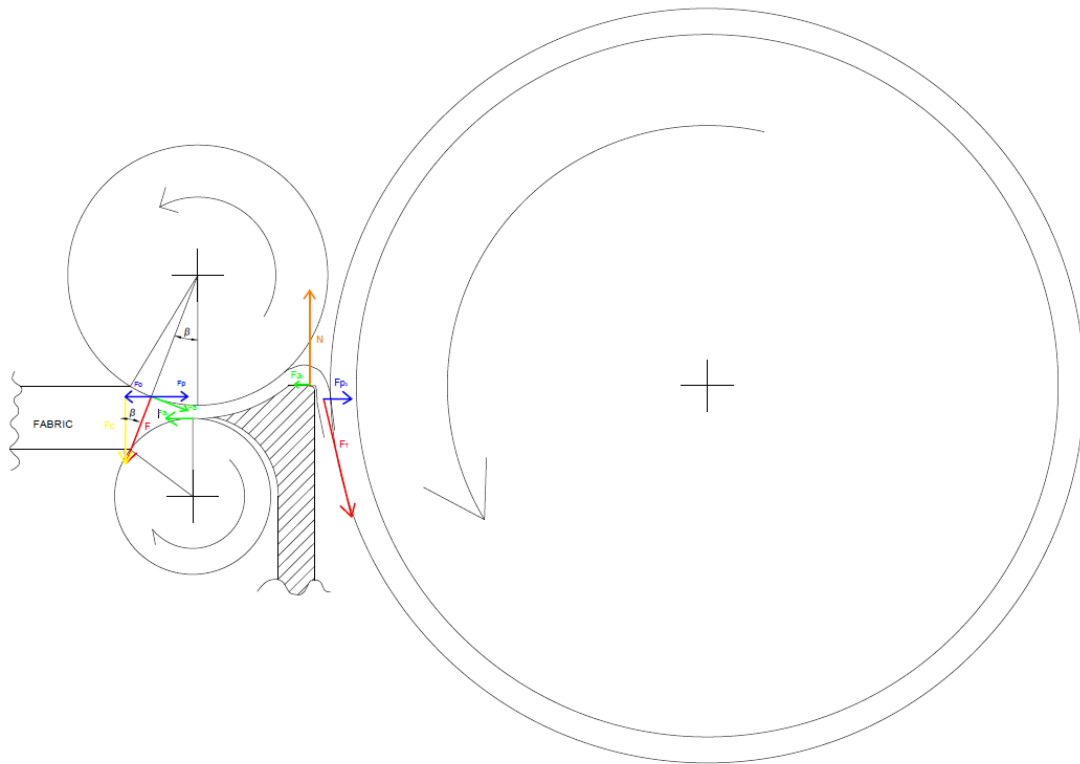


Figure 5.11: Diagram of the forces involved in the tearing process

Figure 5.11 shows in a schematic way the functioning of the machine and there is the scheme of forces acting that allow the tearing of the fabric.

Figure 5.12 shows the detailed diagram of the forces involved during the tearing process, in green there are the friction forces acting and in red the main forces, such as the tensile force of the metal pins and the force generated by the vice of the auxiliary rollers on the fabric.

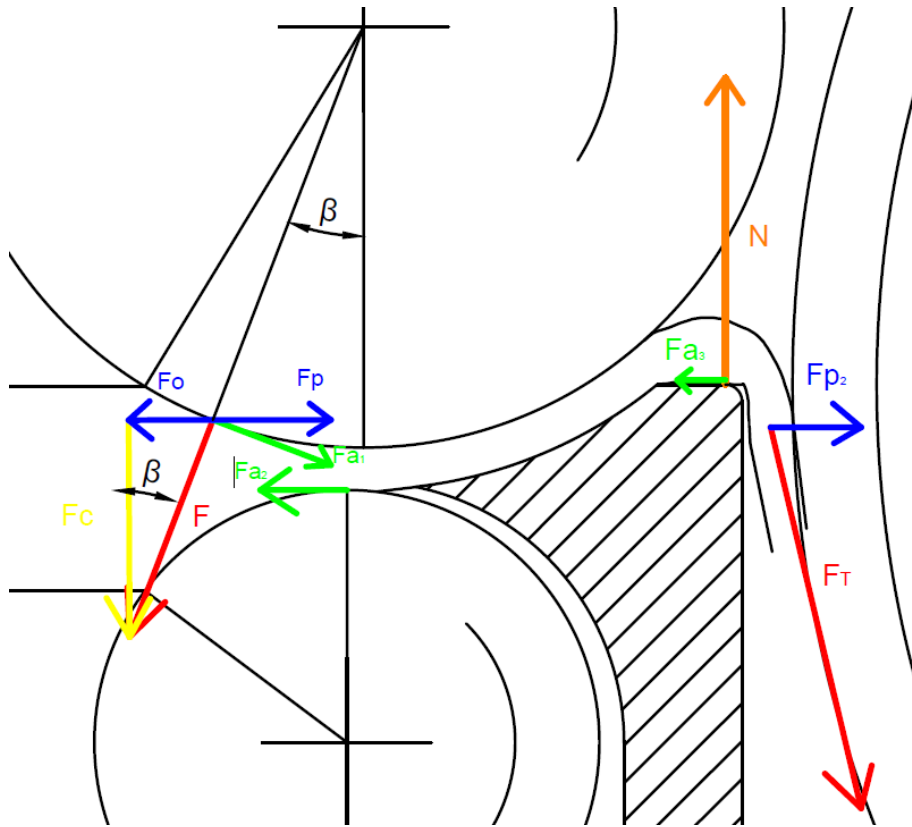


Figure 5.12: Diagram of the forces involved in the tearing process

In order to be able to enter and be fed to the main roller, the fabric must first be compressed, thus passing through a variation of section. This variation of section is permitted thanks to the discordant rotation of the two auxiliary rollers, which, rotating on the fabric, generate a friction force on it that tends to move it in the direction of motion. During the process, the force F is generated on both auxiliary rollers, which is the result of the compressive forces acting on the wire. By breaking down the force F , we obtain F_o in a horizontal direction, and F_c , which represents the compressive force. The passage of the fabric inside the gap between the two rollers is possible only if it results that:

$$F_p \geq F_o \quad (6.1)$$

Once the fabric comes into contact with the metal pins, they apply a tensile force that tends to accelerate the flow of incoming fiber. Due to the difference in speed, a frictional force is generated which tends to break the fabric and, once it has passed the tensile strength limit, it tears. In *Figure 5.12* the force F_{a2} and F_{a3} represent the friction forces generated when the fabric comes into contact with the pins of the main roller.

5.3 Use of the machine

The design of the machine aims to optimize certain parameters that can maximize the operation of a bigger tearing machine.

It is possible to resume the usefulness of the machine in three points:

1. Evaluate the real power required for the process, in order to optimize the choice of any appropriate transmissions and actuation.
2. Evaluate the influence of certain work parameters on the final product, such as:
 - Distance between the centres of the auxiliary rollers
 - Main and auxiliary roller speed
3. Evaluate the best arrangement of the metal tips, their length and possibly their shape, leading to a recycled fiber more suitable for future reuse in the textile company.

5.3.1 Evaluate the real power required

For the first point, it is useful to verify that the power needed to tear the textile waste is in line with the power chosen. Knowing the power required in a more precise way allows you to optimize the choice of transmissions and engine with which to arm a bigger tearing machine. It should be specified that the estimate of the forces involved made in this report is not precise, due to the lack of data available. In this first study, it was considered that each metal tip pulls the textile waste with the same force, i.e. a concentrated load that affects the final part of the metallic pin. In order to obtain an estimate of the forces involved, one could study, through the use of a torque meter, the actual torque to which the main roller shaft is subjected.

5.3.2 Evaluation of the influence of work parameters

This section describes the components that allow the machine to vary some of its working parameters.

- **Changing the rotation speed of the rollers**

Concerning the rotation speed of the main roller, this can be varied going to vary the transmission ratio between the motor and the shaft, the design has been made choosing the most critical condition, that is the one at lower speeds. In order to make the change of the transmission ratio economical, a belt drive was chosen.

- **Changing the distance between the auxiliary rollers**

In order to make the distance between the two auxiliary rollers variable, the upper roller has been made mobile, so it is possible to fix the structure that allows the transport of textile waste. *Figure 5.13* shows the chassis component where the auxiliary shafts are fixed through their supports.

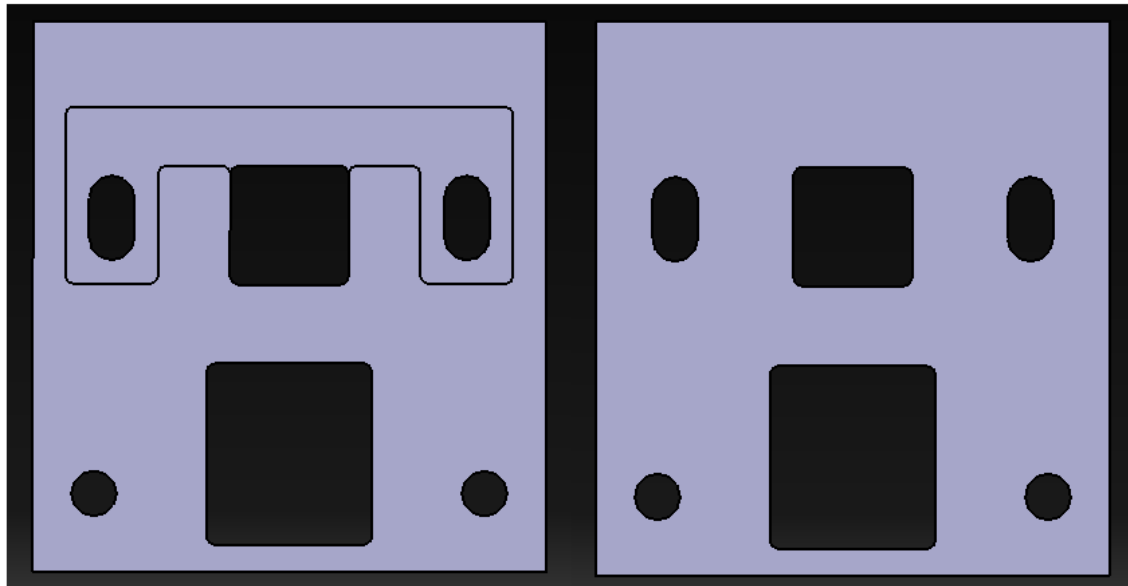


Figure 5.13: chassis elements where the auxiliary rollers are mounted

In order to allow the superior auxiliary shaft to scroll along the pocket created in the chassis in *Figure 5.13*, it was decided to fix the supports to components (23) that could scroll inside the pocket. In *Figure 5.14* is shown the detail of these components.

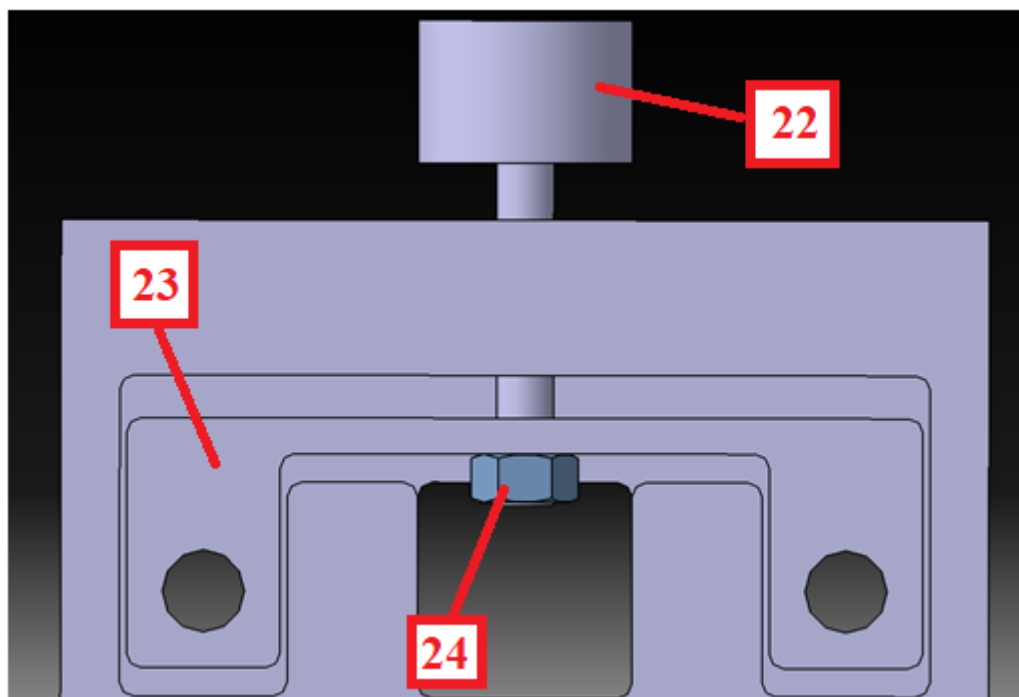


Figure 5.14: Device that allows the variation of the distance between the auxiliary rollers.

The component (22) is the one that allows to regulate the position of the auxiliary shaft. It consists of a graduated handle and a threaded stem. The stem is screwed (Figure 5.16) or unscrewed (Figure 5.17) into the chassis described above, depending on whether you want to reduce or increase the distance between the rollers, to allow the moving of the auxiliary roller along the Z axis.

The auxiliary shaft supports are connected to the component (23) by bolts, and in the same time the component (23) is connected to the stem by interference in the upper part and by a nut (24) in the lower part. This connection allows the roller not to move as a result of possible loads along the Z axis due to the passage of textile waste.

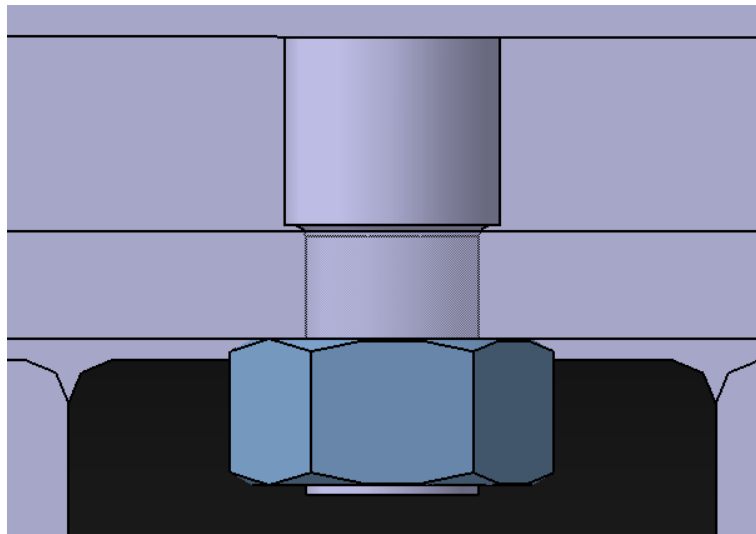


Figure 5.15: Connection between the stem and the component (23)

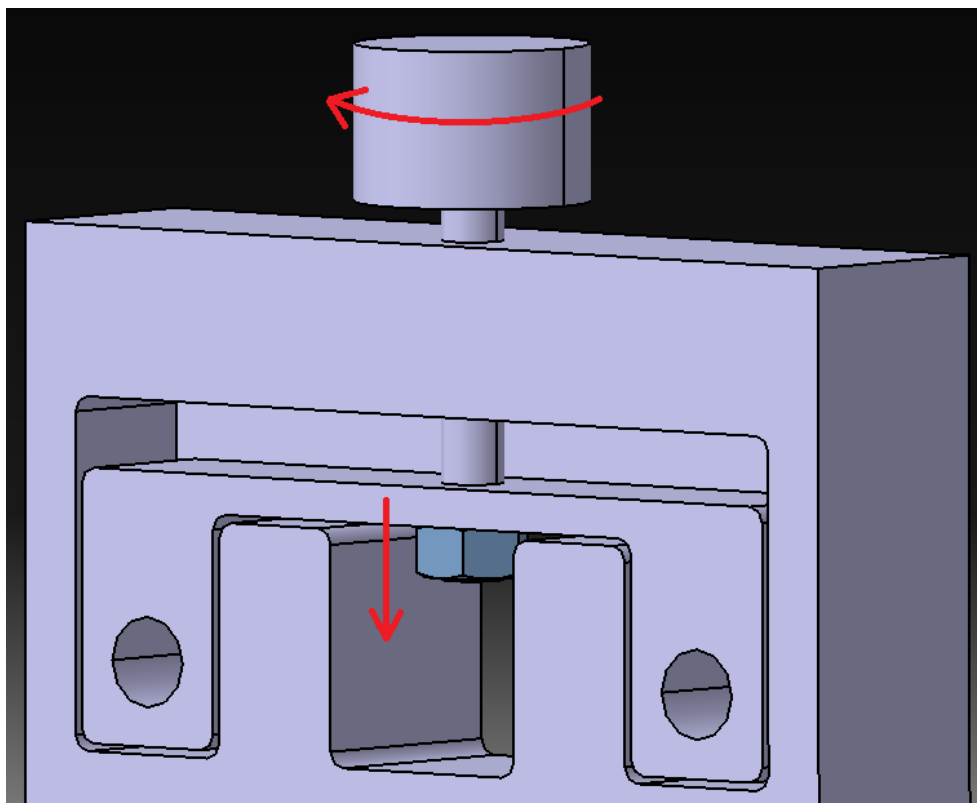


Figure 5.16: Minimum distance between centres condition

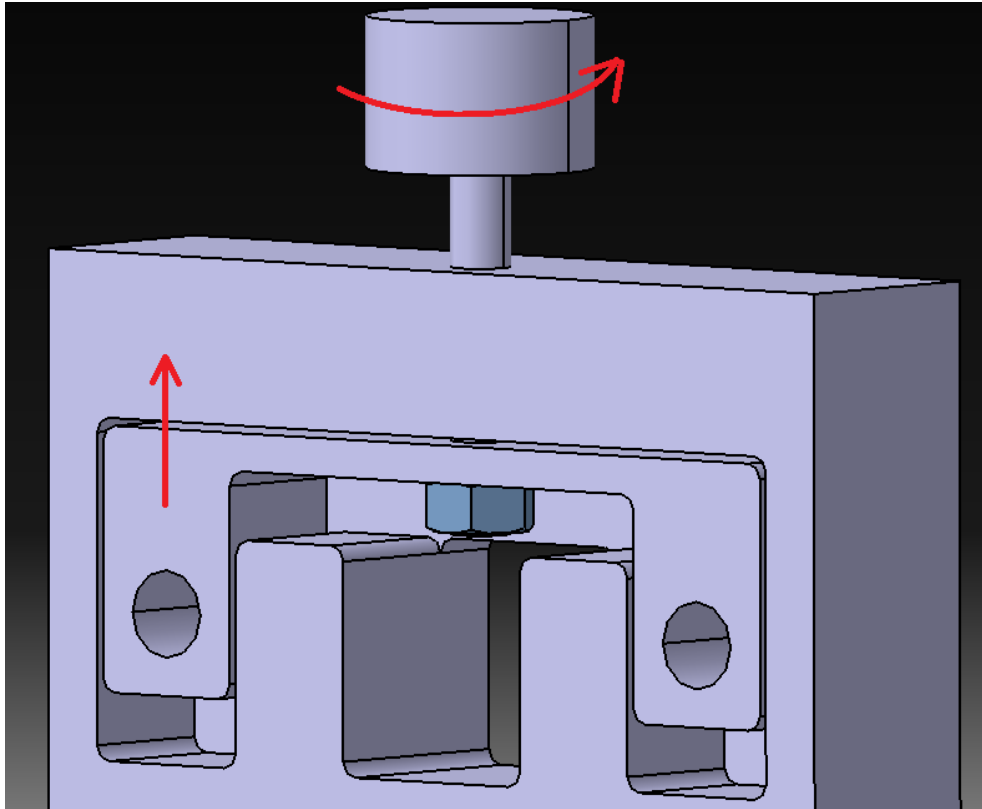


Figure 5.17: Maximum distance between centres condition

In addition, this mechanism is used to insert the toothed belt between the two pulleys. In fact, during assembly, by positioning the auxiliary roller in the position shown in *Figure 5.17*, a minimum distance is obtained between the two pulleys, which allows the belt to be easily installed. Once mounted, the auxiliary roller is returned to the starting position, i.e. where there is a distance of 0.5 mm between the two auxiliary rollers, thus tensioning the belt without the use of external belt tensioners.

5.3.3 Evaluation the location of metallic pins

One of the fundamental tests for which the machine has been designed concerns the position and the choice of the metallic pins that come into contact with the textile waste. The machine in question allows to evaluate different configurations that are shown in the figures below.

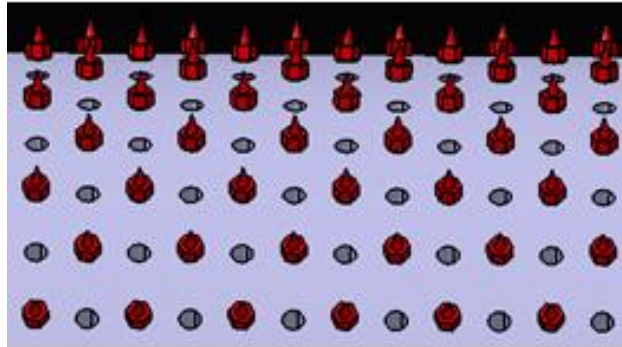


Figure 5.18: Alternate position of the pins on the main roll

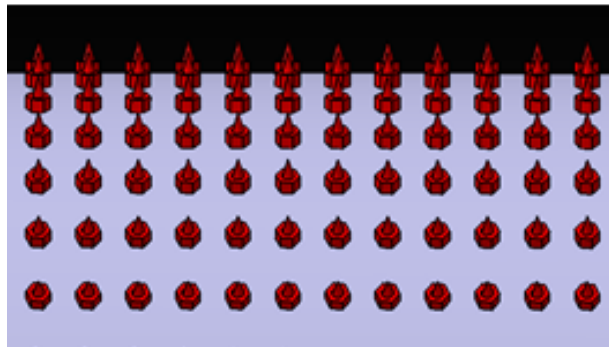


Figure 5.19: Main roll full of pins

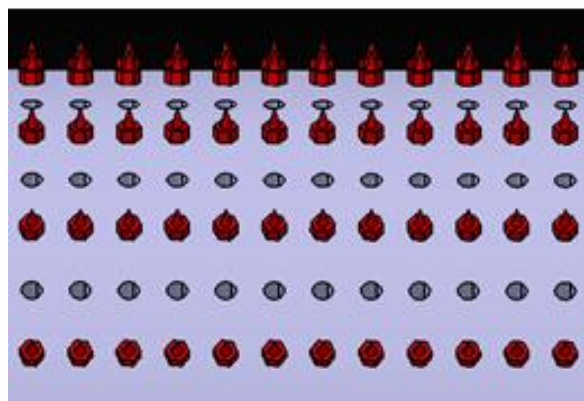


Figure 5.20: Main roll with an alternate row of pins

The *Figure 5.18* and *5.19* take in account the different position of the metallic pins and the *Figure 5.20* take in account the different distance between a metallic pin to the other. The other options to test the effect of the pins is to use different typologies of metallic pins. It was decided to test different types of metal tips that differ from each other for the surface that comes into contact with the fabric.

For example, the metal pin in *Figure 5.22* has a conical truncated shape, with a surface that hits the fabric very small. The metal pin in *Figure 5.23* instead has a larger contact surface, having the face that hits the textile waste of rectangular shape.

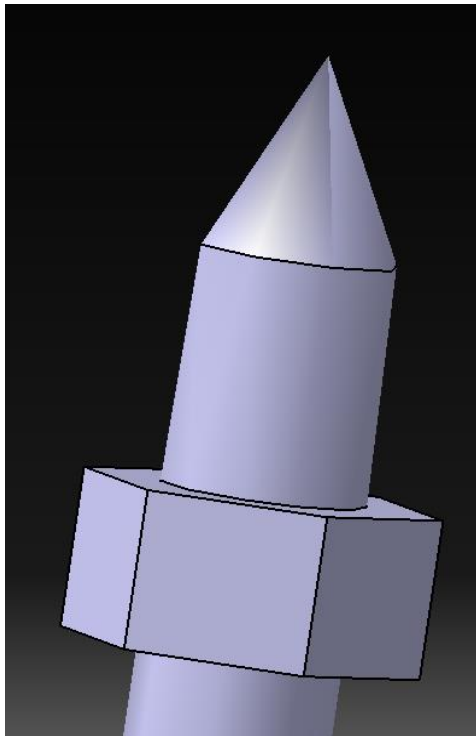


Figure 5.21: Conical truncated shape

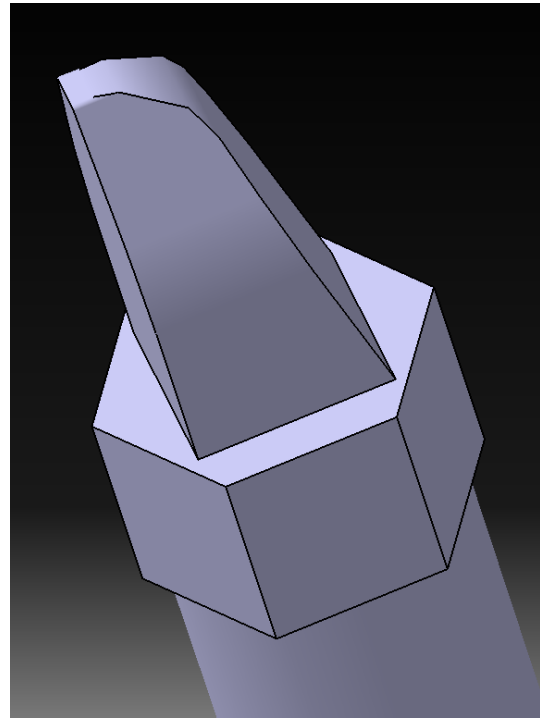


Figure 5.22: Claw shape

6 Prototype design for testing

In this chapter we will explain all the phases of design of the prototype of a tearing machine that will be used in the future to test the influence of some parameters that we considered crucial and that influence the final product or the open fiber that will be spun again.

6.1 Forces involved estimation

The prototype has a main roller that, together with two auxiliary rollers, represents the operating part of the machine, that is, the part that allows the opening of the cloth. The force required to open the fabric is exercised by the pins on the drum of the main roller. The force required to tear the fabric has been obtained through destructive tests made in the mechanical laboratory. To make it we have used this component:

- Screws
- Metal parts
- Dynamometer
- Fabric
- Wood part



Figure 6.1: Simple tool used to simulate and measure the force required to tear the cloth

In *Figure 6.1* is shown the component used to the test. The latter is composed by a screw, which simulated the metallic pin on the main roll, fixed on a wood base which, through a metal link and two screws, is rigidly connected to a metallic component which has at the other extremity a eyelet. A dynamometer (*Figure 6.2*) is connected to the component with using the eyelet. The tear force is given by the dynamometer which is pulled by the hand.



Figure 6.2: Dynamometer

Two different types of fabrics were used for the tests: a very thin (*Figure 6.3*), little worked cotton cloth and a denim cloth (*Figure 6.4*), with a more complex and resistant structure than the first one.



Figure 6.3: Thin cotton fabric



Figure 6.4: Denim fabric

The results obtained are presented in the *Table 6.1 and 6.2*. It's easy to see how the first fabric need less force to be tear than the second one, so we take into account the force needed to tear the denim fabric for ours design. Few tests have been carried out since the first ones gave the same result. It should be borne in mind that the measurement is affected by various errors due to the direction of the force, the accuracy of the naked eye reading of the graduated scale of the dynamometer during tearing, the different composition of the material that may have different predominant directions of the fibers. So that the measurement obtained is to be considered as an orientation value from which to start a first design, then during the design were used strict safety coefficients.

Thin cotton fabric	Force (N)
<i>Test 1</i>	39.3
<i>Test 2</i>	39.3
<i>Test 3</i>	29.4
<i>Test 4</i>	34.4
<i>Test 5</i>	34.4
<i>Average</i>	35.4

Table 6.1: Testing for thin cotton fabric

Denim fabric	Force (N)
<i>Test 1</i>	58.9
<i>Test 2</i>	58.9
<i>Test 3</i>	54.0
<i>Test 4</i>	58.9
<i>Test 5</i>	58.9
<i>Average</i>	57.9

Table 6.2: Testing for denim fabric

6.2 Actuation

The power required for the choice of the motor has been estimated considering the maximum torque needed to tear the fabric that comes into contact with the metallic pines of the main roller. A gearmotor with a maximum power of 1.5 kW and a maximum speed of 150 rpm was chosen. The power connection between the motor and the main roller is made by a rigid joint and through a toothed belt drive the main roller and the auxiliary roller are connected. The following sections describe in detail the solutions adopted.

6.2.1 Gearmotor

In *Figure 6.5* is shown the gearmotor chosen. It has a rated speed of 1461 rpm and an output torque of 89 Nm. It has a K-bevel gearbox which allows a reduction ratio of 9.17. The output shaft has a diameter of 25 mm and a total length of 50 mm. *Figure 6.6* shows the technical data sheet of the gearmotor.

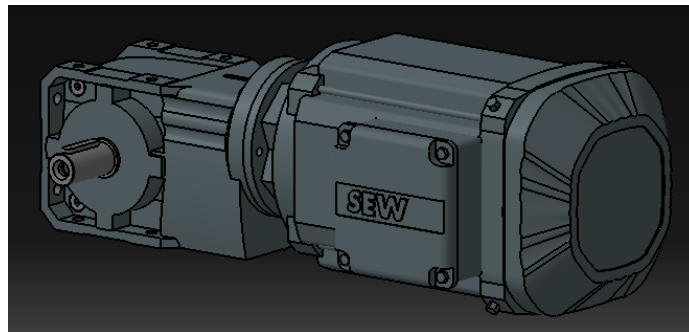


Figure 6.5: Drawing of the motor on CATIA V5

Informazione sul prodotto



Descrizione da catalogo

K29DRN90L4
Riduttori a coppia conica K + Motori trifase DRN.. (IE3)

Dati del prodotto

Velocità nominale motore	[1/min]: 1461
velocità di uscita	[1/min]: 160
Rapporto di riduzione	: 9,17
coppia di uscita	[Nm]: 89
Fattore di servizio SEW-FB	: 1,45
Forma costruttiva	: M1A
Vernice. Base/copertura	: 7031 grigio bluastro (51870310)
Posizione connettore/scatola morsetti	[°]: 0
Entrata cavi/posizione connettore	: X
Albero di uscita	[mm]: 25x50
Carico radiale di uscita ammissibile per n=1400	[N]: 2780
Quantità lubrificante 1. Riduttore	[Litro]: 0,7
Potenza motore	[kW]: 1,5
rapporto di intermittenza	: S1-100%
Classe di efficienza	: IE3
Rendimento (50/75/100% Pn)	[%]: 84,6 / 86,1 / 85,6
Marchio CE	: si
tensione del motore	[V]: 230/400
Schema di collegamento	: R13
Frequenza	[Hz]: 50
Corrente nominale	[A]: 5,9 / 3,4
Cos phi	: 0,74
Classe di isolamento	: 130(B)
Tipo di protezione motore	: IP54
requisito di progettazione	: IEC
Momento d'inerzia di massa del motore	[10 ⁻⁴ kgm ²]: 67,24
Peso netto	[Kg]: 29

Figure 6.6: Gearmotor datasheet

6.2.2 Toothed belt drive

A toothed belt drive was used to connect the central shaft to the auxiliary shafts. In fact, this type of transmission is an economic solution, which does not require maintenance, with a low load on the bearings thanks to the tension-belt content and a high efficiency. The choice was made using the guidelines of the company Sit S.p.A, which are described below.

1. Determination of design power

The design power is defined by the following equation

$$P_d = P_r \cdot KS \quad (6.1)$$

Where

- P_r is the nominal Power
- KS is a service factor chosen from the *Table 6.3*.

Punte massime Istantanee percentuale del carico	100 ÷ 150%	100 ÷ 150%	250 ÷ 400%
Motori a corrente alternata monofase			tutti
Classe del motore	I	II	III
MACCHINE CONDOTTE	MOTORE		
	classe I	classe II	classe III
Macchine tessili telai, banchi a fusi, torcitoi, orditoi bobinatrici, incannatoi, carde	1.6 1.5	1.8 1.7	2.0 ...

Table 6.3: Service factor depending on the type of motor and application

2. Determination of the transmission ratio

The size of the pulleys have been chosen considering the ratio and the recommended minimum diameter. The transmission ratio is equal to:

$$i = \frac{\omega_{in}}{\omega_{out}} = \frac{r_{out}}{r_{in}} = \frac{Z_{out}}{Z_{in}} = \frac{64}{20} = 3.2 \quad (6.2)$$

The drive formed by the toothed belt plus the two pulleys has been calculated using an online tool of the provider Sit S.p.A.

In *Figure 6.7* are shown the result obtained:

SIT S.p.A.

20090 Cusago (MI) - Italy - viale A. Volta, 2

Tel. +39 0289144.1 - Fax +39 0289144291 - 0289181293 - e-mail: info@sitspa.it - export@sitspa.it



BELT DRIVE CALCULATION

INPUT DATA		Printed on: 11/22/2019 4:09 PM	
Family	Rubber timing belts	Required Service Factor	1.8
Drive type	Two pulleys	Power [kW]	0.3
Profile	Mustang Torque	Speed [RPM]	150
Pitch	8	Torque [Nm]	19.11

BELT	
Part Number	CMT640-8M20
Belt length [mm]	640
Selected standard width [mm]	20
Minimum calculated belt width [mm]	11

PULLEYS	Driver	Driven
Part number for Solid Hub Pulley	HD20-8M20	HD64-8M20
Part Number for Taper Bored pulley	-	HDB64-8M20
Number of Teeth	20	64
Pitch diameter [mm]	50.93	162.97
Speed [RPM]	150	47
Selected standard width [mm]	20	20
Teeth in mesh	7.4	40.3
Used belt Static Load on axis [N]	903	
Used belt Dynamic Load on axis [N]	903	

DRIVE		TENSIONING		
Center distance [mm]	140.9	New belt tension [N]	689	
Belt Span length [mm]	129.2	Used belt tension [N]	492	
Gear ratio	0.31	Deflection Method	New belt	Used belt
Power rating [kW]	1.1	Deflection [mm]	2	2
Calculated Service Factor	3.8	Load [N]	46	34
Linear Speed [m/s]	0.4	Vibration Frequency Method	New belt	Used belt
Noise [dB]	-	Vibration Frequency [Hz]	352 ±2%	298 ±2%

Figure 6.7. Datasheet of the toothed belt

6.3 Shaft-hub connections

Although the connection with splined shafts allows to obtain the absolute best performance, due to the problems dictated by the higher costs and the greater difficulty in assembly, the connection with keyways was preferred.

The design is based on the choice of the length of the key. For the choice of the tongue, the UNI 6604 standard has been used (*Figure 5.64*), inserting as input parameter the diameter of the shaft considered.

- **Specific pression check**

The minimum length that is agree with the specific pression check was calculated by the equation (5.45)

$$l_{min} = \frac{4M_t}{p_{amm}^{hd}} \quad (6.3)$$

- **Shear check**

The minimum length that is agree with the shear check was calculated by the equation (5.46)

$$l_{min} = \frac{2M_t}{\tau_{amm}^{hd}} \quad (6.4)$$

The tongue length must be greater than the biggest of the minimum length.

- **Last check**

At the end, it is check that the weakest part of the connection is the tongue in relation to the shaft. This is done to ensure that the tongue fails before the shaft fails. To do this, it must be ensured that:

$$l \leq 1.5d \quad (6.5)$$

The results obtained are as follows in the *Table 6.4 and Table 6.5.*

Campo di Applicazione		Linguetta Sezione			Cava												
					Larghezza						Profondità						
Diametro Albero d		Dimens. Nominali b x h	Tolleranze su b ^h b*		Dimens. Nominale b	Tolleranze su b						Albero		Mozzo			
						Per albero			Per mozzo			t1		t2			
					H9	N9	P9	D10	Js9	P9	Nom.	Toil.	Nom.	Toil.			
da fino a	6 8	2 x 2	0	0	2	+0,025 0	0 -0,004	-0,006 -0,031	+0,060 +0,020	±0,012	-0,006 -0,031	1,2		1			
da fino a	8 10	3 x 3	-0,025	-0,025	3							1,8		1,4			
oltre fino a	10 12	4 x 4			4							2,5		1,8			
oltre fino a	12 17	5 x 5			5							3		2,3			
oltre fino a	17 22	6 x 4	-0,030	0 -0,030	6	+0,030 0	0 -0,030	-0,012 -0,042	+0,078 +0,030	±0,015	-0,012 -0,042	+0,1 0	1,8	+0,1 0	3,5		
		6 x 5			6											3	2,3
		6 x 6			6											3,5	3,5
oltre fino a	22 30	8 x 5	0 -0,036	0 -0,090	8	+0,036 0	0 -0,036	-0,015 -0,051	+0,098 +0,040	±0,018	-0,015 -0,051	3,3	3,3	+0,2 0	4,3		
		8 x 6			8											3,5	2,8
		8 x 7			8											4	3,3
		8 x 8			8											5	3,3
oltre fino a	30 38	10 x 8	0 -0,090	0 -0,090	10	+0,043 0	0 -0,043	-0,018 -0,061	+0,120 +0,050	±0,021	-0,018 -0,061	5,4	+0,2 0	5,4			
		10 x 10			10										6	4,3	
oltre fino a	38 44	12 x 8	0 -0,090	0 -0,090	12	+0,043 0	0 -0,043	-0,018 -0,061	+0,120 +0,050	±0,021	-0,018 -0,061	5,4	+0,2 0	5,4			
		12 x 12			12										7,5	4,9	
oltre fino a	44 50	14 x 9	0 -0,090	0 -0,090	14	+0,043 0	0 -0,043	-0,018 -0,061	+0,120 +0,050	±0,021	-0,018 -0,061	5,4	+0,2 0	5,4			
		14 x 14			14										9	5,4	
oltre fino a	50 58	16 x 10	0 -0,090	0 -0,090	16							6		4,3			

Figure 6.8: UNI 6604 standard for the choice of tongues.

Shaft-hub connection: <i>main shaft</i>			Shaft-hub connection: <i>auxiliary shaft</i>		
Mt	76	Nm	Mt	76	Nm
p _{amm}	110	MPa	p _{amm}	110	MPa
t ₁ (shaft)	3,5	mm	t ₁ (shaft)	3	mm
t ₂ (pulley)	2,8	mm	t ₂ (pulley)	2,3	mm
h	6	mm	h	5	mm
d	25	mm	d	20	mm
b	8	mm	b	6	mm
τ _{amm}	55	MPa	τ _{amm}	55	MPa
Specific pression check			Specific pression check		
L _{min}	18.42	mm	L _{min}	27.63	mm
Shear check			Shear check		
L _{min}	13.81	mm	L _{min}	23.03	mm
L	20	mm	L	30	mm

Table 6.4: Shaft-hub connection for the pulleys

Shaft-hub connection: <i>auxiliary shaft</i>			Shaft-hub connection: <i>auxiliary shaft</i>		
Mt	76	Nm	Mt	76	Nm
p_{amm}	110	MPa	p_{amm}	110	MPa
t_1 (shaft)	3,5	mm	t_1 (shaft)	3,5	mm
t_2 (gear)	2,8	mm	t_2 (gear)	2,8	mm
h	6	mm	h	6	mm
d	30	mm	d	25	mm
b	8	mm	b	8	mm
τ_{amm}	55	MPa	τ_{amm}	55	MPa
Specific pression check			Specific pression check		
L_{min}	15.35	mm	L_{min}	18.42	mm
Shear check			Shear check		
L_{min}	11.52	mm	L_{min}	13.81	mm
L	18	mm	L	20	mm

Table 6.5: Shaft-hub connection for the gears.

6.4 Drive joint

To connect the gearmotor to the main shaft a rigid joint was chosen, in particular a bolt coupling. This solution allow to joint easily the gearmotor to the main shaft without the using of shaft-hub. In *Figure 6.9* is shown the bolt coupling chosen.



Figure 6.9: Bolt coupling made by ComInTec.

6.5 Design: Gear drive

The gears are designed with modular proportions. This means that the teeth are from a geometric point of view, completely defined according to standard measures with respect to the module; this type of proportioning is recommended because it can ensure at least one pair of teeth always in grip and protect the wheels from interference phenomena.

6.5.1 Static Design

- Design with Lewis method

For a design calculation, in which both the module, “ m ” and the width gear b are to be determined, the following relationship is to be verified:

$$m \geq \left(\frac{2 \cdot C_{max} \cdot y_{LW}(Z_v)}{\lambda \cdot Z_1 \cdot \sigma_{adm,LW}} \right)^{\frac{1}{3}} \quad (6.6)$$

With:

- $\sigma_{adm,LW}$ permissible stress of Lewis equal to:

$$\sigma_{adm,LW} = \frac{R_{Po,2}}{SF} \quad (6.7)$$

Where SF is the security factor, equal to 1,5;

- y_{LW} is obtained from the *Table 6.6*, knowing the number of teeth and the pressure angle of the gear.

$\alpha_n = 20^\circ$			
Z, Z_v	y_{LW}	Z, Z_v	y_{LW}
12	4,08	28	2,84
13	3,83	30	2,79
14	3,62	34	2,70
15	3,46	38	2,61
16	3,39	43	2,53
17	3,31	50	2,45
18	3,25	60	2,38
19	3,18	75	2,30
20	3,13	100	2,24
21	3,06	150	2,18
22	3,03	300	2,12
24	2,98	∞	2,07
25	2,89		

Table 6.6: y_{LW} depending on Z

- **Design with Hertz method**

For a design calculation, in which both the module, “*m*” and the width gear “*b*” are to be determined, the following relationship is to be verified:

$$m \geq \left(\frac{0.418^2 \cdot 4 E C_{max} \cdot \left(1 + \frac{1}{i}\right)}{\lambda \cdot z_1^2 \cdot \sigma_{adm,HZ}^2 \cdot \cos \theta \cdot \sin \theta} \right)^{\frac{1}{3}} \quad (6.8)$$

With:

- $\sigma_{adm,HZ}$ permissible stress of Hertz equal to:

$$\sigma_{adm,HZ} = \frac{C \cdot \sigma_{Hlim}}{CS} \quad (6.9)$$

Where SF is the security factor, equal to 3;

The useful data and the results obtained are shown below:

USEFUL DATA		
Power	0,3	<i>Kw</i>
Speed	50	<i>rpm</i>
	5,24	<i>rad/s</i>
Torque	57,30	<i>Nm</i>
r	34	<i>mm</i>

GEAR DATA		
SF	1,5	-
$R_{Po,2}$	335	<i>MPa</i>
Material	<i>C 45 – UNI 7845</i>	
v	0,178	<i>m/s</i>
F_t	1685	<i>N</i>
F_r	613	<i>N</i>

Static design - Lewis test		
θ	20,0	°
	0,35	Rad
Z_{min}	17,1	-
Z_{eff}	17	-
Y_{lew}	3,31	-
m_{min}	2,15	<i>mm</i>
m_{eff}	4	<i>mm</i>
r	34	<i>mm</i>
λ	10	-
b	40	<i>mm</i>

Static design - Hertz test		
σ_{Hlim}	1030	-
SF	3	-
C	1,6	-
$\sigma_{adm,HZ}$	549	<i>MPa</i>
m_{min}	3,91	<i>mm</i>
m	4	<i>mm</i>
b	40	<i>mm</i>

6.5.2 Fatigue test: Standard ISO 6336

This section shows the procedure used to perform fatigue tests. The guideline given by the ISO 6336 standard has been used.

- **Calculation of the surface durability (Standard ISO 6336 -2)**

To be valid the bending fatigue test, it must be shown that:

$$\sigma_F \leq \sigma_{FP} \quad (6.10)$$

where:

- σ_{FP} is the *permissible tooth root stress*, and equal to:

$$\sigma_{FP} = \sigma_{Flim} \frac{Y_{ST} \cdot Y_{NT}}{S_{F,min}} Y_x \cdot Y_{RrelT} \cdot Y_{\delta relT} \quad (6.11)$$

- Y_{ST} called *stress correction factor*, which can be obtained from *Haigh diagram*;
- Y_{NT} called *life factor for tooth root stress for reference test conditions*, which can be obtained from *Wohler diagram (Figure 6.11)*;
- Y_{RrelT} called *relative surface factor*, obtained from the diagram in the *Figure 6.13*;
- $Y_{\delta relT}$ called *relative notch sensitivity factor*, obtained from the diagram in the *Figure 6.12*;
- Y_x called *size factor*, which can be obtained from the diagram in the *Figure 6.10*;
- $S_{F,min}$ defined *minimum safety coefficient for tooth breakage*, assumed to be equal to 1 during the test, and then calculated subsequently by verifying that it is equal to or greater than 1;

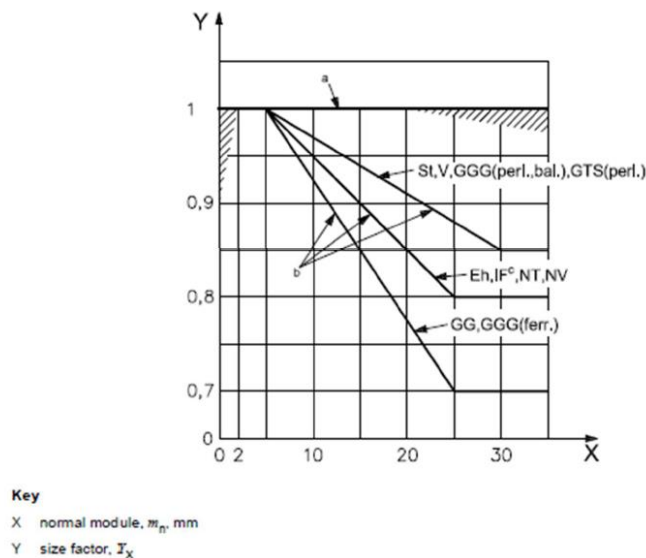
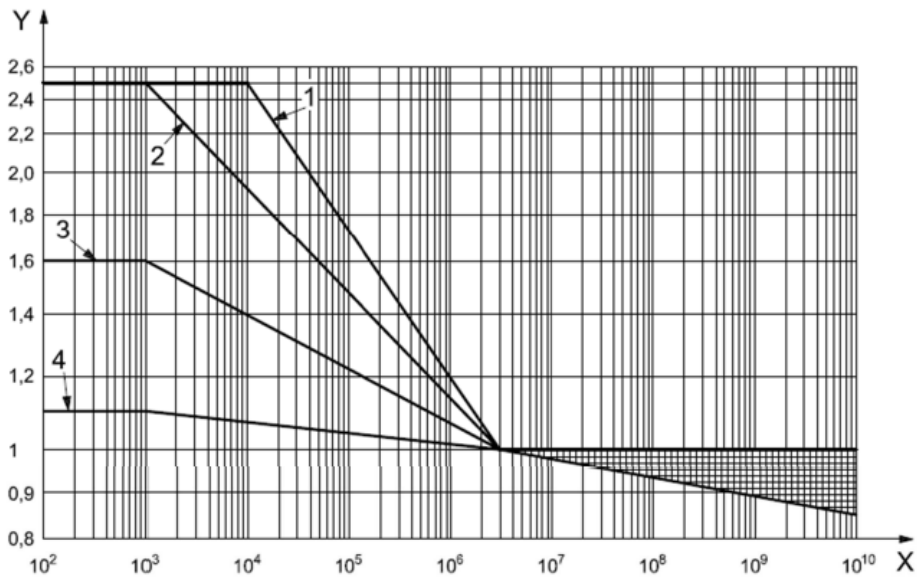
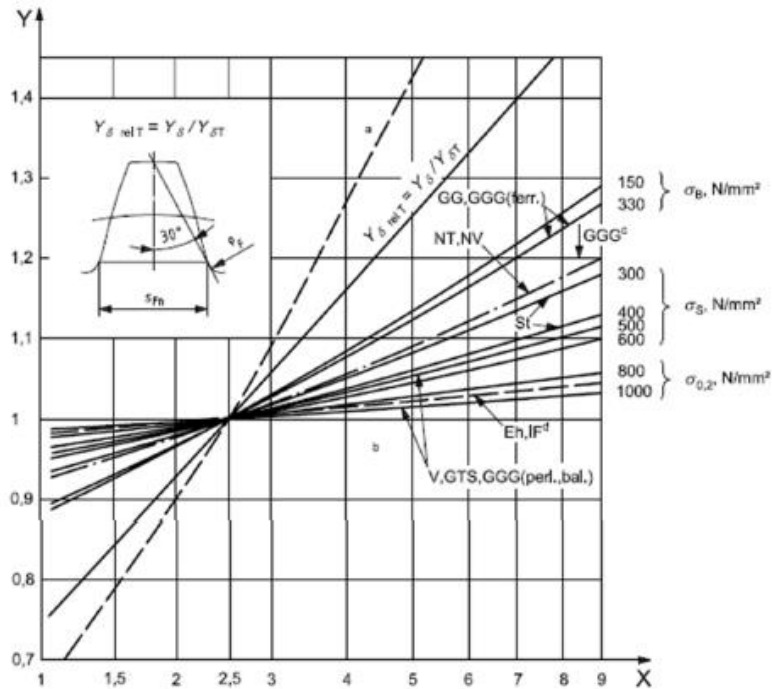


Figure 6.10: Size factor, Y_x , for tooth bending strength



Key
 X number of load cycles, N_L
 Y life factor, Y_{NT}

Figure 6.11: Life factor, Y_{NT} , depending on number of load cycles

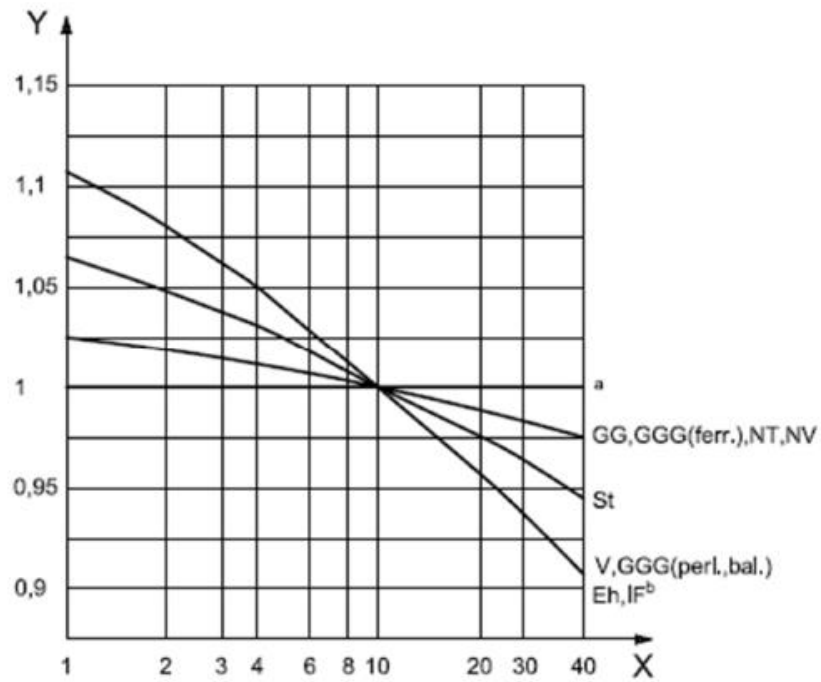


Key
 X notch parameter, $q_s = r_n / 2r_s$
 Y relative notch sensitivity factor, $Y_{\delta rel T}$, for reference stress

NOTE 1 Values of σ in newtons per square millimetre (N/mm²).
 NOTE 2 See ISO 6536-1:2006, Table 2, for an explanation of the abbreviations used.
 NOTE 3 Based on bending flat bar complying with VDI 2226^[7].

- a Fully insensitive to notches.
- b Fully sensitive to notches.
- c With increasingly pearlitic structure.
- d (root).

Figure 6.12: Relative notch sensitivity factor, $Y_{\delta rel T}$, for reference stress



- Key**
- X roughness, R_z , μm
 - Y relative surface factor, $Y_{Rrel T}$
 - a For static stress and all materials.
 - b (root).

Figure 6.13: Relative surface factor, $Y_{Rrel T}$

- σ_F is the *actual tooth root stress* equal to:

$$\sigma_F = \sigma_{F0} K_A K_V K_{F\alpha} K_{F\beta} \quad (6.12)$$

where σ_{F0} is the *nominal tooth root stress* equal to:

$$\sigma_{F0} = \frac{F_t}{b m_{n,uni}} Y_F Y_S Y_B Y_{DT} Y_\beta \quad (6.13)$$

- Y_B called *rim thickness factor*;
- Y_{DT} called *deep tooth factor*;
- Y_F called *form factor*;
- Y_S called *stress correction factor*;
- $Y_F * Y_S = Y_{Lw}$ obtained from the *Table 6.6*;
- Y_β called *helix angle factor*, which is equal to 1 for the spur wheel;

Returning to the equation (6.12), the terms that compose it must be explained:

- K_A called *application factor*, obtained from the *Table 6.7*;

Working characteristic of driving machine	Working characteristic of driven machine			
	Uniform	Light shocks	Moderate shocks	Heavy shocks
Uniform	1,00	1,25	1,50	1,75
Light shocks	1,10	1,35	1,60	1,85
Moderate shocks	1,25	1,50	1,75	2,00
Heavy shocks	1,50	1,75	2,00	$\geq 2,25$

Table 6.7: Application factor, K_A

- K_v called *dynamic factor* equal to:

$$K_v = 1 + \left(\frac{K_1}{K_A \cdot \frac{F_t}{b}} + K_2 \right) \cdot \frac{v \cdot z_1}{100} \cdot K_3 \cdot \sqrt{\frac{u^2}{1 + u^2}} \quad (6.14)$$

subject to the following constraints being respected

$$\begin{cases} \frac{v \cdot z_1}{100} \cdot \sqrt{\frac{i_{1-2}^2}{1 + i_{1-2}^2}} \leq 10 \frac{m}{s} \\ \mathcal{E}_\beta \geq 1 \quad ; \quad \beta \leq 30^\circ \\ z_1 \leq 50 \end{cases}$$

Where:

- K_1 e K_2 obtained from the *Table 6.8*;

	K_1 Accuracy grades as specified in ISO 1328-1										K_2 All accuracy grades
	3	4	5	6	7	8	9	10	11	12	
Spur gears	2,1	3,9	7,5	14,9	26,8	39,1	52,8	76,6	102,6	146,3	0,019 3
Helical gears	1,9	3,5	6,7	13,3	23,9	34,8	47,0	68,2	91,4	130,3	0,008 7

Table 6.8: K_1 and K_2 depending on the accuracy grades

- K_3 which depend on the following ratio:

$$\frac{v \cdot z_1}{100} \cdot \sqrt{\frac{i_{1-2}^2}{1 + i_{1-2}^2}} \quad (6.15)$$

$$K_3 = \begin{cases} 2 & \text{se } \frac{v \cdot z_1}{100} \cdot \sqrt{\frac{i_{1-2}^2}{1 + i_{1-2}^2}} \leq 0,2 \\ -0,357 \cdot \frac{v \cdot z_1}{100} \cdot \sqrt{\frac{i_{1-2}^2}{1 + i_{1-2}^2}} + 2,071 & \text{se } \frac{v \cdot z_1}{100} \cdot \sqrt{\frac{i_{1-2}^2}{1 + i_{1-2}^2}} > 0,2 \end{cases} \quad (6.16)$$

- K_{Fa} called *transverse load factor* assumed equal to 1;
- $K_{F\beta}$ called *face load factor* assumed equal to 1;

The results obtained are shown below:

Calculation of tooth bending strength (Standard ISO 6336 -3)					
Y_{NT}	1	K_A	1,25	$Y_F \cdot Y_S$	3,25
Y_{ST}	2	K_V	1,02	Y_ϵ	1
$Y_{\delta relT}$	1	K_1	39,1	Y_β	1
Y_{RrelT}	1	K_2	0,019	Y_B	1
Y_X	1	K_3	2		
σ_{Flim} [MPa]	270	K_{Fa}	1		
σ_{Fp} [MPa]	540	$K_{F\beta}$	1		
		σ_{F0} [MPa]	34,23	$\sigma_F \leq \sigma_{Fp}$	
S_F	8,3476	σ_F [MPa]	32,34	TRUE	

- **Calculation of the surface durability (Standard ISO 6336 -2)**

To be valid the pitting fatigue test, it must be shown that:

$$\sigma_H \leq \sigma_{HP} \quad (6.17)$$

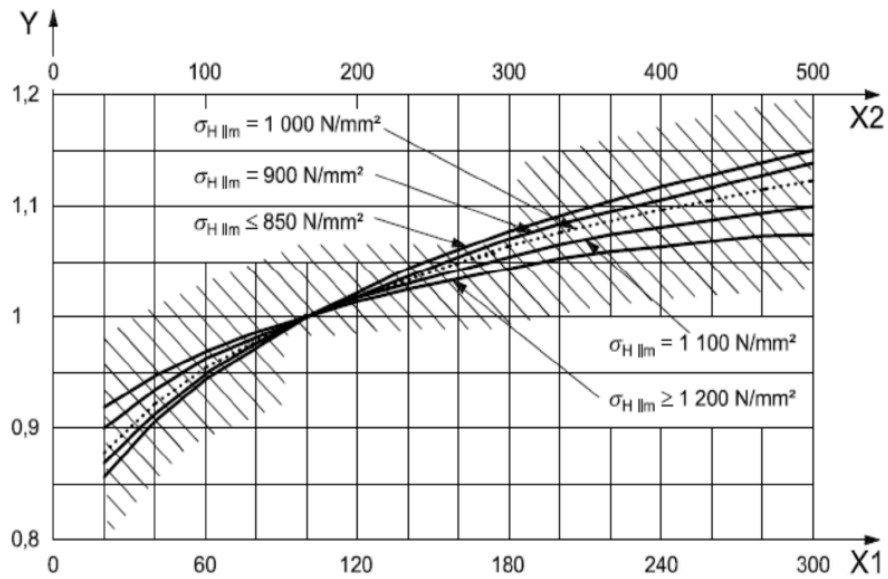
where σ_{HP} is the *permissible contact stress* equal to:

$$\sigma_{HP} = \sigma_{Hlim} \frac{Z_{NT}}{S_{H,min}} Z_L \cdot Z_V \cdot Z_R \cdot Z_W \cdot Z_X \quad (6.18)$$

With:

- σ_{Hlim} is the *allowable stress numbers(contact)*;
- Z_{NT} called *life factor for contact stress for reference test conditions*, which can be obtained from *Wohler diagram*;
- Z_L called *lubricant factor*, obtained from the diagram in *Figure 6.14*;
- Z_V called *velocity factor*, obtained from the diagram in *Figure 6.15*;
- Z_R called *roughness factor*, obtained from the diagram in *Figure 6.16*;
- Z_W called *work hardening factor*, obtained from the diagram in *Figure 6.17*;
- Z_X called *size factor*, which in part 2 of ISO 6336 is taken to be 1;

- $S_{H,min}$ defined *minimum safety factor for pitting*, assumed to be equal to 1 during the test, and then calculated subsequently by verifying that it is equal to or greater than 1;



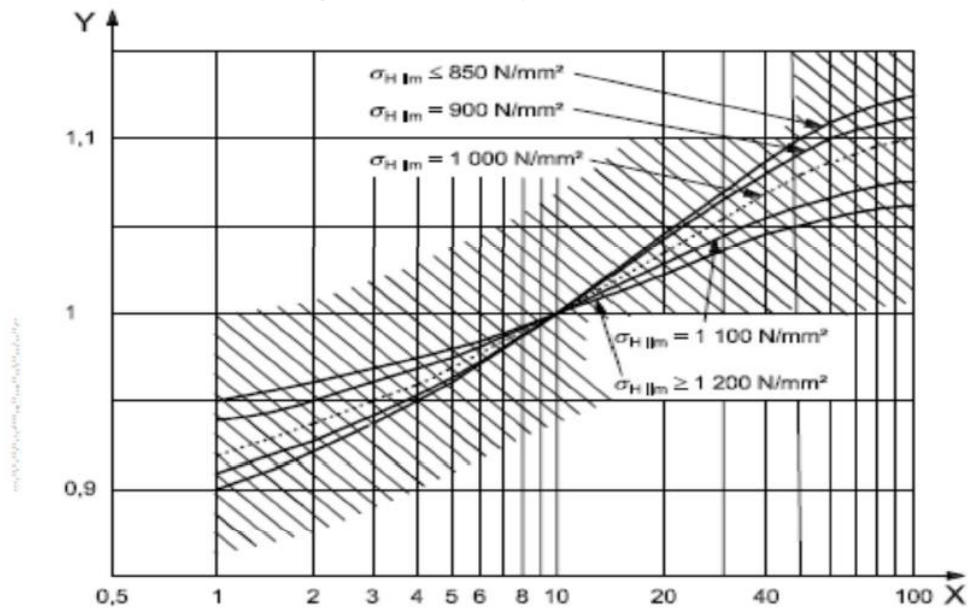
Key

X1 nominal viscosity at 50 °C, ν_{50} , mm²/s

X2 nominal viscosity at 40 °C, ν_{40} , mm²/s

Y facteur lubrifiant, Z_L

Figure 6.14: Lubricant factor Z_L

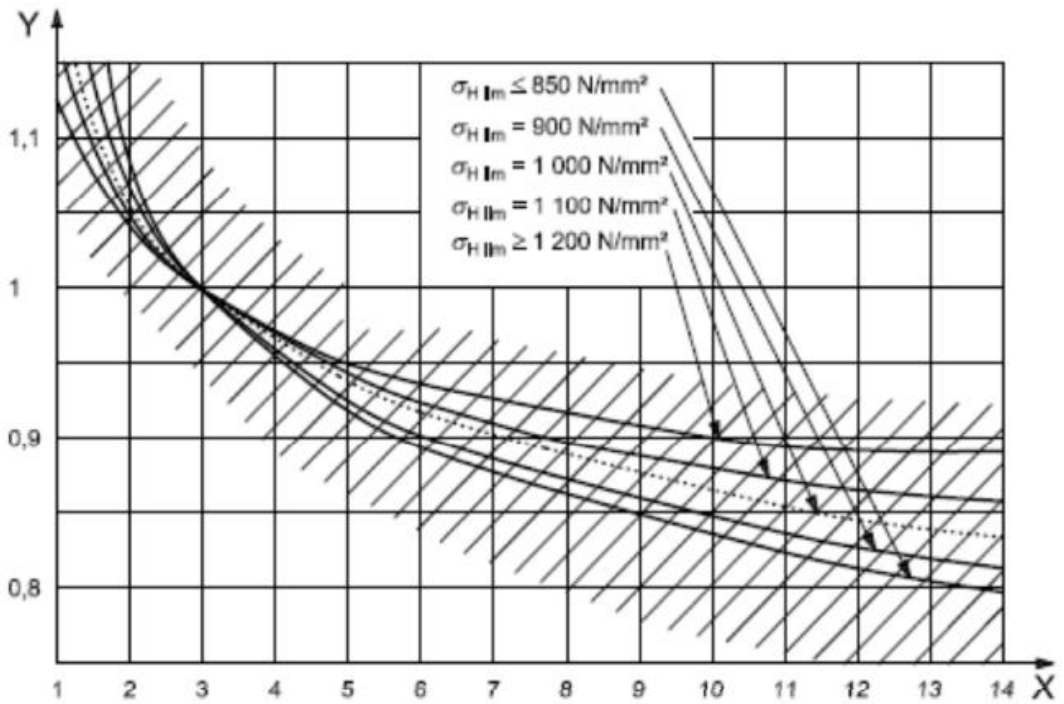


Key

X pitch line velocity, v , m/s

Y velocity factor, Z_v

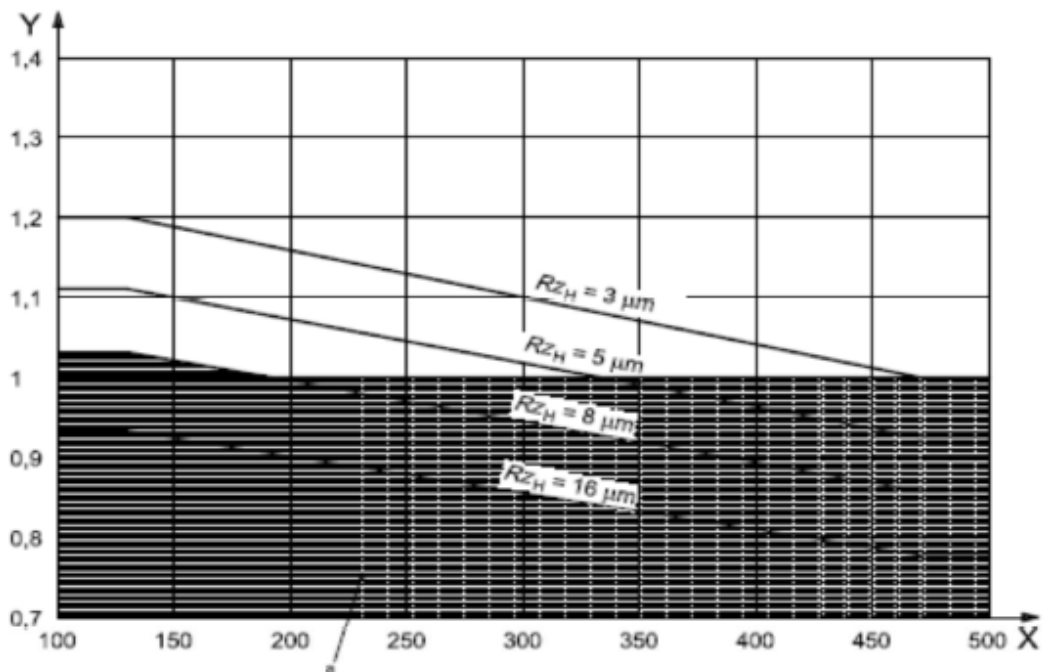
Figure 6.15: Velocity factor, Z_v



Key

- X mean relative peak-to-valley roughness, Rz_{10} , μm
- Y roughness factor, Z_R

Figure 6.16: Roughness factor, Z_R



Key

- X tooth flank hardness of softer wheel, HB
- Y work hardening factor, Z_W

^a Shaded area: $Z_W = 1$. Effects of wear (not covered by ISO 6336).

Figure 6.17: Work hardening factor Z_W for through-hardened gear/case-hardened pinion, reference stress

Returning to the equation (6.16), σ_H is the *contact stress* equal to:

$$\sigma_H = \sigma_{H0} \cdot \sqrt{K_A \cdot K_V \cdot K_{H\alpha} \cdot K_{H\beta}} \quad (6.18)$$

where σ_{H0} is the *nominal contact stress* equal to:

$$\sigma_{H0} = \sqrt{\frac{F_t}{2 \cdot r \cdot b} \cdot \frac{1 + i_{1-2}}{i_{1-2}} \cdot Z_E \cdot Z_H \cdot Z_\beta \cdot Z_\varepsilon} \quad (6.19)$$

- Z_E called *elasticity factor*, in this case, since the same material was used, it is equal to:

$$Z_E = 0,418 \cdot \sqrt{E} \quad (6.20)$$

- Z_H called *zone factor* and equal to:

$$Z_H = \sqrt{\frac{2}{\sin \theta \cdot \cos \theta}} \quad (6.21)$$

- Z_β called *helix angle factor*, and equal to 1 for spur gear

- Z_ε called *contact ratio factor*, for spur wheel equal to:

$$Z_\varepsilon = \sqrt{\frac{4 - \varepsilon_\alpha}{3}} \quad (6.22)$$

With ε_α called *transverse contact ratio* equal to

$$\varepsilon_\alpha = \frac{\sqrt{R_{\alpha_2}^2 - R_{b_2}^2} + \sqrt{R_{\alpha_1}^2 - R_{b_1}^2} - (R_1 + R_2) \cdot \sin \theta}{\pi \cdot m_u \cdot \cos \theta} \quad (6.23)$$

Returning to the equation (6.18), the terms that compose it must be explained:

- K_A called *application factor*, obtained from the *Table 6.7*;
- K_V called *dynamic factor*, calculated with the equation (6.14);
- $K_{H\alpha}$ called *transverse load factor (contact stress)* equal to 1 for industrial transmissions;
- $K_{H\beta}$ called *face load factor (contact stress)* equal to 1 for industrial transmissions;

The results obtained are shown below:

Calculation of the surface durability (Standard ISO 6336 -2)					
Z _{NT}	1	Z _H	2,49457	K _A	1,25
Z _L	0,8	Z _E	191,552	K _V	1,01755
Z _V	0,92	Z _ε	0,82041	K _{Hα}	1
Z _R	0,86	ε _α	1,98	K _{Hβ}	1
Z _W	1			σ _H ≤ σ _{HP}	
Z _X	1			TRUE	
σ _{Hlimite}	1030	σ _{H0}	436,38		
σ _{HP}	651,949	σ _H	555,046	S _F	1,8557

In Figure 6.18 is shown the propriety of the steel chosen for the gears.

C45		Normativa di riferimento UNI 7845 Reference Standard UNI 7845					ims IMS S.p.A. acciai speciali	
Corrispondenze Comparable standards	SIAU	DIN	W.N.	AFNOR	BS	AISI/SAE		
	-	CK45	1.1191	(XC48)	(080M46)	-		
Composizione Chemical analysis	C	Mn	Si	Cr	Ni	Mo	Altri	
	.42+.50	.50+.80	.15+.35	-	-	-	P e S ≤ .035	
Caratteristiche meccaniche / Mechanical properties								
Stato Condition	Saggio Ø mm. Specimen Ø mm.	Re min. N/mm ²	Rm N/mm ²	A min. %	KCU min. J	Durezza HB allo stato HB hardness in the following conditions		
Bonificato Hardened and tempered	16	510	730+870	14	20	Ricotto lavorabile / Soft-annealed	≤ 235	
	16+40	460	690+830	15	17,5	Ricotto isothermico/ Isothermal annealed	163+217	
	40+100	410	640+780	16	15	Ricotto sferoidale/Spheroidal annealed	≤ 188	
Normalizzato/Normalized	16+100	335	590+740	17				

Materiale	Abbreviazione DIN o UNI	Stato di trattamento	Allungam. a rottura A _r (%)	Durezza	Resistenza al piede del dente, σ _{FE} (MPa)	Resistenza a vaiolatura σ _{H,lim} (MPa)
Acciai da bonifica	C 45	normalizzato	-	560 HV 10	540	1030
DIN 17220, induriti	34 CrMo4	bonificato	-	590 HV 10	860	1070
alla fiamma o per induzione	42 CrMo4	bonificato	-	610 HV 10	720	1170
	34 CrNiMo6	bonificato	-	590 HV 10	760	1270
Acciai da bonifica e cementazione nitrurati.	42 CrMo4	bonificati	-	550 HV 10	770	1070
	16 MnCr5	prima	-	550 HV 10	810	1110
Acciai da nitrurazione	31 CrMoV9	della	-	700 HV 10	840	1230
nitrurati	14 CrMoV6	truciolatura	-	770 HV 10	860	1270
Acciai da bonifica e da cementazione	C 45	normalizzato	-	420 HV 10	620	710
	16 MnCr5	normalizzato	-	560 HV 10	650	770
nitrocarburi	42 CrMo4	bonificato	-	610 HV 10	680	830

Figure 6.18: Propriety of the steel chosen for the gears.

6.6 Static evaluation of metallic pins

The pins that come into contact with the fabric were seen as beams embedded with a concentrated load at their ends. With this simplification it is easy to calculate the stresses acting on the metal pins and then be able to verify in this case the minimum diameter needed to prevent the phenomenon of breakage or yielding.

Figure 6.19 shows the graph of the forces related to one of the metal pins.

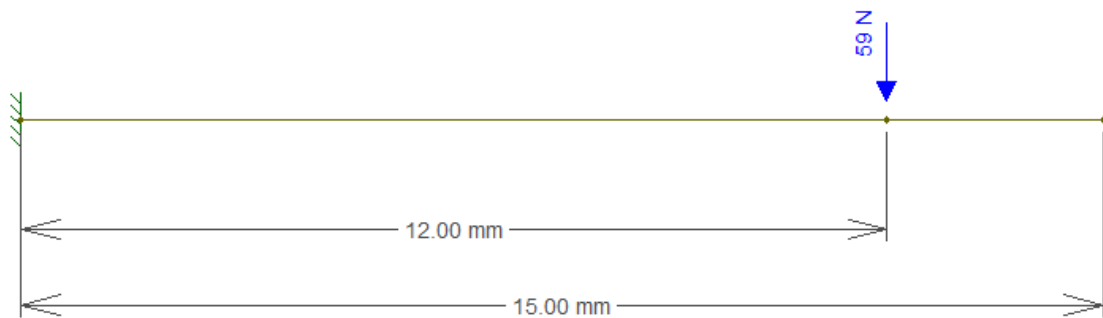


Figure 6.19: graph of the forces acting on the pins

We have calculated the constraining reactions that result from it and we have been able to calculate the diagram of the stresses of the *Shear* and of the *bending Moment* shown in Figure 6.20 and Figure 6.21.

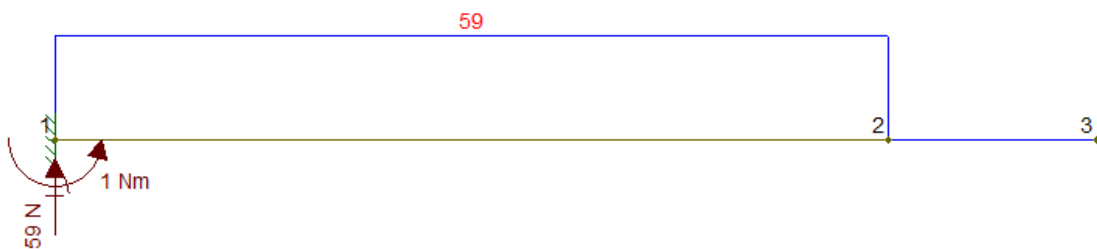


Figure 6.20: Shear diagram

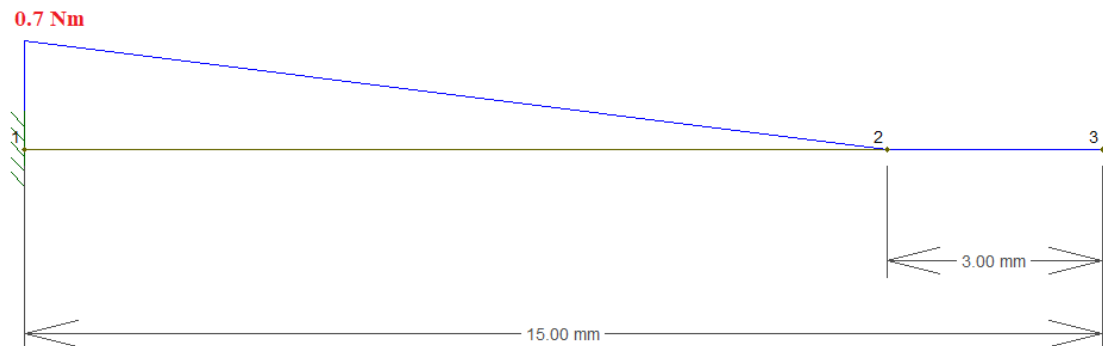


Figure 6.21: Bending moment diagram

To determine the minimum diameter of the pins, a static verification was carried out. For the pins, the use of a common type of steel was chosen.

The sizing was carried out considering only the contribution of the bending moment, considering the most loaded section, which in this case is the final part of the metal pin. Statically dimensioning the tip means ensuring that the ideal tension is lower than the allowable tension of the material with which it is intended to be made, providing for the use of a safety factor. The relationship must therefore be satisfied:

$$\sigma_{id} \leq \sigma_{amm} = \frac{R_{P,02}}{CS} \quad (6.24)$$

With

- $R_{P,02}$ Yield stress
- CS safety factor, in this case equal to 3

The ideal stress σ_{id} is calculated by *Tresca criterion*:

$$\sigma_{id} = \frac{32 \cdot \sqrt{M_f^2}}{\pi \cdot d^3} \quad (6.25)$$

With the equations 1 and 2, is get the minimum diameter d_{min} :

$$d_{min} \geq \sqrt[3]{\frac{32 \cdot CS \cdot \sqrt{M_f^2}}{\pi \cdot R_{P,02}}} \quad (6.26)$$

The result obtained are as follow:

Metallic Pins		
$R_{P,02}$	270,0	MPa
σ_{id}	90,0	MPa
M_f	0.7	Nm
CS	3	-
d_{min}	4,29	mm

The metal pins will have a conical truncated shape, with the diameter in correspondence to the most stressed section of 5 mm.

6.7 Estimated of the forces involved: *main shaft*

Once the forces acting on the pins that have the function of tearing the cloth have been estimated, it is easy to estimate the forces acting on the main roller. For the main roller, the choice of steel to be used has been constrained by the various catalogues of companies that manufacture steel tubes. Due to the not excessive forces, it was decided to reduce the weight of the structure by selecting a hollow shaft, i.e. a tube with a certain thickness, which will be our unknown factor when designing it.

The main shaft consists of two parts, the external part formed by a tube with a certain thickness "s" and an internal part, formed by a shaft with a diameter "d". The two parts will be bound by a junction ring.

6.7.1 Design: *hollow shaft*

The hollow shaft is the part that contains the various metal tips that are used to tear the fabric. The latter is characterized by 40 perforated rows, which can contain up to 12 metal pins.

Figure 6.22 shows the graph of the forces acting on the shaft.

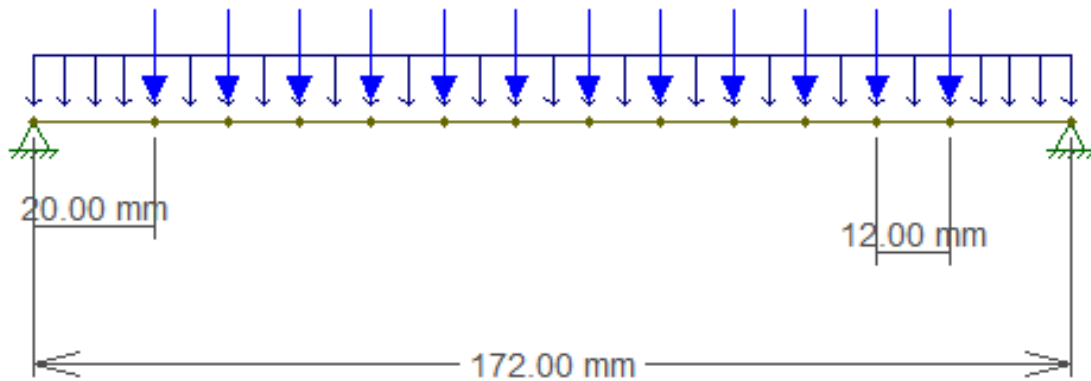


Figure 6.22: graph of the forces acting on the hollow shaft

In blue are represented the forces acting on the metal pins used to tear the fabric, with a value of 59 N. The distributed charge represents the weight force of the shaft itself, which causes the shaft to bend. The latter strongly depends on the thickness of the shaft, because it is a hollow shaft. As a first approximation for the calculation of the minimum thickness, the tube in the catalogue with its maximum thickness was considered in order to calculate the weight force acting. Secondly, the minimum thickness of the hollow shaft in question was checked by static evaluation.

Figure 6.23 shows the diagram of the solicitations relative to the bending moment, with the relative constraint reactions.

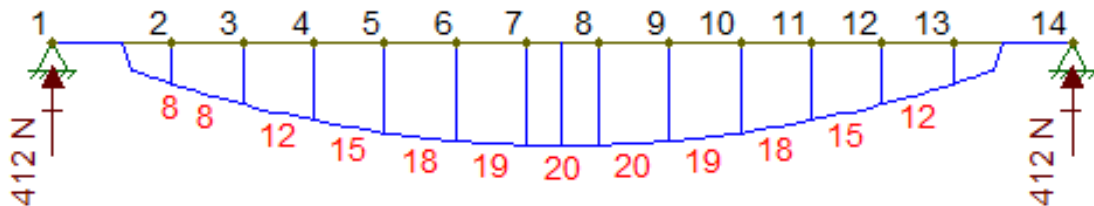


Figure 6.23: Bending moment diagram

In addition to being subject to bending moment, a torque also acts on the shaft. As a first approximation, the total torque acting was equal to the sum of the various torque moments generated by the forces acting on each metal pin.

The design was made taking into account the contribution of the torque acting together with the bending moment. The most loaded section, which is the central section of the shaft, has been considered.

Statically dimensioning the hollow shaft means ensuring that the ideal stress is lower than the allowed stress of the material with which it is intended to be made unless an appropriate safety coefficient. The relationship must therefore be satisfied:

$$\sigma_{id} \leq \sigma_{amm} = \frac{R_{P,02}}{CS} \quad (6.27)$$

The ideal stress σ_{id} is calculated by *Tresca criterion*:

$$\sigma_{id} = \frac{d_e \cdot 32 \cdot \sqrt{M_f^2 + M_t^2}}{\pi \cdot (d_e^4 - d_i^4)} \quad (6.28)$$

With:

- d_e external diameter of the shaft;
- d_i internal diameter of the shaft;

With equation (6.27) and (6.28) is obtained the minimum thickness t_{min} :

$$d_{i_max} = \sqrt[4]{d_e^4 - \frac{d_e \cdot 32 \cdot \sqrt{M_f^2 + M_t^2}}{\pi \cdot \sigma_{id}}} \quad (6.29)$$

$$t_{min} = \frac{d_e - d_{i_max}}{2} \geq \frac{d_e - \sqrt[4]{d_e^4 - \frac{d_e \cdot 32 \cdot \sqrt{M_f^2 + M_t^2}}{\pi \cdot \sigma_{id}}}}{2} \quad (6.30)$$

The results obtained are as follow:

Hollow shaft		
$R_{P,02}$	241,0	MPa
σ_{id}	80,3	MPa
M_{fyz}	20	Nm
M_t	67.3	Nm
CS	3	-
d_e	160,00	mm
d_{i_max}	159,91	mm
s_{min}	0,09	mm

Because the minimum thickness of the hollow shaft is very small, the thickness of it will be determined according to the need to be able to anchor the metal tips to it.

6.7.2 Design: *Internal shaft*

The internal shaft is mounted on two supports which contain two bearings that allow the shaft to rotate. As for the forces acting on the shaft, it is characterized by two concentrated forces acting at the point where the two shafts are joint and corresponding to the constraint reactions calculated in paragraph 6.7.1.

At the end of the left part of the shaft is acting a concentrated force resulting from the connection of the shaft to the auxiliary roll made by belt. Following are shown the force diagram of the shaft, on the two cartesian plane, YX and YX.

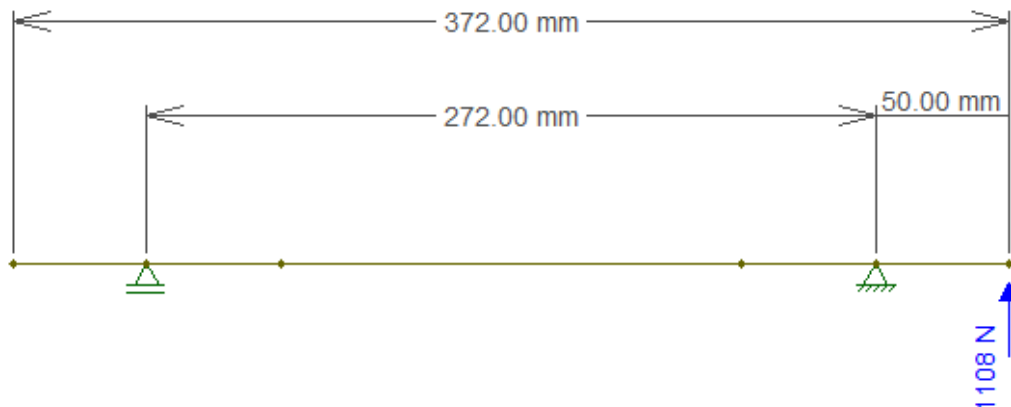


Figure 6.24: graph of the forces acting on the shaft – YX plane

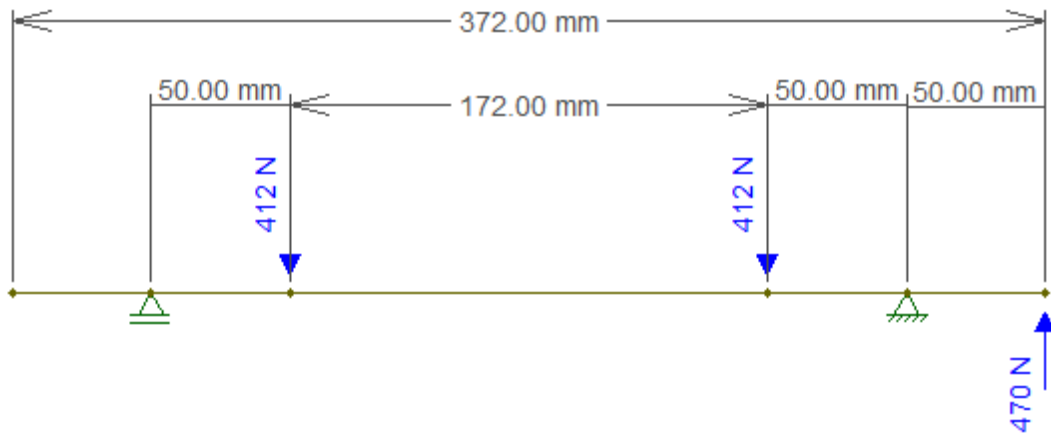


Figure 6.25: graph of the forces acting on the shaft – YZ plane

Figure 6.26 and Figure 6.27 show the diagram of the bending moment on the two different planes with its reactions' values.



Figure 6.26: Bending moment diagram – YX plane

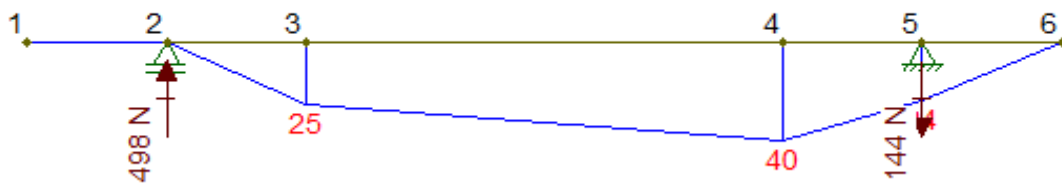


Figure 6.27: Bending moment diagram – YZ plane

In addition to being affected by bending moment, the shaft also presents a stress due to the torque, in the first approximation the total torque acting was the sum of the various torques generated by the forces acting on each metal pin.

Also, in this case, the minimum thickness of the shaft was checked primarily by means of a static check. The dimensioning was carried out taking into consideration the contribution of the torque acting together with the bending moment. The most heavily loaded section, which is represented shortly before the right bearing, has been considered, or section 4 in Figure 6.27.

Statically dimensioning the shaft means ensuring that the ideal stress is lower than the allowed stress of the material with which it is intended to be made unless an appropriate safety coefficient. The relationship must therefore be satisfied:

$$\sigma_{id} \leq \sigma_{amm} = \frac{R_{P,02}}{CS} \quad (6.31)$$

The ideal stress σ_{id} is calculated by *Tresca criterion*:

$$\sigma_{id} = \frac{32 \cdot \sqrt{M_f^2 + M_t^2}}{\pi \cdot d} \quad (6.32)$$

With equation (6.31) and (6.32) is obtained the minimum diameter d_{min} :

$$d_{min} \geq \sqrt[3]{\frac{32 \cdot CS \cdot \sqrt{\sqrt{M_{f_{xy}}^2 + M_{f_{zx}}^2} + M_t^2}}{\pi \cdot R_{P,02}}} \quad (6.33)$$

The results obtained are as follow:

Internal shaft		
$R_{P,02}$	240,0	MPa
σ_{id}	80,0	MPa
M_{byx}	45	Nm
M_{byz}	40	Nm
M_t	67.3	Nm
CS	3	-
d_{min}	22,57	mm

- **The Fatigue test**

The fatigue test carried out in the most critical sections of shaft 2 is described in detail below.

- **Effect of the average stress**

The objective of this verification is to evaluate the fatigue behaviour of the shafts since, during operation, they are subjected to an alternating symmetrical stress attributable to the alternation of the stresses deriving from the bending moment and varying in the section during the rotation of the shaft itself, as shown in *Figure 6.28*.

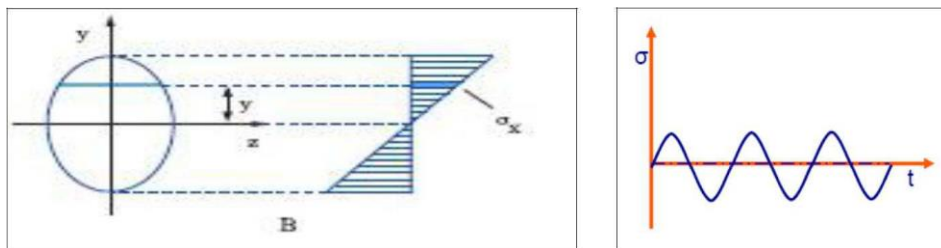


Figure 6.28: Stress due to bending moment, and its value as the time changes

The verification must be carried out in the sections of the shaft in which high σ_{bm} stresses are associated, which vary with the resistant section, which in turn varies along the axis of the shaft due to connections provided to satisfy construction requirements. We want to specify that the alternating stress has been attributed only to the presence of the bending moment, having in fact neglected the effects of shear.

All fatigue tests will be carried out considering the nominal values of the transmitted torques, supposed to be those associated with the operation in operation. The next step is to calculate the SC safety coefficient, verifying that it is higher than 2.

The design choices adopted have led to the verification of several sections for various causes attributable to notch effects, *Figure 6.29* shows the sections in which the fatigue test was carried out for the shaft.

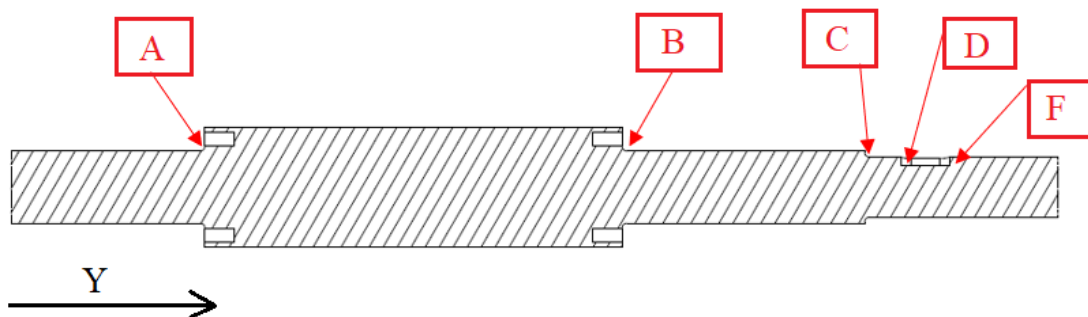


Figure 6.29: Sections verified at Fatigue, seen in the YZ plan

	Description	Cordinate [Y]
Section A	Corner radius	80 mm
Section B	Corner radius	252 mm
Section C	Corner radius	352 mm
Section D	Corner radius of tongue	367 mm
Section F	Corner radius of tongue	387 mm

Table 6.9: Description and position of the sections verified at Fatigue

The procedure for calculating the stresses is the *Sines method*, according to which the shear stress is neglected because it does not affect the fatigue. The uniaxial case is considered. Once the sections have been determined, it is possible to calculate for each of them

- σ_m mean stress in the section, defined as

$$\sigma_m = \frac{4 \cdot N}{\pi \cdot d^2} + \frac{M_{f_{max}} - M_{f_{min}}}{2} \quad (6.34)$$

- σ_a stress amplitude in the section, defined as

$$\sigma_a = \frac{32 \cdot M_f}{\pi \cdot d^3} \quad (6.35)$$

A useful graphic representation is the Haigh plot in which on the x-axis there is σ_m and on the y-axis σ_a . These axes are both intersected by the straight line of Goodman whose equation

$$\frac{\sigma_a}{\sigma_{D-1}^c} + \frac{\sigma_m}{R_m} = 1 \quad (6.36)$$

It allows to understand how it intersects the x-axis at the point identified by the static strength R_m and y-axis in the point defined as *fatigue limit* σ_{D-1}^c .

The fatigue test is satisfied when the point P identified by the coordinates

$$P: (\sigma_m^P ; \sigma_a^P)$$

It's located inside the area between the axis of Goodman's line.

In this way a safety factor SF is determined equal to the ratio between the joining of the origin of the axes and a point on the Goodman line obtained by intersecting the latter with a line passing through the origin and the point P and the joining of the origin of the axes and the point P.

The SF can be determined in an analytical way according to the equation

$$SF = \frac{1}{\frac{\sigma_a}{\sigma_{D-1}^c} + \frac{\sigma_m}{R_m}} \geq 3 \quad (6.37)$$

With

- σ_{D-1}^c corresponding to

$$\sigma_{D-1}^c = \sigma_{D-1} \cdot \frac{C_S \cdot C_L \cdot C_F}{K_f} \quad (6.38)$$

With

- σ_{D-1} fatigue limit equal to

$$\sigma_{D-1} = \frac{R_m}{2} \quad (6.39)$$

- C_S size effect and C_L stress coefficient obtained from the chart in *Figure 6.30*

$$C_S, C_L = f(d; M_f, M_t, N)$$

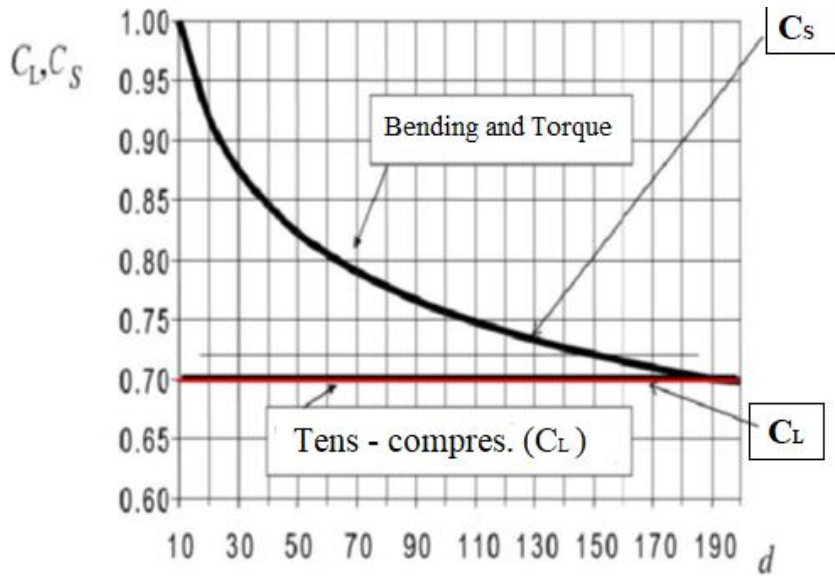


Figure 6.30: C_L and C_S chart depending on load

- C_F surface finish factor obtain from the chart in Figure 6.31

$$C_F = f(R_m, R_a = 10\mu m)$$

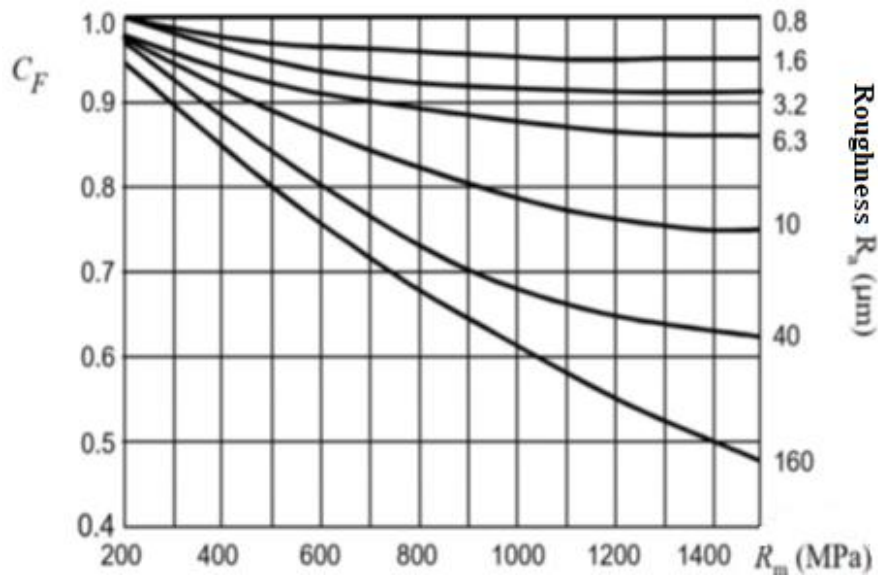


Figure 6.31: C_F chart depending on the roughness

- K_f fatigue notch factor defined to

$$K_f = 1 + q \cdot (K_t - 1) \quad (6.40)$$

With

- q notch sensitivity factor obtained from the chart in Figure 6.32 and equal to $q = f(r, material)$

- K_t stress concentration factor obtained from the chart in Figure 6.33 and equal to

$$K_t = f\left(\frac{D}{d}, \frac{r}{d}\right)$$

With r notch root radius, d smaller diameter and D bigger diameter of the shaft in the section of the notch

$$q = \frac{1}{1 + \frac{A}{\sqrt{r}}}$$

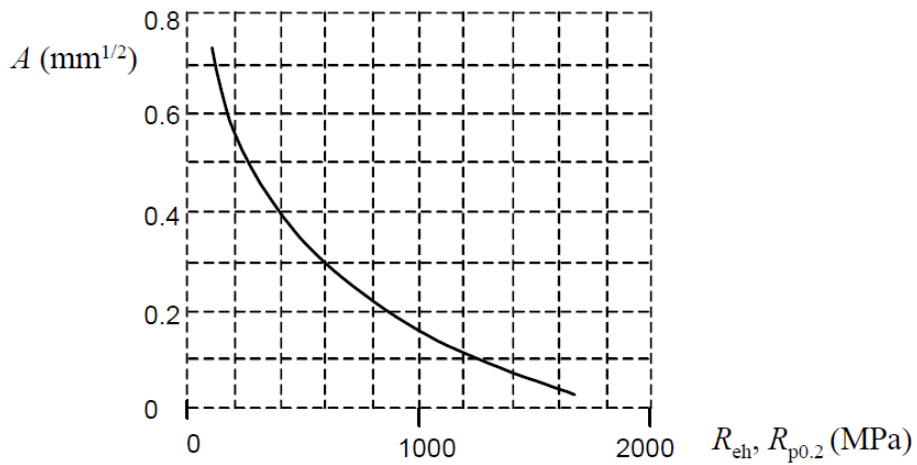


Figure 6.32: A chart depending on $R_{p0.2}$ of the material

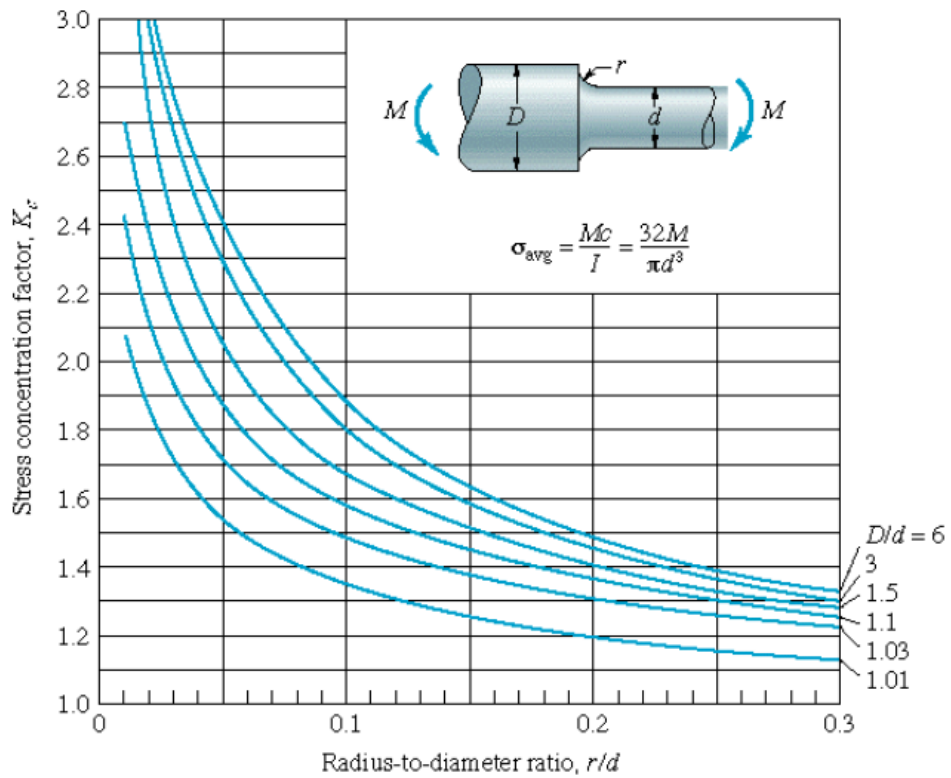


Figure 6.33: K_t chart depending on (r/D) and (D/d)

The results obtained are shown below:

Section A			Section B		
$M_{b_{yx}}$	10	Nm	$M_{b_{yx}}$	45	Nm
$M_{b_{yz}}$	25	Nm	$M_{b_{yz}}$	40	Nm
M_t	67.3	Nm	M_t	67.3	Nm
N	0	N	N	0	N
d	30	mm	d	30	mm
$\sigma_{M_{b_{max}}}$	10,16	MPa	$\sigma_{M_{b_{max}}}$	22,71	MPa
σ_N	0,00	MPa	σ_N	0,00	MPa
$\tau_{M_t_{max}}$	39,85	MPa	$\tau_{M_t_{max}}$	39,85	MPa
Useful Data			Useful Data		
σ_m	0,00	MPa	σ_m	0,00	MPa
σ_a	10,16	MPa	σ_a	22,71	MPa
τ_m	39,85	MPa	τ_m	39,85	MPa

Fatigue test			Fatigue test		
R_m	450	MPa	R_m	450	MPa
σ_{D-1}	225	MPa	σ_{D-1}	225	MPa
C_L	0.7	-	C_L	0.7	-
C_S	0,875	-	C_S	0,875	-
C_F	0,9	-	C_F	0,9	-
r	2	mm	r	2	mm
K_t	2,08	-	K_t	2,08	-
$\rho^{0,5}$	0,5		$\rho^{0,5}$	0,5	
q	0,74	-	q	0,74	-
K_f	1,80	-	K_f	1,80	-
σ_{D-1_e}	98,55	MPa	σ_{D-1_e}	98,55	MPa
σ_{DC}	98,55	MPa	σ_{DC}	98,55	MPa
Secure factor			Secure factor		
SF	9,70	True	SF	4,34	True

Section C			Section D		
M _{b_yx}	23	Nm	M _{b_yx}	12	Nm
M _{b_yz}	10	Nm	M _{b_yz}	6	Nm
M _t	67.3	Nm	M _t	67.3	Nm
N	0	N	N	0	N
d	25	mm	d	21,5	mm
σ _{Mb_max}	16,35	MPa	σ _{Mb_max}	13,75	MPa
σ _N	0,00	MPa	σ _N	0,00	MPa
τ _{Mt_max}	68,86	MPa	τ _{Mt_max}	108,25	MPa
Useful Data			Useful Data		
σ _m	0,00	MPa	σ _m	0,00	MPa
σ _a	16,35	MPa	σ _a	13,75	MPa
τ _m	68,86	MPa	τ _m	108,25	MPa
Fatigue test			Fatigue test		
R _m	450,00	MPa	R _m	450	MPa
σ _{D-1}	225,00	MPa	σ _{D-1}	225	MPa
C _L	10.7	-	C _L	0.7	-
C _S	0,88	-	C _S	0,875	-
C _F	0,90	-	C _F	0,9	-
r	2,00	mm	r	0,6	mm
K _t	1,70	-	K _t	2,3	-
ρ ^{0,5}	0,5		ρ ^{0,5}	0,5	
q	0,74	-	q	0,61	-
K _f	1,52	-	K _f	1,79	-
σ _{D-1_e}	116,79	MPa	σ _{D-1_e}	98,99	MPa
σ _{DC}	116,79	MPa	σ _{DC}	98,99	MPa
Secure factor			Secure factor		
SF	7.14	True	SF	7.20	True

6.8 Design: Auxiliary shafts

As with the main shaft, the auxiliary shafts have also been dimensioned using the same procedure. There are three auxiliary shafts as shown in *Figure 6.34*.

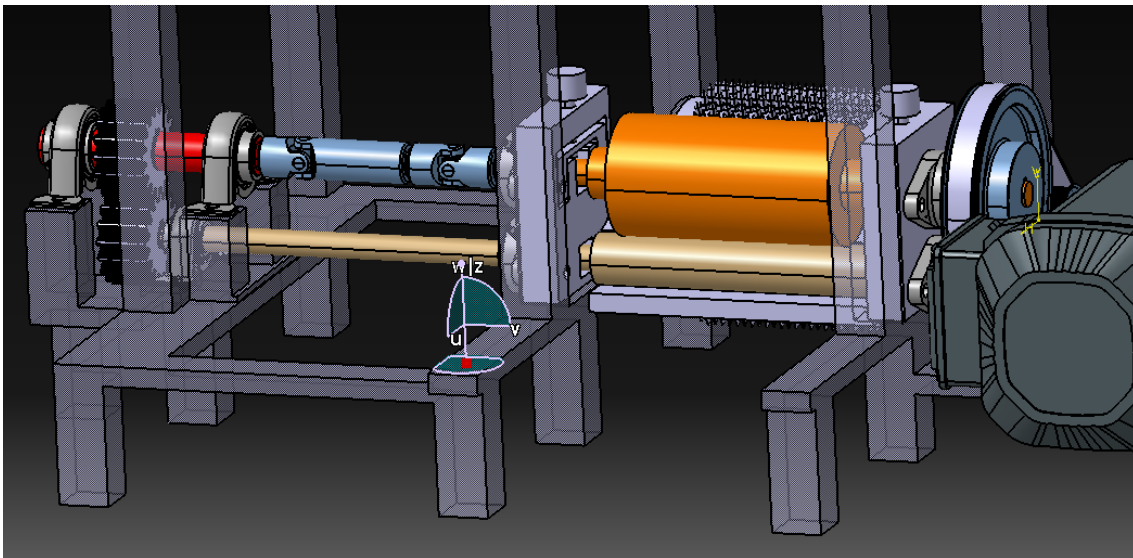


Figure 6.34: drawing of the prototype showing the auxiliary shafts

The orange coloured shaft has the function to normalize and limit the flow of material entering the machine and to simplify the entry of the fabric that will come into contact with the main roller.

The gold coloured shaft carries out the task of transporting the material to be recycled and together with the orange one press the textile waste.

The red coloured shaft only has the function of supporting the gear and to transfer the torque to the gold coloured shaft.

- **Orange shaft**

The orange shaft is mounted on two supports which contain two bearings that allow the shaft to rotate. This shaft can be moved on the Z-axis and it is characterized by a concentrated force acting at the end of the right part of the shaft, resulting from the belt drive. This force act on the YX-plane and YZ-plane and it has been determined by knowing the belt drive stress on the axis and the torque which is transmitted.

In the *Figure 5.21* is showed the forces diagram of the belt transmission. The force S represent the stress on the axis made by the tension of the belt, it is decomposed on the ZY-plane, S_x , and on XY- plane, S_y .

The module of this forces is calculated as follow:

$$S = 1209 \text{ N}$$

$$\alpha = \tan^{-1} \left(\frac{55}{130} \right) = 23^\circ$$

$$S_x = S \cdot \cos \alpha = 1113 \text{ N}$$

$$S_y = S \cdot \sin \alpha = 473 \text{ N}$$

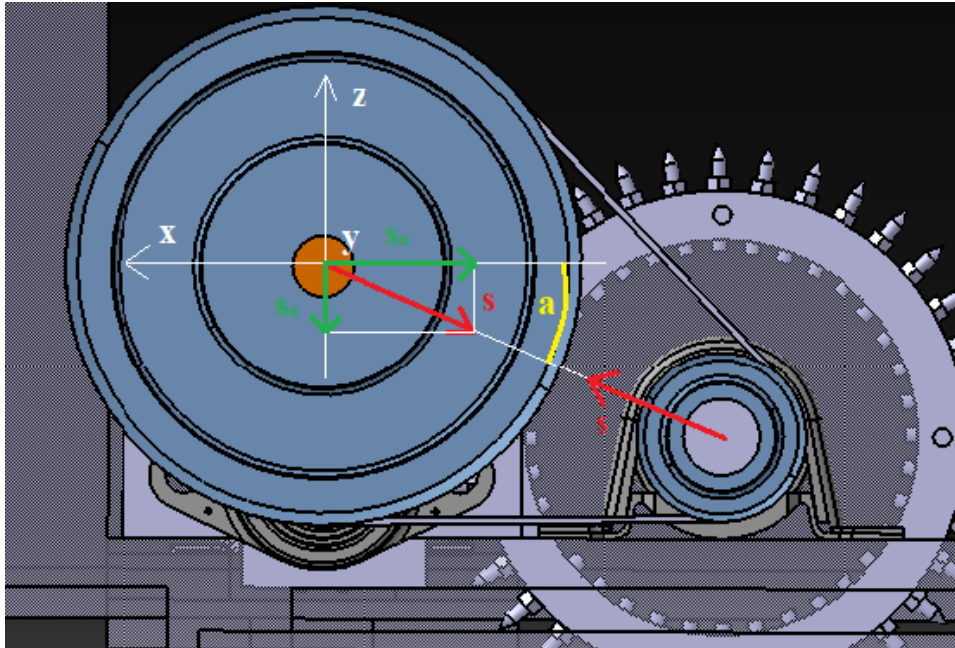


Figure 6.35: Diagram of forces for belt drive

Figure 6.36 and Figure 6.37 show the graph with the forces acting on the shaft.

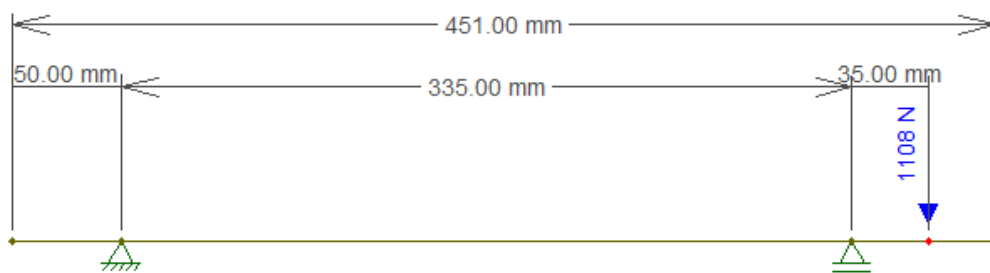


Figure 6.36: graph of the forces acting on the shaft – YX plane

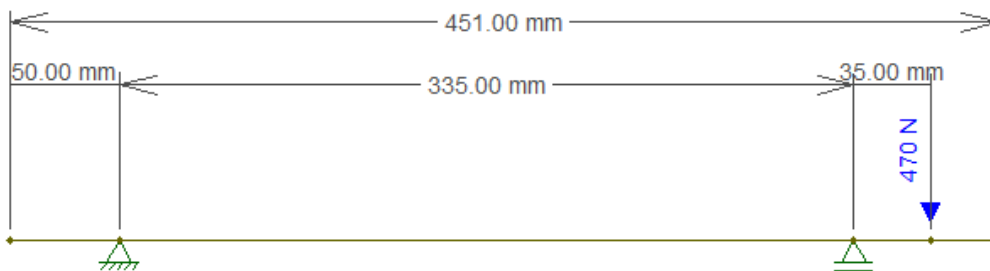


Figure 6.37: graph of the forces acting on the shaft – YZ plane

Figure 6.38 and Figure 6.39 show the diagram of the shaft, with the relative constraint reactions.

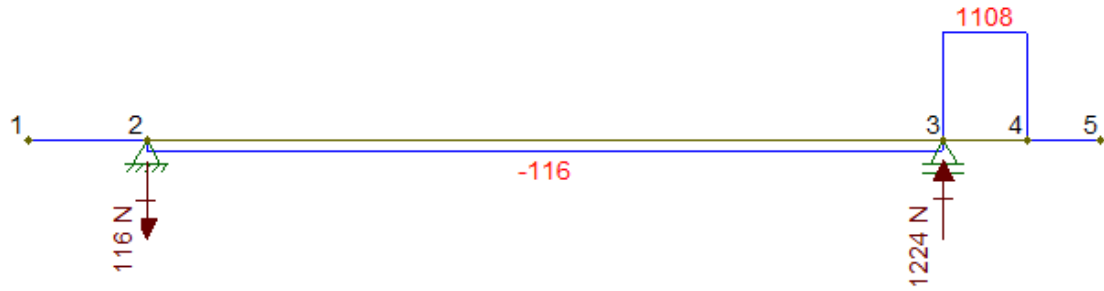


Figure 6.38: Shear diagram – YX plane

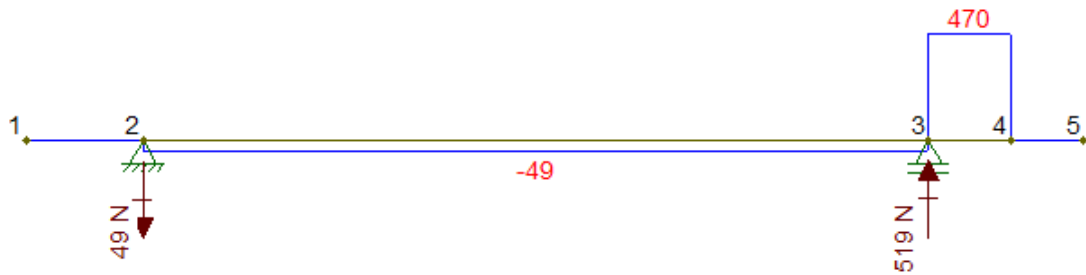


Figure 6.39: Shear diagram – YZ plane

Figure 6.40 and Figure 6.41 show the diagram of the bending moment.



Figure 6.40: Bending moment diagram – YX plane

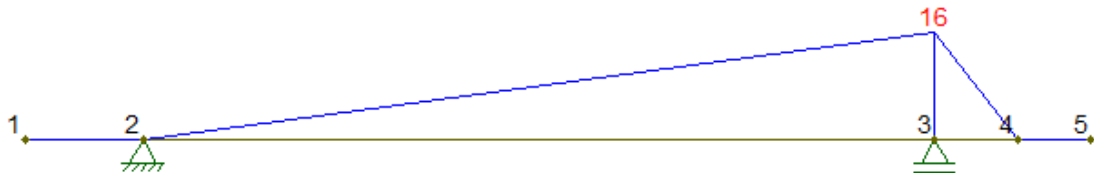


Figure 6.41: Bending moment diagram – YZ plane

In addition to being affected by bending moment, the shaft also presents a stress due to the torque. The dimensioning was carried out taking into consideration the contribution of the torque acting together with the bending moment. The most heavily loaded section, which is represented shortly before the right bearing, has been considered, or section 3 in Figure 6.41.

Statically dimensioning the shaft means ensuring that the ideal stress is lower than the allowed stress of the material with which it is intended to be made unless an appropriate safety coefficient. The relationship that must be satisfied is the (6.31), using the equations (6.32) and (6.33) are obtained the results below:

Orange shaft		
$R_{P,02}$	440	MPa
σ_{id}	146.7	MPa
M_{byx}	39	Nm
M_{byz}	16	Nm
M_t	57.3	Nm
CS	3	-
d_{min}	17,03	mm

After the static design, the shaft was subjected to an indefinite fatigue test. The same procedure as for the main shaft was used for the test. In *Figure 6.42* is shown the sections in which carried out the fatigue test.

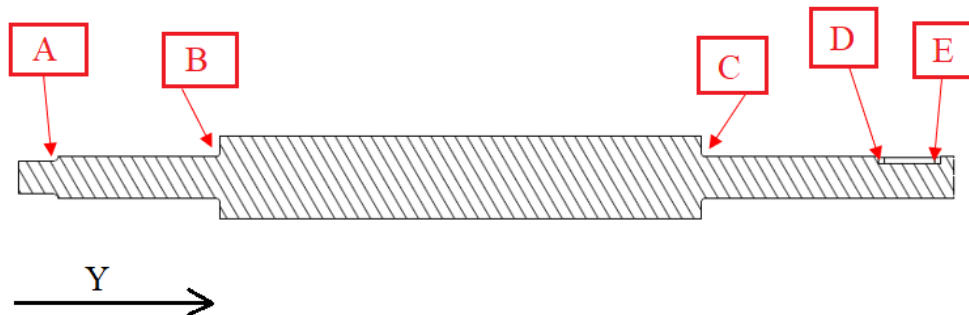


Figure 6.42: Section in which carried out the fatigue test

	Description	Cordinate [Y]
Section A	Corner radius for joint	17 mm
Section B	Corner radius	97 mm
Section C	Corner radius	330 mm
Section D	Corner radius of tongue	415 mm
Section E	Corner radius of tongue	445 mm

Table 6.10: Description and position of the sections verified at Fatigue

The results obtained are shown below:

Section A			Section B		
$M_{b_{yx}}$	32	Nm	$M_{b_{yx}}$	16	Nm
$M_{b_{yz}}$	14	Nm	$M_{b_{yz}}$	7	Nm
M_t	57324	Nm	M_t	57324	Nm
N	0	N	N	0	N
d	20	mm	d	17	mm
$\sigma_{M_{b_{max}}}$	44,47	MPa	$\sigma_{M_{b_{max}}}$	36,21	MPa
σ_N	0,00	MPa	σ_N	0,00	MPa
$\tau_{M_t_{max}}$	114,60	MPa	$\tau_{M_t_{max}}$	186,57	MPa
Useful Data			Useful Data		
σ_m	0,00	MPa	σ_m	0,00	MPa
σ_a	44,47	MPa	σ_a	36,21	MPa
τ_m	114,60	MPa	τ_m	186,57	MPa

Fatigue test			Fatigue test		
R_m	690	MPa	R_m	690	MPa
σ_{D-1}	345	MPa	σ_{D-1}	345	MPa
C_L	0.7	-	C_L	0.7	-
C_S	0,92	-	C_S	0,92	-
C_F	0,85	-	C_F	0,85	-
r	2	mm	r	2	mm
K_t	1,85	-	K_t	2,15	-
$\rho^{0,5}$	0,37		$\rho^{0,5}$	0,37	
q	0,79	-	q	0,79	-
K_f	1,67	-	K_f	1,91	-
σ_{D-1_e}	161,19	MPa	σ_{D-1_e}	141,14	MPa
σ_{DC}	161,19	MPa	σ_{DC}	141,14	MPa
Secure factor			Secure factor		
SF	3,62	True	SF	3,90	True

- **Red shaft**

The red shaft is mounted on two supports which contain two bearings that allow the shaft to rotate. The force generated by the gear drive has two components, one in the YX-plane and one in the YZ- plane. In the *Figure 6.43* is showed the forces diagram of the gear transmission. To determinate this force it is useful consider how the gear drive was made. The gear drive is made by two spur wheel which are used to transfer a torque of 57.3 Nm, so knowing the gear dimension is possible to determinate the *tangential force* F_t and *radial force* F_r like:

$$F_t = \frac{C}{r} = \frac{57.3 \text{ Nm}}{0.034 \text{ m}} = 1686 \text{ N} \qquad F_r = F_t \cdot \tan \theta = 614 \text{ N}$$

Where θ is the pressure angle and it is equal to 20° .

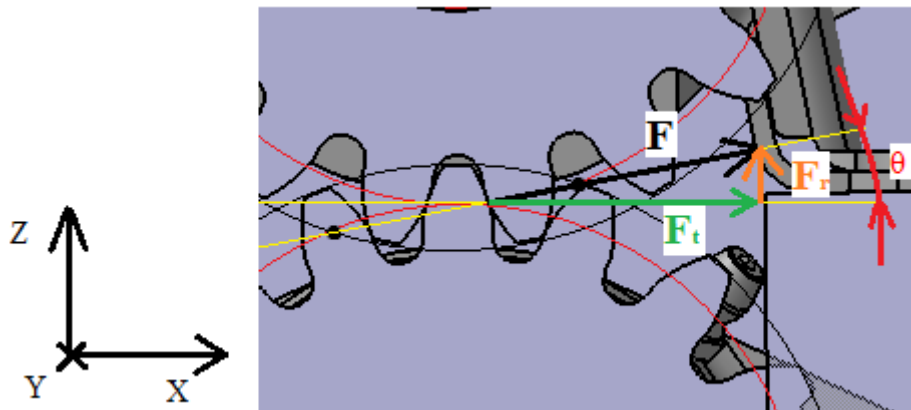


Figure 6.43: Diagram of forces for gear drive

Figure 6.44 and Figure 6.45 show the graph with the forces acting on the shaft.

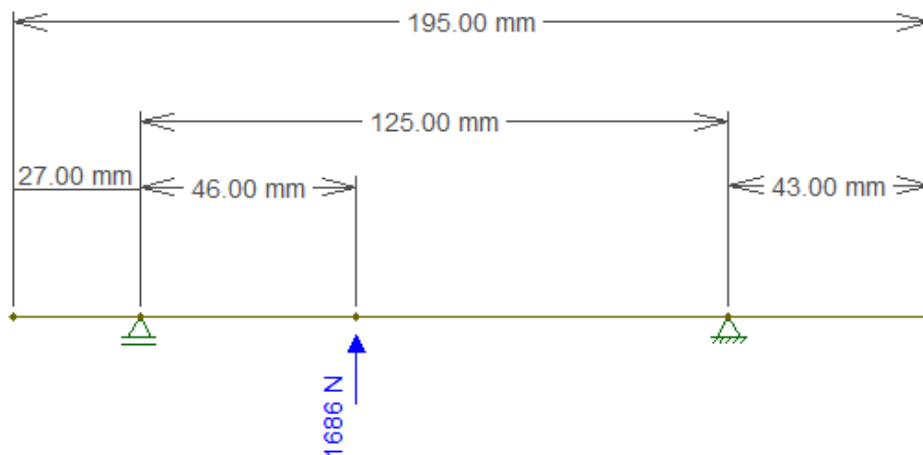


Figure 6.44: graph of the forces acting on the shaft – YX plane

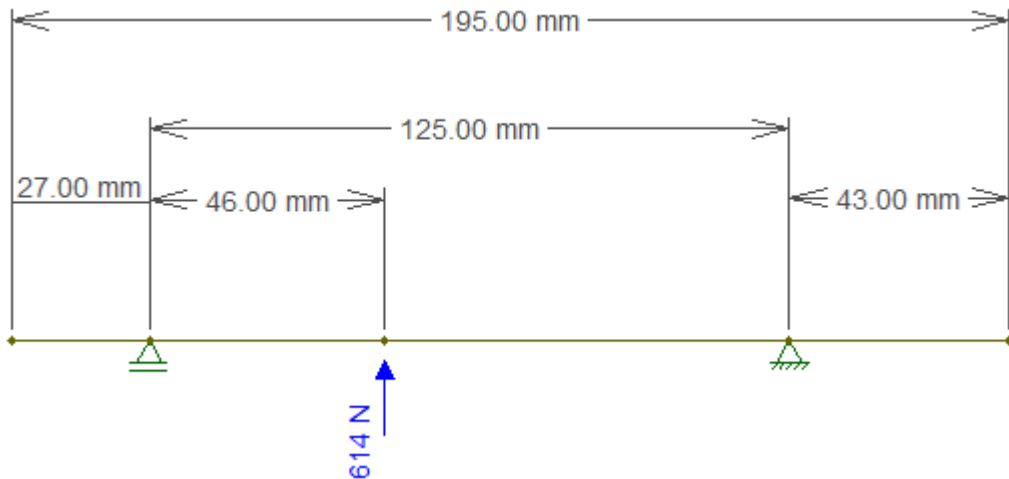


Figure 6.45: graph of the forces acting on the shaft – YZ plane

Figure 6.46 and Figure 6.47 show the diagram of the bending moment, with the relative constraint reactions.

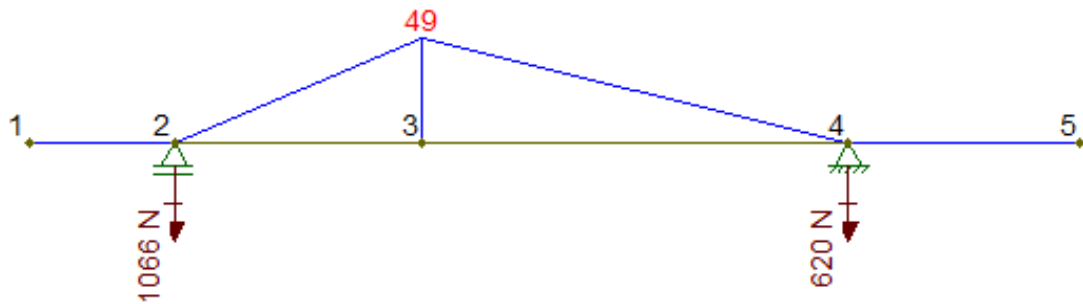


Figure 6.46: Bending moment diagram – YX plane

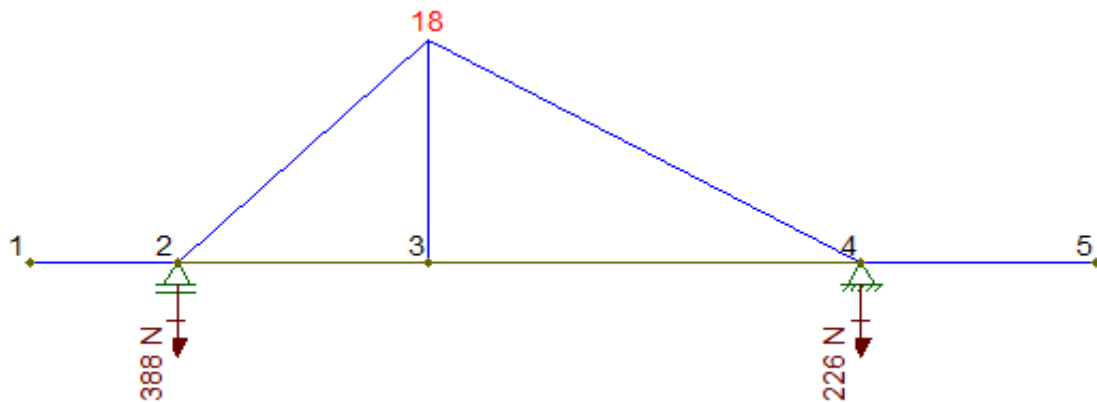


Figure 6.47: Bending moment diagram – YZ plane

In addition to being affected by bending moment, the shaft also presents a stress due to the torque. The dimensioning was carried out taking into consideration the contribution of the torque acting together with the bending moment. The most heavily loaded section has been considered, the section 4 in Figure 6.47.

Statically dimensioning the shaft means ensuring that the ideal stress is lower than the allowed stress of the material with which it is intended to be made unless an appropriate safety coefficient. The relationship that must be satisfied is the (6.31), using the equations (6.32) and (6.33) are obtained the results below:

Red shaft		
$R_{P,02}$	440	MPa
σ_{id}	146.7	MPa
M_{byx}	49	Nm
M_{byz}	18	Nm
M_t	57.3	Nm
CS	3	-
d_{min}	17,03	mm

After the static design, the shaft was subjected to an indefinite fatigue test. The same procedure as for the main shaft was used for the test. In Figure 6.48 is shown the sections in which carried out the fatigue test.

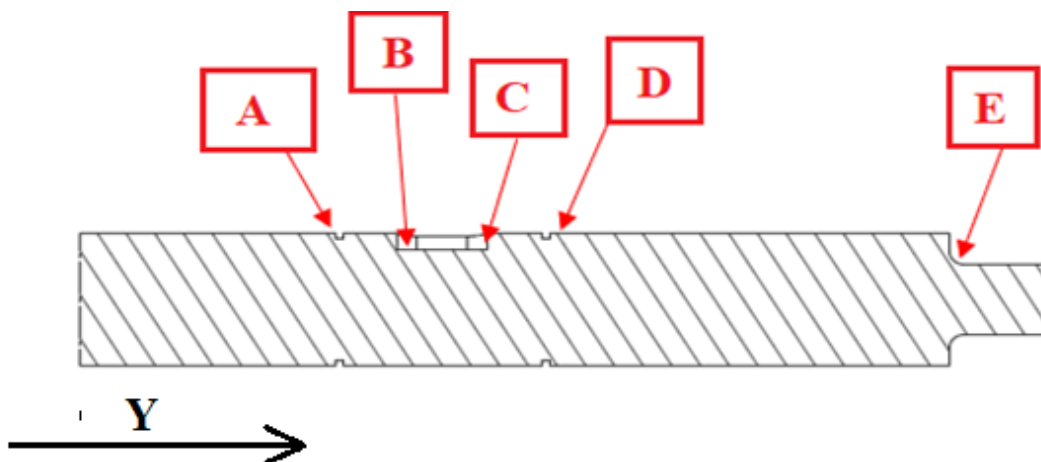


Figure 6.48: Section in which carried out the fatigue test

	Description	Cordinate [Y]
Section A	Corner radius for joint	17 mm
Section B	Corner radius	97 mm
Section C	Corner radius	330 mm
Section D	Corner radius of tongue	415 mm
Section E	Corner radius of tongue	445 mm

Table 6.11: Description and position of the sections verified at Fatigue

The results obtained are shown below:

Section A			Section B		
$M_{b_{yx}}$	28	Nm	$M_{b_{yx}}$	40	Nm
$M_{b_{yz}}$	14	Nm	$M_{b_{yz}}$	10	Nm
M_t	57.3	Nm	M_t	57.3	Nm
N	0	N	N	0	N
d	27,9	mm	d	26,5	mm
$\sigma_{M_{b_{max}}}$	14,68	MPa	$\sigma_{M_{b_{max}}}$	22,57	MPa
σ_N	0,00	MPa	σ_N	0,00	MPa
$\tau_{M_t_{max}}$	42,21	MPa	$\tau_{M_t_{max}}$	49,26	MPa
Useful Data			Useful Data		
σ_m	0,00	MPa	σ_m	0,00	MPa
σ_a	10,16	MPa	σ_a	22,57	MPa
τ_m	39,85	MPa	τ_m	49,26	MPa

Fatigue test			Fatigue test		
R_m	690	MPa	R_m	690	MPa
σ_{D-1}	345	MPa	σ_{D-1}	345	MPa
C_L	1	-	C_L	1	-
C_S	0,875	-	C_S	0,875	-
C_F	0,85	-	C_F	0,85	-
r	0,2	mm	r	0,6	mm
K_t	2,5	-	K_t	2,4	-
$\rho^{0,5}$	0,37		$\rho^{0,5}$	0,37	
q	0,55	-	q	0,68	-
K_f	1,82	-	K_f	1,95	-
σ_{D-1_e}	140,92	MPa	σ_{D-1_e}	131,76	MPa
σ_{DC}	140,92	MPa	σ_{DC}	131,76	MPa
Secure factor			Secure factor		
SF	9,60	True	SF	5,84	True

Section C			Section D		
$M_{b_{yx}}$	44	Nm	$M_{b_{yx}}$	36	Nm
$M_{b_{yz}}$	16	Nm	$M_{b_{yz}}$	13	Nm
M_t	57.3	Nm	M_t	57.3	Nm
N	0	N	N	0	N
d	26,5	mm	d	27,9	mm
$\sigma_{Mb_{max}}$	25,63	MPa	$\sigma_{Mb_{max}}$	17,95	MPa
σ_N	0,00	MPa	σ_N	0,00	MPa
$\tau_{Mt_{max}}$	49,26	MPa	$\tau_{Mt_{max}}$	42,21	MPa
Useful Data			Useful Data		
σ_m	0,00	MPa	σ_m	0,00	MPa
σ_a	25,63	MPa	σ_a	17,95	MPa
τ_m	49,26	MPa	τ_m	42,21	MPa
Fatigue test			Fatigue test		
R_m	690	MPa	R_m	690	MPa
σ_{D-1}	345	MPa	σ_{D-1}	345	MPa
C_L	1	-	C_L	1	-
C_S	0,875	-	C_S	0,875	-
C_F	0,85	-	C_F	0,85	-
r	0,6	mm	r	0,2	mm
K_t	2,4	-	K_t	2,5	-
$\rho^{0,5}$	0,37		$\rho^{0,5}$	0,37	
q	0,68	-	q	0,55	-
K_f	1,95	-	K_f	1,82	-
σ_{D-1_e}	131,76	MPa	σ_{D-1_e}	140,92	MPa
σ_{DC}	131,76	MPa	σ_{DC}	140,92	MPa
Secure factor			Secure factor		
SF	5.14	True	SF	7,85	True

- **Gold shaft**

The gold shaft is mounted on three supports which contain two bearings that allow the shaft to rotate. As the red coloured shaft, the force generated by the gear drive has two components, one in the YX-plane and one in the YZ- plane. *Figure 6.50* and *Figure 6.51* show the graph with the forces acting on the shaft.

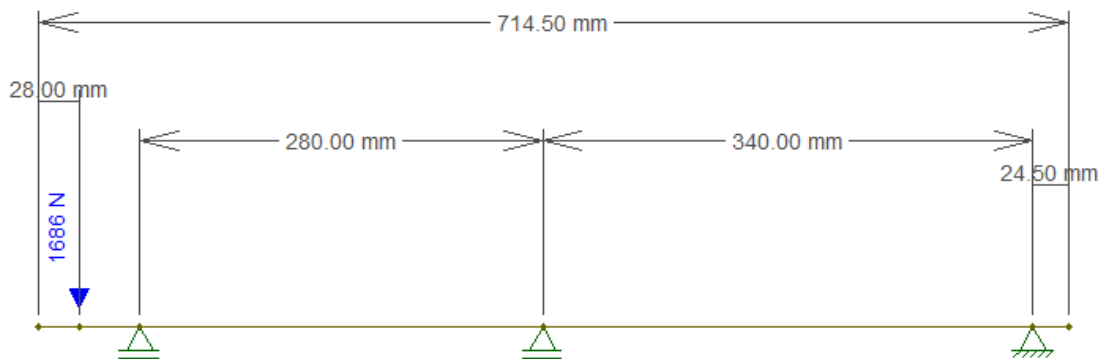


Figure 6.49: graph of the forces acting on the shaft – YX plane

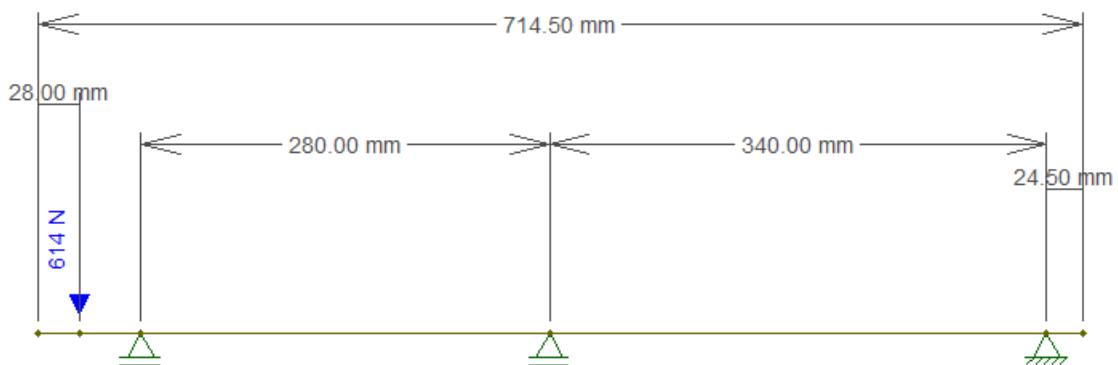


Figure 6.50: graph of the forces acting on the shaft – YZ plane

In the *Figure 6.51* and *Figure 6.52* are shown the constraint reactions.

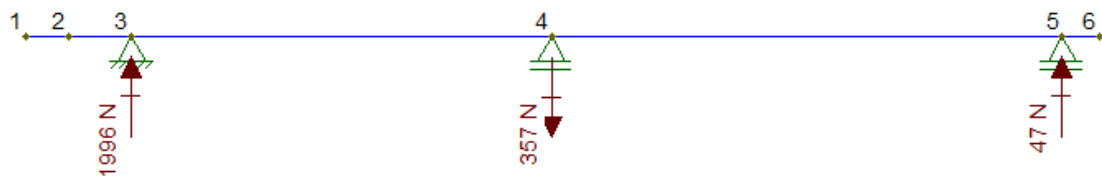


Figure 6.51: graph of the constrain reactions on the shaft – YX plane

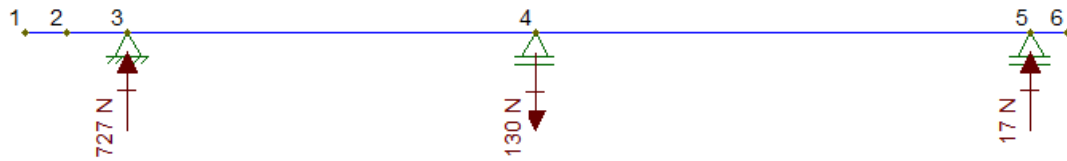


Figure 6.52: graph of the constrain reactions on the shaft – YZ plane

Figure 6.53 and Figure 6.54 show the diagram of the banding moment.

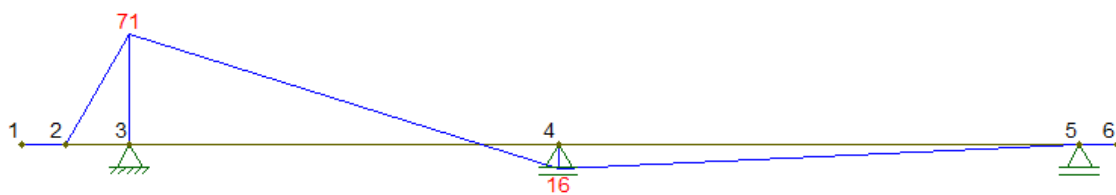


Figure 6.53: Bending moment diagram – YX plane

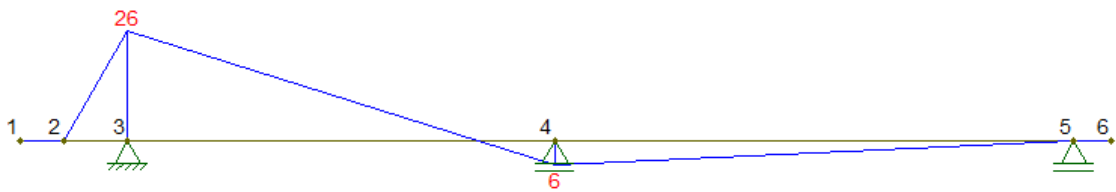


Figure 6.54: Bending moment diagram – YZ plane

In addition to being affected by bending moment, the shaft also presents a stress due to the torque. The dimensioning was carried out taking into consideration the contribution of the torque acting together with the bending moment. The most heavily loaded section has been considered, the section 3 in Figure 6.54.

Statically dimensioning the shaft means ensuring that the ideal stress is lower than the allowed stress of the material with which it is intended to be made unless an appropriate safety coefficient.

The relationship that must be satisfied is the (6.31), using the equations (6.32) and (6.33) are obtained the results below:

Gold shaft		
$R_{P,02}$	605,0	MPa
σ_{id}	201,7	MPa
M_{fyz}	47	Nm
M_t	65.52	Nm
CS	3	-
d_{min}	14,90	mm

After the static design, the shaft was subjected to an indefinite fatigue test. The same procedure as for the main shaft was used for the test. In *Figure 6.55* is shown the sections in which carried out the fatigue test.

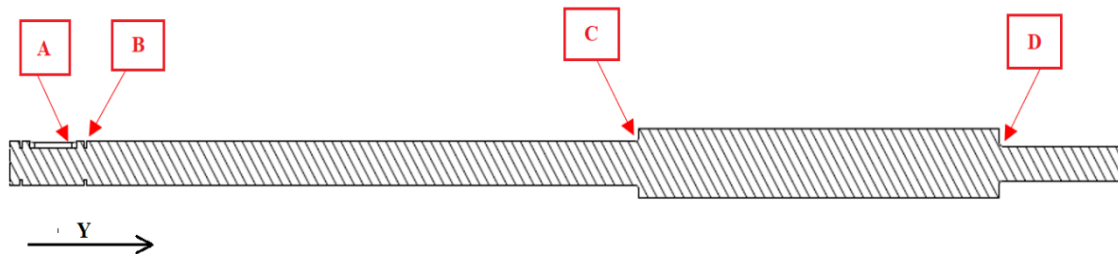


Figure 6.55: Section in which carried out the fatigue test

	Description	Cordinate [Y]
Section A	Corner radius for joint	17 mm
Section B	Corner radius	97 mm
Section C	Corner radius	330 mm
Section D	Corner radius of tongue	415 mm
Section E	Corner radius of tongue	445 mm

Table 6.12: Description and position of the sections verified at Fatigue

The results obtained are shown below:

Section A			Section B		
$M_{b_{yx}}$	10	Nm	$M_{b_{yx}}$	45	Nm
$M_{b_{yz}}$	25	Nm	$M_{b_{yz}}$	40	Nm
M_t	67.3	Nm	M_t	67.3	Nm
N	0	N	N	0	N
d	21,5	mm	d	23,9	mm
$\sigma_{M_{b_{max}}}$	65,50	MPa	$\sigma_{M_{b_{max}}}$	49,34	MPa
σ_N	0,00	MPa	σ_N	0,00	MPa
$\tau_{M_t_{max}}$	92,26	MPa	$\tau_{M_t_{max}}$	67,17	MPa
Useful Data			Useful Data		
σ_m	0,00	MPa	σ_m	0,00	MPa
σ_a	65,50	MPa	σ_a	49,34	MPa
τ_m	92,26	MPa	τ_m	67,17	MPa

Fatigue test			Fatigue test		
R_m	690	MPa	R_m	690	MPa
σ_{D-1}	345	MPa	σ_{D-1}	345	MPa
C_L	1	-	C_L	1	-
C_S	0,91	-	C_S	0,9	-
C_F	0,9	-	C_F	0,9	-
r	0,5	mm	r	0,2	mm
K_t	2,2	-	K_t	2,5	-
$\rho^{0,5}$	0,38		$\rho^{0,5}$	0,38	
q	0,65	-	q	0,54	-
K_f	1,78	-	K_f	1,81	-
σ_{D-1_e}	158,69	MPa	σ_{D-1_e}	154,31	MPa
σ_{DC}	158,69	MPa	σ_{DC}	154,31	MPa
Secure factor			Secure factor		
SF	2,42	True	SF	3,13	True

Section C			Section D		
M _{b_yx}	23	Nm	M _{b_yx}	12	Nm
M _{b_yz}	10	Nm	M _{b_yz}	6	Nm
M _t	67.3	Nm	M _t	67.3	Nm
N	0	N	N	0	N
d	25	mm	d	20	mm
σ _{Mb_max}	7,02	MPa	σ _{Mb_max}	17,32	MPa
σ _N	0,00	MPa	σ _N	0,00	MPa
τ _{Mt_max}	58,69	MPa	τ _{Mt_max}	114,60	MPa
Useful Data			Useful Data		
σ _m	0,00	MPa	σ _m	0,00	MPa
σ _a	7,02	MPa	σ _a	17,32	MPa
τ _m	58,69	MPa	τ _m	114,60	MPa
Fatigue test			Fatigue test		
R _m	690	MPa	R _m	690	MPa
σ _{D-1}	345	MPa	σ _{D-1}	345	MPa
C _L	1	-	C _L	1	-
C _S	0,9	-	C _S	0,92	-
C _F	0,9	-	C _F	0,9	-
r	2	mm	r	2	mm
K _t	1,8	-	K _t	1,75	-
ρ ^{0,5}	0,38		ρ ^{0,5}	0,38	
q	0,79	-	q	0,79	-
K _f	1,63	-	K _f	1,59	-
σ _{D-1_e}	171,38	MPa	σ _{D-1_e}	179,53	MPa
σ _{DC}	171,38	MPa	σ _{DC}	179,53	MPa
Secure factor			Secure factor		
SF	24.41	True	SF	10.37	True

In Figure 6.56 and 6.57 are shown the characteristics of the steels chosen for the main shaft and auxiliary shafts.

EUROPA		ITALIA		GERMANIA		FRANCIA		UK		USA	
EN 10083-2: 2006		(UNI 7845-78)		(DIN 17200-86)		(NF A 35-52-86)		(BS 970 pt.3-96)		ASTM A 29	
Qualità	N°			Werkstoff	N°						
C22E	1.1151	-		Cl. 22	1.1151	XC 18		070M20		1020	

EUROPA	C	Si / max	Mn	P / max	S	Cr / max	Mo / max	Ni / max	Al	Pb
C22E	0,17-0,24	0,40	0,40-0,70	0,035	≤ 0,035	0,40	0,10	0,40	-	-
C22Epb					0,020-0,040				0,020-0,050	0,15-0,30

Spessore mm	Laminato + Pelato rollato (+SH)			Trafilato a freddo (+C)		
	Durezza HB	R _m (MPa)	R _{p0,2} (MPa) min	R _m (MPa)	A ₅ (%) min	
≥ 5 ≤ 10	-	-	425	550-900	7	
> 10 ≤ 16	-	-	340	500-800	8	
> 16 ≤ 40	136-200	460-650	270	470-770	9	
> 40 ≤ 63	136-200	460-650	240	450-750	10	
> 63 ≤ 100	136-200	460-650	215	425-700	10	

Figure 6.56: Datasheet of steel for the main shaft

EUROPA		ITALIA		GERMANIA		FRANCIA		UK		USA	
EN 10083-2: 2006 EN 10277-5: 2008		(UNI 7845-78)		(DIN 17200-86)		(NF A 35-52-86)		(BS 970 pt.3-96)		ASTM A 29	
Qualità	N°			Werkstoff	N°						
C50E	1.1206	C50		Cl. 50	1.1206	-		080M50		1050	
C50R Pb	1.0542	C50		Cl. 50	1.0542	-		080M50 LEADED		10L50	

EUROPA	C	Si	Mn	P / max	S / max	Cr / max	Mo / max	Ni / max	Cu / max	Pb
C50E	0,47-0,55	0,10-0,40	0,60-0,90	0,025	0,035	0,40	0,10	0,40	0,30	-
C50Rpb					0,020-0,040					0,015-0,030

Spessore mm	Pelato rollato (+SH)		Bonificato + Pelato (+QT+SH)*				Bonificato + Trafilato a freddo (+QT+C)			Trafilato a freddo (+C)		
	Durezza HB	R _m (MPa)	R _{p0,2} (MPa) min	R _m (MPa)	A ₅ (%) min	KV (J) min	R _{p0,2} (MPa) min	R _m (MPa)	A ₅ (%) min	R _{p0,2} (MPa) min	R _m (MPa)	A ₅ (%) min
≥ 5 ≤ 10	-	-	-	-	-	-	610	870-1070	7	590	770-1100	5
> 10 ≤ 16	-	-	-	-	-	-	580	830-1030	7	520	730-1080	6
> 16 ≤ 40	179-269	610-910	460	700-850	15	-	555	790-990	8	440	690-1050	7
> 40 ≤ 63	179-269	610-910	400	650-800	16	-	510	730-930	9	390	650-1030	8
> 63 ≤ 100	179-269	610-910	400	650-800	16	-	475	680-880	9	-	-	-

Figure 6.57: Datasheet of steel for the auxiliaries shafts

6.9 Design: main shaft joint ring

In this section the dimensioning of the ring (*Figure 6.58*) that joins the internal shaft with the external roller by using screws, thus allowing the transmission of the torque from the first to the second one was examined.

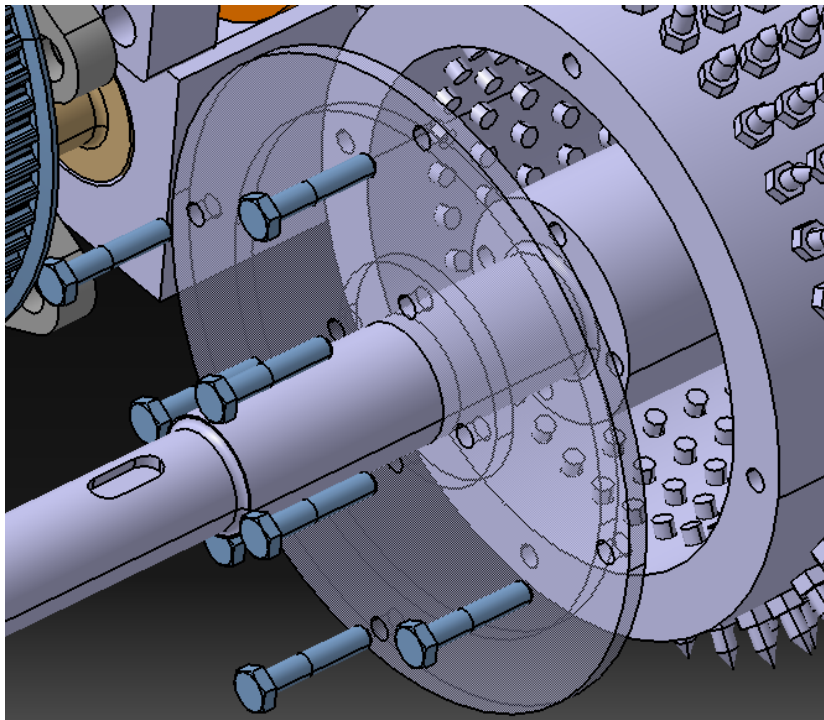


Figure 6.58: Ring joint

In this case, a minimum thickness of the latter was determined using the theory of the fracture mechanics. In particular, the disc was considered as a plate, on which an average force is exerted on both sides, resulting from the tangential force resulting from the torque transmitted by the internal shaft to the external roller. In this case, the present case was approximated with the one in *Figure 6.59*.

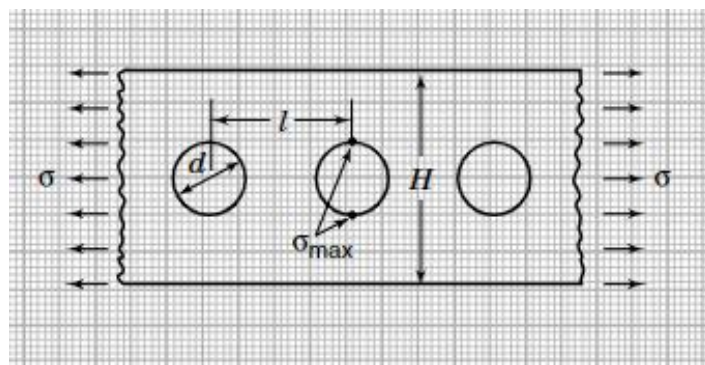


Figure 6.59: Stress parallel to the axis of the holes to a finite-width thin element [20]

Where

- **d** is the hole diameter equal to 6 mm
- **l** is the distance between the holes and (considering the most external holes) is equal to:

$$l = \frac{\pi D}{4} = \frac{\pi \cdot 170}{4} = 133.5 \text{ mm}$$

- **H** is the thinnest part of the ring, and is equal to the thickness of the hollow shaft and it is equal to 16 mm.

To design the component to an infinite life we can use the fatigue theory, when has been ensure the following equation:

$$SF = \frac{1}{\frac{\sigma_a}{\sigma_{D-1}^c} + \frac{\sigma_m}{R_m}} \geq 2 \quad (6.41)$$

Where

- $\sigma_a = \sigma_{max} = \frac{F}{B(W-d)}$
- $\sigma_m = 0$ for a symmetric stress.
- $k_f = 1 + q(K_t - 1) = 2.07$ it has obtained using the charts in *Figure 6.60* and *Figure 6.61*.
- $\sigma_{ef} = \frac{R_m}{2 \cdot K_f}$ it represent the fatigue limit of the steel used to make the joint.

$$q = \frac{1}{1 + \frac{A}{\sqrt{r}}}$$

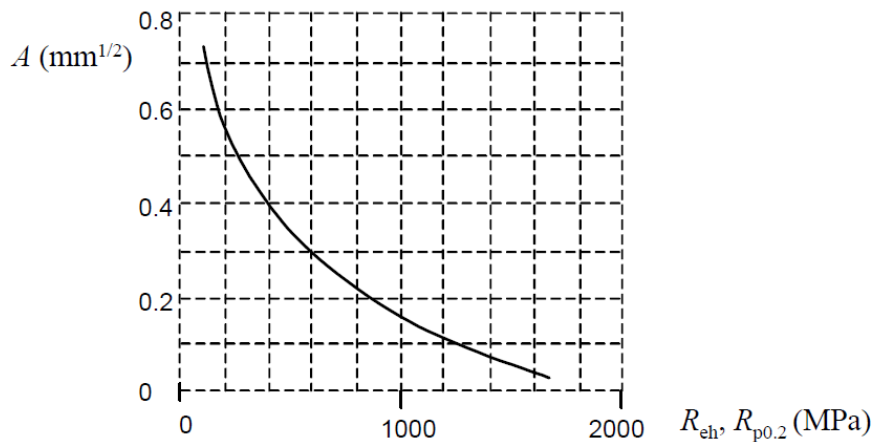


Figure 6.60: A chart depending on $R_{p0.2}$ of the material

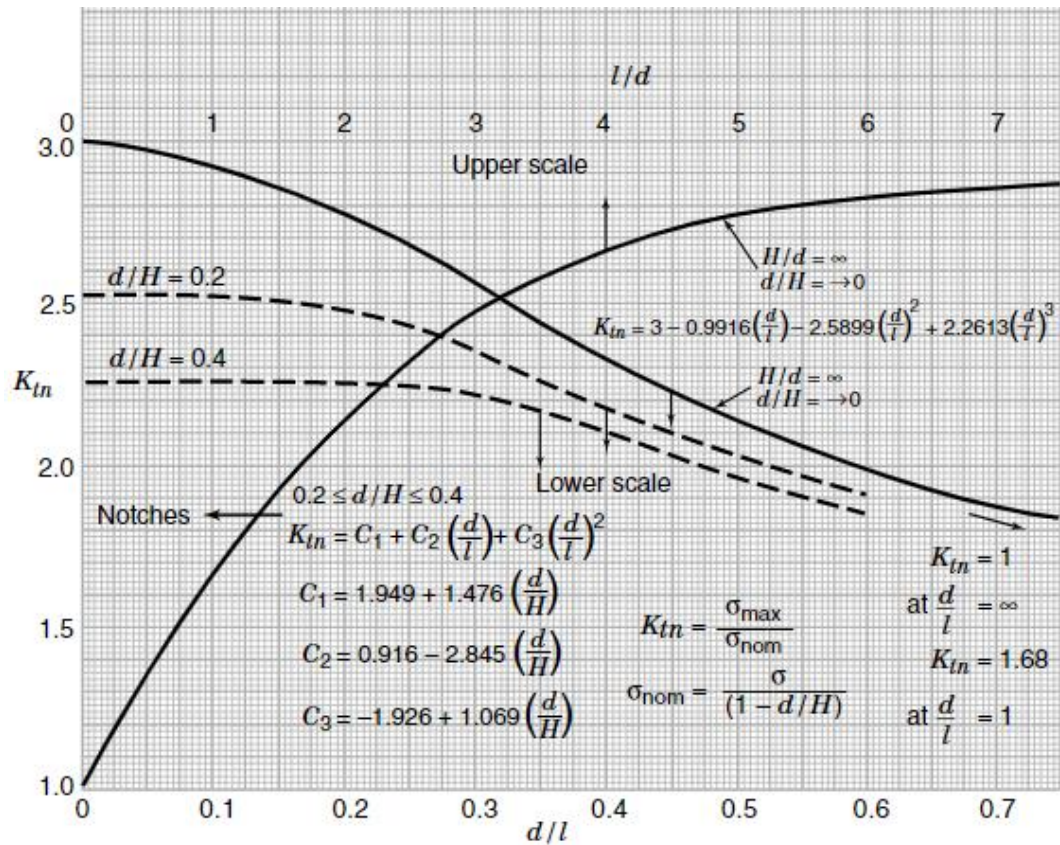


Figure 6.61: Stress concentration factor K_t for uniaxial tension of a finite-width element. Stress parallel to the axis of the holes.[20]

To estimate the force (P) it was considered the case in Figure 6.62, where P represent the resultant of the stress generated with the join between the ring and the hollow shaft using a screw connection.

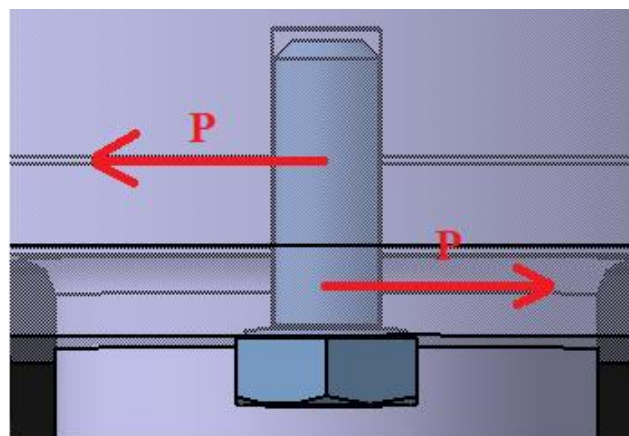


Figure 6.62: share force in the screw connection

It has been possible to determine a minimum thickness using the equation (6.41) the result is shown below:

$$B \geq \frac{3 \cdot P}{\sigma_{ef} \cdot (W - d)} \geq \frac{3 \cdot 1272}{108,7 \cdot 10} \geq 3.51 \text{ mm}$$

6.9.1 Checking the screws used

- **Tensile strength**

To carry out the calculation of the tensile strength of a screw was used the following formula:

$$F_{Rd,t} = \frac{0.9 \cdot f_{tb} \cdot A_{res}}{Y_{M2}} \quad (6.42)$$

Where

- $F_{Rd,t}$ is the tensile strength of the screw
- f_{tb} is the breaking strength of the selected screw (*Table 6.13*)
- A_{res} is the resistant section of the threaded part of the screw (*Table 6.14*)
- Y_{M2} is the safety factor that in this case is equal to 1.25

Classe	4.6	5.6	6.8	8.8	10.9
f_{yb} (N/mm ²)	240	300	480	649	900
f_{tb} (N/mm ²)	400	500	600	800	1000

Table 6.13: Breaking strength according to UNI EN ISO 898-1:2001

Nominal Diameter	Pitch mm	Resistant Area (A_{res}) mm ²
M.4	0,70	8,78
M.5	0,80	14,20
M.6	1,00	20,10
M.8	1,25	36,60

Table 6.14: Resistant Area for nominal diameter of screw

A hexagonal head screw with a fully threaded shank M6, class 8.8 has been selected for this application according to the following standards *ISO 4017 – UNI 5739 – DIN 933*. Using equation (6.42) it is possible to verify that the preload force applied on the screw shank is less than the maximum permissible force, the result are shown below:

$$F_{Rd,v} = \frac{0.7 \cdot 800 \cdot 20.1}{1.25} = 11577 \text{ N} > \frac{P \cdot 1.5}{\mu_{steal}} > 3347 \text{ N}$$

- **Shear strength**

To carry out the calculation of the shear strength of a screw was used the following formula:

$$F_{Rd,v} = \frac{0.6 \cdot f_{tb} \cdot A_{res}}{Y_{M2}} \quad (6.43)$$

Where

- $F_{Rd,v}$ is the shear strength of the screw
- f_{tb} is the breaking strength of the selected screw (*Table 6.13*)
- A_{res} is the resistant section of the threaded part of the screw (*Table 6.14*)
- Y_{M2} is the safety factor that in this case is equal to 1.25

Using equation (6.43) it is possible to verify that the shear force applied on the screw shank is less than the maximum permissible force, the result are shown below:

$$F_{Rd,v} = \frac{0.6 \cdot 800 \cdot 20.1}{1.25} = 7718 \text{ N} > 1272 \text{ N}$$

6.10 Bearing choose

The following lines of the discussion are dedicated to the analysis of the calculations and parameters used for the selection and sizing of the bearings. In this regard, the SKF catalogue has been taken as a reference, from which all the data necessary for the established purpose will be extracted. For the project under consideration it was decided to use, for all the cases present, types of toroidal roller bearing. The choice of bearings depends on several parameters, which are described in detail below. One of them, which is fundamental for the treatment, is the life. The life of the bearings must be within the range of values from 25000 to 50000 hours, if possible, or in any case have a value around the maximum life established.

6.10.1 Calculation criteria

- **Static test**

The first step to be carried out for the calculation of the bearings is the static verification expressed by the calculation of the safety factor S_0 :

$$S_0 = \frac{C_0}{P_0} \quad (6.44)$$

With:

- C_0 basic static load rating
- P_0 equivalent static bearing load

The value of C_0 is given in the catalogue for each individual bearing. It can be expressed as P_0 in the following way:

$$P_0 = F_r \quad (6.45)$$

The safety factor must respect the equation below:

$$S_0 \geq S_{min} \quad (6.46)$$

In which the value of S_{min} is provided by the catalogue according to the type of application considered.

- **Fatigue test**

Fatigue testing is the main step in the calculation of bearings. It can be used to check if the bearing in question satisfies the life restriction mentioned above. The relationship expressing the service life in millions of cycles is as follows, in accordance with ISO 281:1990/Amd 2:2000

$$L_{10m} = a_1 a_{SKF} \cdot \left(\frac{C}{P}\right)^p \quad (6.47)$$

With

- a_1 life adjustment factor for reliability
- a_{SKF} SKF life modification factor equal to

$$a_{SKF} = f_{a_{SKF}}\left(\eta_c, \frac{P_u}{P}, k\right) \quad (6.48)$$

- η_c the contamination level in the bearing, whose value depends on the working conditions and can be chosen from the following table:

Conditions	Factor η_c ¹⁾ for bearings with mean diameter	
	$d_m < 100$ mm	$d_m \geq 100$ mm
Extreme cleanliness • particle size approximately the same as the lubricant film thickness • laboratory conditions	1	1
High cleanliness • oil filtered through an extremely fine filter • typical conditions: sealed bearings that are greased for life	0,8 ... 0,6	0,9 ... 0,8
Normal cleanliness • oil filtered through a fine filter • typical conditions: shielded bearings that are greased for life	0,6 ... 0,5	0,8 ... 0,6
Slight contamination • typical conditions: bearings without integral seals, coarse filtering, wear particles and slight ingress of contaminants	0,5 ... 0,3	0,6 ... 0,4
Typical contamination • conditions typical of bearings without integral seals, coarse filtering, wear particles and ingress from surroundings	0,3 ... 0,1	0,4 ... 0,2
Severe contamination • typical conditions: high levels of contamination due to excessive wear and/or ineffective seals • bearing arrangement with ineffective or damaged seals	0,1 ... 0	0,1 ... 0
Very severe contamination • typical conditions: contamination levels so severe that values of η_c are outside the scale, which significantly reduces the bearing life	0	0

¹⁾ The scale for η_c refers only to typical solid contaminants. Contaminants like water or other fluids detrimental to bearing life is not included. Due to strong abrasive wear in highly contaminated environments ($\eta_c = 0$) the useful life of a bearing can be significantly shorter than the rated life.

Table 6.15: Values for the η_c for different levels of the contamination, according to SKF standard.

- P_u/P fatigue load limit ratio, where the P_u is the fatigue limit load from the catalogue for each individual bearing.
- k viscosity ratio as the ratio of the actual viscosity ν to the rated viscosity ν_1 for adequate lubrication, when the lubricant is at normal operating temperature.

$$k = \frac{\nu}{\nu_1} \quad (6.49)$$

The viscosity ν depend by the work temperature and is obtained from the chart below:

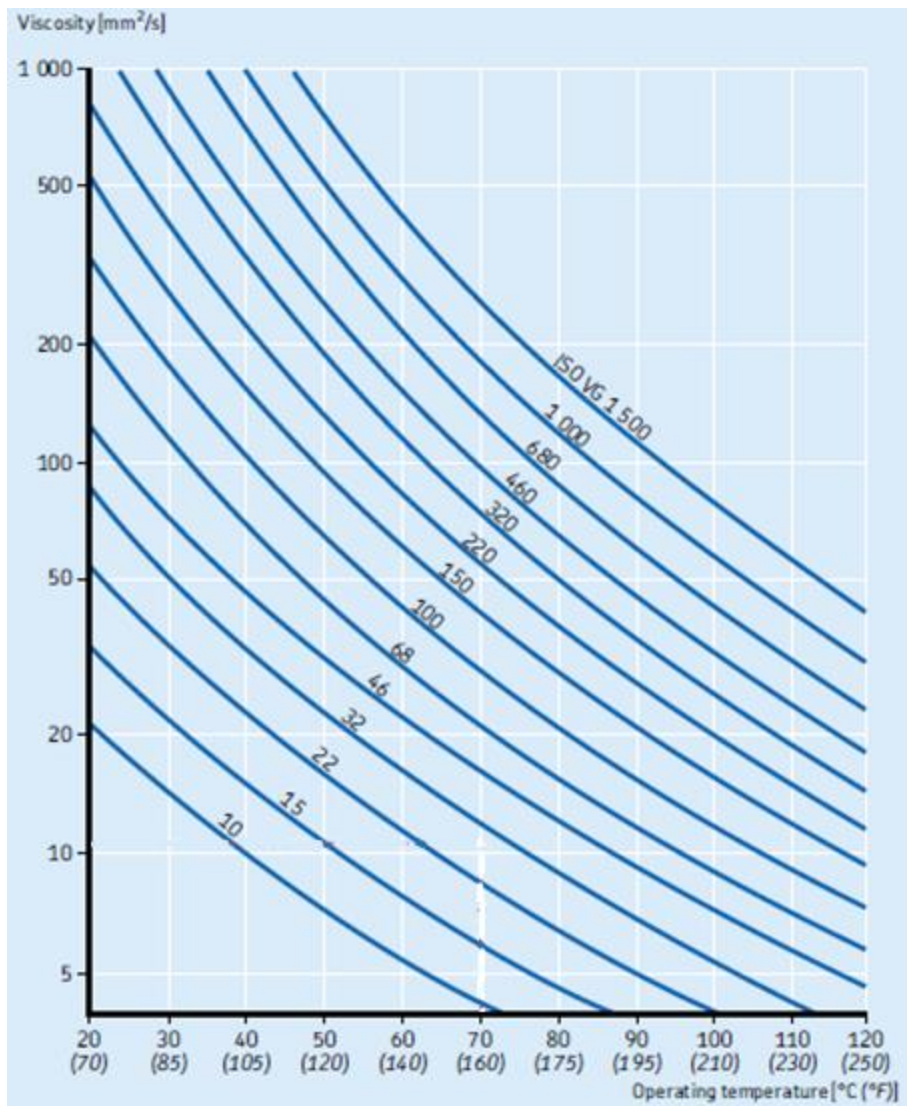


Figure 6.63: Viscosity-temperature diagram for ISO viscosity grades

The minimum required viscosity ν_1 is instead a function of the average diameter of the bearing used and the number of revolutions of the shaft n and it is obtained from the chart in *Figure 6.63*.

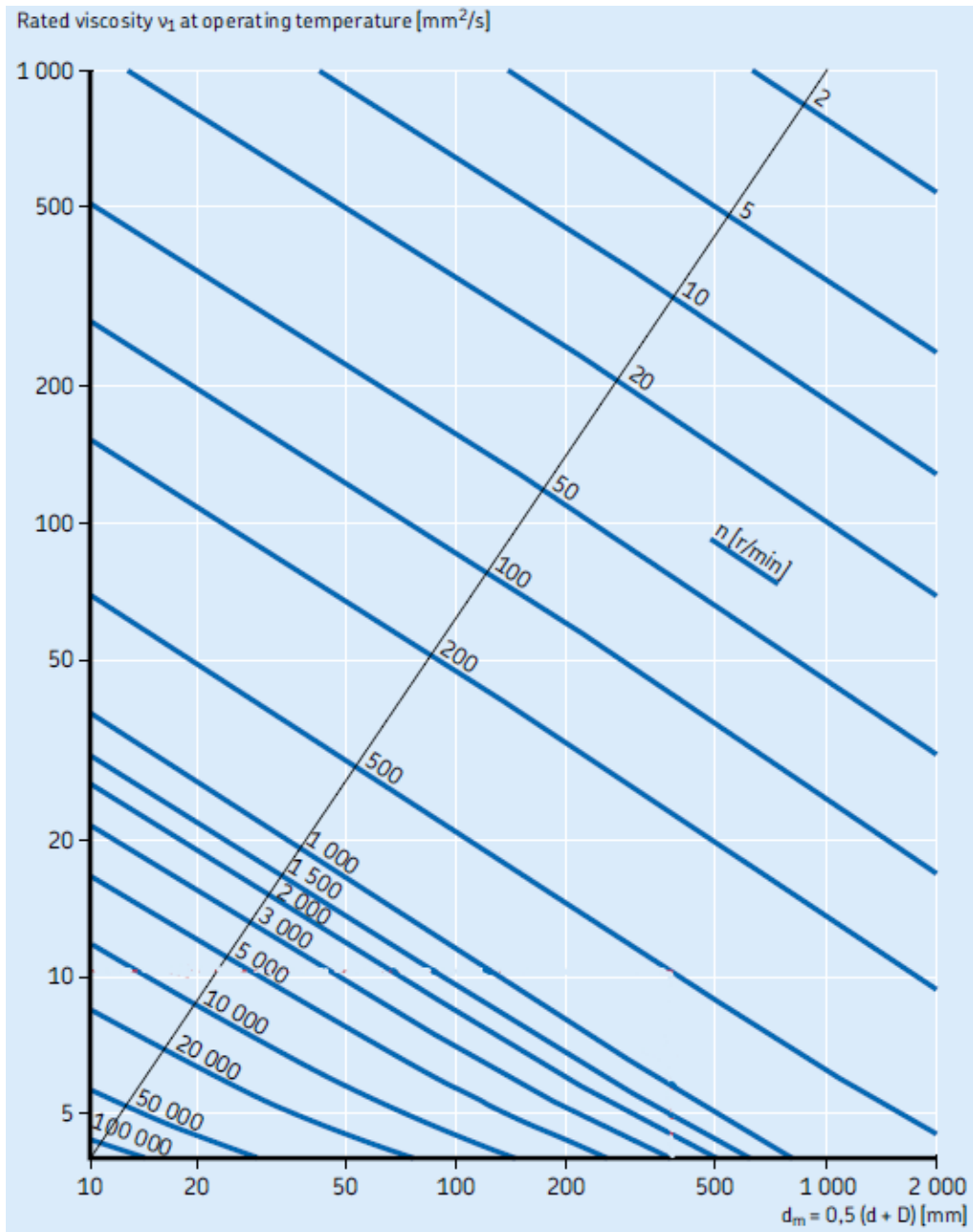


Figure 6.64: Minimum rated viscosity v_1 required depending on the average diameter of the bearing

Once all parameters have been calculated, the value of the correction factor a_{SKF} can be identified from the chart in Figure 6.64, which already relates to a type of radial roller bearing

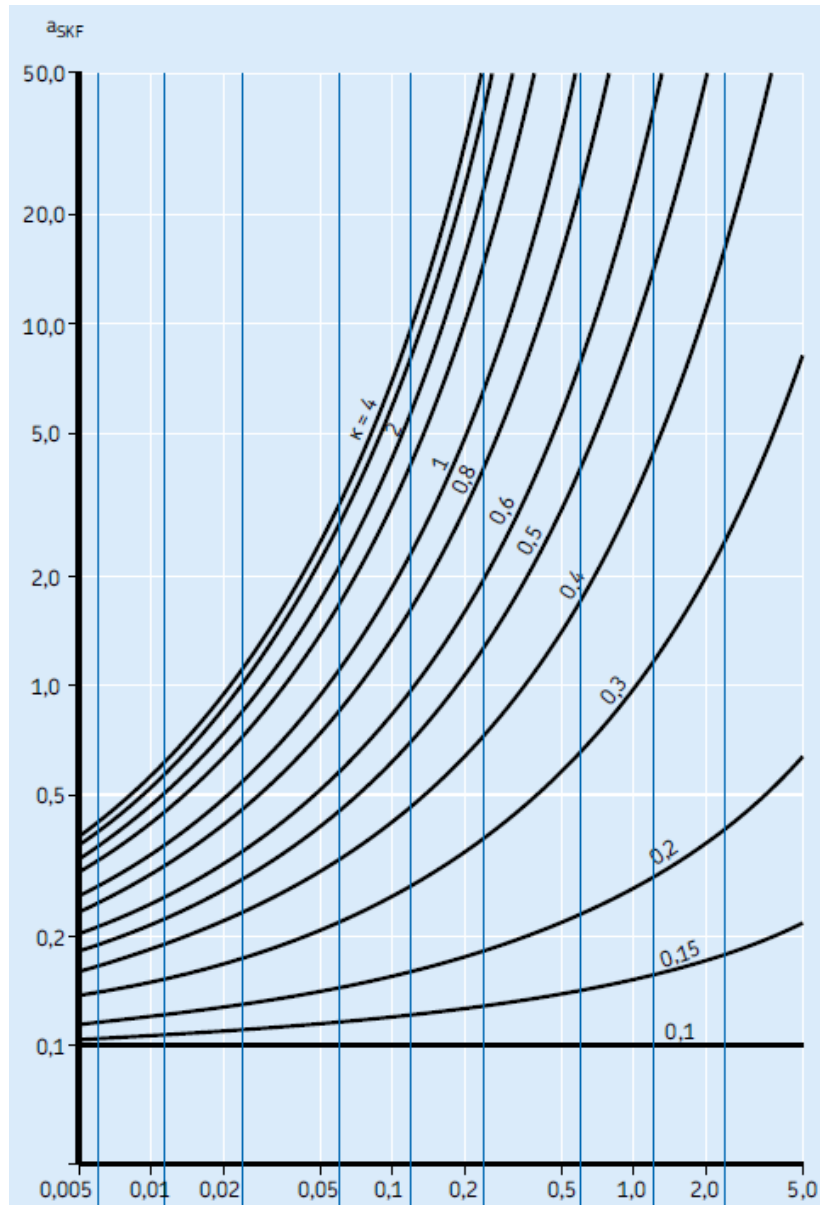


Figure 6.65: Factor a_{SKF} for radial ball bearings

- C basic dynamic load rating
- P equivalent dynamic bearing load, usually P is equal to:

$$P = \begin{cases} X_1 F_r + Y_1 F_a & \text{se } \frac{F_a}{F_r} \leq e \\ X_2 F_r + Y_2 F_a & \text{se } \frac{F_a}{F_r} \geq e \end{cases}$$

In this case $P = F_r$

- p exponent of the life equation equal to

$$p = \begin{cases} 3 & \text{for ball bearings} \\ \frac{10}{3} & \text{for roller bearings} \end{cases}$$

6.10.2 Bearing for main shaft

For the main shaft, the *SKF* catalogue has been used to choose a type of bearing suitable for our application. The latter already have bearings supported in the catalogue. For the main shaft, the support with the code *P 30 TF* was chosen, which recommended as bearing the one with the code *YAR 206-2F*. The bearing in question was checked for our application. In this case, the life limit motioned above was not taken into account as it is excessive for a testing machine. However, the service life of the testing machine has been calculated and it has been decided if it is acceptable or not. The results obtained are as follows:

YAR 206-2F		
Static check		
C_0	11200	N
P_0	1320	N
R_{rX}	1312	N
R_{rY}	144	N
R_r	1320	N
F_r	1320	N
S_0	8.49	-
S_{min}	2	-

Fatigue check		
a_1	1	-
v	40	mm ² /s
v_1	90	mm ² /s
P_u	475	N
R_r	1320	N
F_r	1320	N
η_c	0,7	-
K	0.44	-
$\eta_c \frac{p_u}{p}$	0.25	-
a_{skf}	0.8	-
C	19500	N
P	1320	N
(E)	47775	h
p	3	-
L_{mn}	235,4	-

6.10.3 Bearing for auxiliary shafts

For the auxiliary shaft called "orange coloured shaft" above, the *SKF* catalogue has been used to choose a type of bearing suitable for our application. The latter already have bearings supported in the catalogue. For this shaft, the support with the code *FYTB 20 TF* was chosen, which recommended the bearing with the code *YAR 204-2F*. The bearing in question was checked for our application. The results obtained are as follows:

YAR 204-2F		
Static check		
C_0	6550	N
P_0	1329	N
R_{rX}	1224	N
R_{rY}	519	N
R_r	1329	N
F_r	1329	N
S_0	4.93	-
S_{min}	2	-

Fatigue check		
a_1	1	-
v	180	mm ² /s
v_1	300	mm ² /s
R_{rX}	1329	N
P_u	280	N
R_r	1329	N
F_r	1329	N
η_c	0,9	-
K	0.6	-
$\eta_c \frac{p_u}{p}$	0.19	-
a_{skf}	1.8	-
C	12700	N
P	1329	N
(E)	29056	h
p	3	-
L_{mn}	1569	-

For the auxiliary shaft called "red coloured shaft" above, the *SKF* catalogue has been used to choose a type of bearing suitable for our application. The latter already have bearings supported in the catalogue. For this shaft, the support with the code *P 30 TF* was chosen, which recommended the bearing with the code *YAR 206-2F*. The bearing in question was checked for our application. The results obtained are as follows:

YAR 206-2F		
Static check		
C_0	11200	N
P_0	1134	N
R_{rX}	1066	N
R_{rY}	388	N
R_r	1134	N
F_r	1134	N
S_0	9,87	-
S_{min}	2	-

Fatigue check		
a_1	1	-
v	40	mm ² /s
v_1	90	mm ² /s
R_{rX}	1134	N
P_u	475	N
R_r	1134	N
F_r	1134	N
η_c	0,7	-
K	0,444	-
$\eta_c \frac{p_u}{p}$	0,29	-
a_{skf}	1	-
C	19500	N
P	1134	N
(E)	94057	h
p	3,00	-
L_{mn}	5079	-

For the auxiliary shaft called "gold coloured shaft" above, the SKF catalogue has been used to choose a type of bearing suitable for our application. The latter already have bearings with integrate supported in the catalogue. For this shaft, the supports with the code *P 25 TF*, *FYTB 25 TF* and *FYTB 20 TF* have been chosen, which recommended the bearing with the code *YAR 205-25* for the first two and *YAR 204-25* for the last. The most loaded bearing was checked for our application. The results obtained are as follows:

YAR 205-2F		
Static check		
C_0	7800	N
P_0	2124	N
R_{rX}	1996	N
R_{rY}	727	N
R_r	2124	N
F_r	2124	N
S_0	3,67	-
S_{min}	2	-

Fatigue check		
a_1	1	-
v	180	mm ² /s
v_1	300	mm ² /s
R_{rX}	2124	N
P_u	335	N
R_r	2124	N
F_r	2124	N
η_c	0,9	-
K	0,600	-
$\eta_c \frac{p_u}{p}$	0,14	-
a_{skf}	1,6	-
C	14000	N
P	2124	N
(E)	8482	h
p	3,00	-
L_{mn}	458	-

7 Conclusion and future development

Waste has always been one of the problems of our society. In particular, the need for textile waste recycling stems from the fact that the world's population is constantly increasing and we will no longer be able to meet the demand for raw materials necessary for the production of clothing (i.e. the demand for organic raw materials) nor will we be able to dispose of and accumulate waste in landfills because there will be a lack of areas that can meet this purpose. This thesis' work enable to make a first tearing machine prototype with variables parameters which can be used to recycling the textile waste.

The work starts with the introduction of statistics data about the topic which still sees that 85% of the recyclable textile waste going to landfills.

After a classification of textile waste, it introduces the recycling technologies used to recycle the textile waste, in particular this thesis' work is focus on the first approach, the reclaiming of fibers.

In the 3rd chapter is described the recycling process to obtain reclaimed fiber and the work has focused on the tearing process, in fact in the 4th chapter is explaining how some old tearing machine patents work.

Using a disruptive test, the force needed to tear the fabric was estimated, this allowed to start the design of the prototype.

The next step is to build the tearing machine prototype to make possible to test it. In particular is useful to know which the correct power is needed to tear the fabric for minimized the power waste and choose a smaller gearmotor, this allow to minimize also the cost of the machine.

The machine can be used to do tests changing some work's parameters.

It is useful know the best rollers' speed to tearing the textile waste also verifying that is not change for different material such as cotton, wool or others.

It is useful know which is the best distance between the centres of the auxiliary rollers to compress the textile waste as enough to allow the tearing of the latter.

With the final product, namely the recycled fibers, it is possible to create also other type of material mixing the recycling fiber with other kind of recycling products.

References

- [1] <https://www-statista-com.ezproxy.biblio.polito.it/topics/1542/cotton/>
- [2] Bojana Voncina, (2000). *Recycling of textile materials* -, University of Maribor, Faculty of Mechanical Engineering, Smetanova 17, Maribor, Slovenia
- [3] <http://worldwearproject.com/about-us/global-responsibility>
- [4] <http://www.smartasn.org/> | Secondary Materials and Recycling Textiles [SMART]
- [5] Youjiang Wang, (2006). *Recycling in textiles*. Cambridge CB1 6AH, England: Woodhead Publishing Ltd
- [6] Samy Yousefa,d, Maksym Tatariantsb, Martynas Tichonovasb, Zahid arwarb, Ilona Jonuškienėc, Linas Kliucininkasb, (2019). *A new strategy for using textile waste as a sustainable source of recovered cotton*
- [7] <https://www.statista.com/statistics/741296/world-fiber-consumption-distribution-by-fiber-type/>
- [8] Hawley J. M. (2000), Textile recycling as a system: A micro/macro analysis. *Journal of Family and Consumer Sciences*, 93(5), 35–40.
- [9] Nattha Pensupa, Shao-Yuan Leu³, Yunzi Hul, Chenyu Du⁴, Hao Liu, Houde Jing³, Huaimin Wang, Carol Sze Ki Lin, (2017). *Recent Trends in Sustainable textile Waste Recycling Methods: Current Situation and Future Prospects*. Springer International Publishing
- [10] Rota F., inventor; Satrind, Srl, assignee. Two-shaft industrial shredder. United States patent US 2005/0242221 A1. 2003 Jun. 2.
- [11] Sarah Wroe, (2013). *The Recycling of Resorcinol Formaldehyde Latex Coated Nylon 66*. University of Manchester, Manchester, UK.
- [12] Nattha Pensupa, Shao-Yuan Leu, Yunzi Hu, Chenyu Du, Hao Liu, Houde Jing, Huaimin Wang, Carol Sze Ki Lin, (2017). *Recent Trends in Sustainable Textile Waste Recycling Methods: Current Situation and Future Prospects*. Innovation and Technology Commission, Hong Kong: Springer International Publishing.
- [13] Azam Jeihanipour, Keikhosro Karimi, Claes Niklasson, Mohammad J.Taherzadeh, (2010). *A novel process for ethanol or biogas production from cellulose in blended-fibers waste textiles*.

- [14] Mahalakshmi, M., Angayarkanni, J., Rajendran, R., Rajesh, R., (2011). *Bioconversion of cotton waste from textile mills to bioethanol by microbial Saccharification and fermentation*. Scholars Research Library, India: Annals of Biological Research, 2011, Vol. 2, No. 3, pp. 380-388.
- [15] Jeihanipour A, Karimi K, Niklasson C, Taherzadeh MJ, (2010). *A novel process for ethanol or biogas production from cellulose in blended-fibers waste textiles*.
- [16] Wolfgang W., inventor; H Schirp & Co KG GmbH, assignee. Reisswolf für die Textilindustrie. European Patent Office EP 0293590 B1. 1991 Jan 30.
- [17] Robert G. Rowe, inventor; John D Hollingsworth on Wheels, Inc. Textile recycling machine. United States patent US 6061876. 2000 May 16.
- [18] Morel A., inventor; Constructions Mecaniques F Laroche and Fils, assignee. Shredding machine for recycling textile fibers and method. United States patent US 4484377. 1984 Nov 27.
- [19] S Dhamija, Manisha Chopra (2007). *Tearing strength of cotton fabrics in relation to certain process and loom parameters*. The Technological Institute of Textile & Sciences, Birla Colony, Bhiwani 127 021, India: Indian Journal of Fibre & Textile Research.
- [20] Walter D. Pilkey, Deborah F. Pilkey (2007). *Peterson's stress concentration factors*. Hoboken, New Jersey, John Wiley & Sons, Inc, Section 4.4.4, pp 315-344.